SUSCEPTIBILITY OF SERVICE EXPOSED CREEP RESISTANT MATERIALS TO REHEAT CRACKING DURING REPAIR WELDING

By

Riaan Loots

Submitted in partial fulfillment of the requirements for the degree Masters in Metallurgical Engineering in the Faculty of Engineering, the Build Environment and Information Technology

UNIVERSITY OF PRETORIA

2003

TABLE OF CONTENTS

ABSTRACT

High temperature steam generating boilers constructed from creep resistant alloys are designed for specific operating parameters for the estimated safe operating life. Design life calculations of a boiler are based on material data available at that time and also on previous experience. During the life of the boiler new material data becomes available through long-term research projects, in some cases showing weak characteristics and behaviour that can compromise the original design life. That plant operator needs to launch a remedial maintenance and inspection programme or review the operating parameters to ensure safe and reliable remnant life for the affected components. A significant proportion of Eskom's boiler fleet accumulated more than 100 000 operating hours thus requiring close evaluation of component health in view of life extension beyond the original design life estimates.

Creep resistant alloys used on Eskom plant are shown in Table 1:

German Spec DIN17 715	British Spec BS3604 Grade HFS :	Also known as
15Mo3	-	½Mo
13CrMo4 4	620	1Cr-½Mo
10CrMo9 10	622	2¼Cr-1Mo
14MoV6 3	660	½Cr-½Mo-¼V
X20CrMoV12 1	762	12Cr or X20
X10CrMoVNb91		Steel 91 or P91

Table 1: Pipe and tube material chemical composition comparisons

Critical steam containing components manufactured from a combination of the above alloys accumulated sufficient operating hours for creep damage to take appreciable effect. In theory it would be possible to safely operate material which is creep aged to the upper limit of the secondary creep phase, just before the rapid creep deformation associated with tertiary creep commences.

Research work included specifically the susceptibility of four of the above mentioned materials (½Cr-½Mo-¼V, 2¼Cr-1Mo, X20, P91) with regards to reheat cracking, as these types of materials, especially the older ferritic

grades (½Cr-½Mo-¼V and 2¼Cr-1Mo) are prone to reheat cracking. The tests involved the material undergoing a simulated welding thermal cycle and then being subjected to constant load tests. This was done for new as well as service exposed material.

The results indicate that for service exposed materials where creep damage (voids in the microstructure) are below a certain limit the material show no susceptibility to reheat cracking for the testing conditions employed. For the new material it was confirmed that mainly ½Cr-½Mo-¼V showed susceptibility towards reheat cracking.

OPSOMMING

Stoom ketels, in die elektrisiteits generasie industrie, word vervaardig van kruip-bestaande stale en is ontwerp vir spesifieke operasionele parameters vir die beplande, veilige operasionele leeftyd van die ketel. Ontwerpslewe berekeninge van so 'n ketel word gebasseer op beskikbare materiaal inligting op daardie tydstip en ook op vorige ondervinding van die ontwerpspan. Tydens die leeftyd van 'n ketel word nuwe materiaaldata dikwels bekend gestel. Hierdie resultate is as gevolg van lang termyn navorsings projekte. In sommige gevalle word swak materiaal eienskappe uitgewys wat 'n sterk invloed het op die ontwerp leeftyd van die ketel. Aanlegbestuur en operateurs het dus nodig om 'n voorkomende inspeksie en onderhoudsprogram in te stel of 'n volledige studie van aanlegparameters moet gedoen word en dalk aangepas word, om te verseker dat geaffekteerde komponente veilig gebruik kan word vir die res van die leeftyd. 'n Relatiewe groot hoeveelheid van Eskom se stoomketels het al meer as 100 000 operasionele ure geakumuleer. 'n Filosofie is in plek gebring wat baie deeglike inspeksie van komponente vereis, met die oog op verlenging van die operasionele leeftyd, verby die oorspronklike ontwerp leeftyd.

Kruip bestande legerings soos gebruik op Eskom aanlegte word aangedui in Tabel 1:

Duitse Spesifikasie DIN17 715	Britse Spesifikasie BS3604 Graad HFS :	Ook bekend as
15Mo3	-	½Mo
13CrMo4 4	620	1Cr-½Mo
10CrMo9 10	622	2¼Cr-1Mo
14MoV6 3	660	½Cr-½Mo-¼V
X20CrMoV12 1	762	12Cr or X20
X10CrMoVNb91		Staal 91 of P91

Tabel 1: Pyp en buis materiaal chemiese samestelling vergelyking

Kritieke stoomdraende komponente wat vervaardig is van 'n kombinasie van die bogenoemde legerings, het al genoeg operasionele ure geakumuleer vir

kruip skade om te manifesteer in die mikrostruktuur. In teorie sal dit moontlik wees om die komponente veilig te gebruik tot in die boonste limiet van die sekondêre kruip fase. Dit is tot net voor hoë kruip vervorming wat geassosieer word met tersiêre kruip begin.

Navorsingswerk tydens hierdie studie het gefokus op die vatbaarheid van vier van die bogenoemde legerings (½Cr-½Mo-¼V, 2¼Cr-1Mo, X20 en P91) vir herverhittings krake. Hierdie tipe materiale, veral die ouer ferritiese legerings (½Cr-½Mo-¼V en 2¼Cr01Mo), is vatbaar vir herverhittingskrake tydens sweiswerk. Die toetse het behels dat die materiaal 'n gesimuleerde termiese sweis siklus ondergaan en dan onderwerp word aan konstante belasting toetse. Dit was uitgevoer op nuwe sowel as diensverouderde materiaal.

Die resultate het aangedui dat vir diensverouderde materiaal waar kruip skade (holtes in die mikrostruktuur) onder 'n sekere hoeveelheid is, die materiaal nie vatbaar is vir herverhittingskrake nie, vir die toets kondisies wat gebruik is. Vir nuwe materiaal was dit bevestig dat ½Cr-½Mo-¼V die meeste vatbaar is vir herverhittingskrake.

ACKNOWLEDGEMENTS

I would like to thank Professor G.T. van Rooyen for his invaluable guidance and input for the duration of this project.

The following persons and institutions are all worth mentioning:

Professor P.C. Pistorius, Mr J. Borman and Mr C. Smal from the Department of Metallurgical Engineering for always being available and offering assistance.

Mr P Doubell, a colleague from Eskom TSI for his help and guidance.

Mr G von dem Bongart, for his assistance with the various microstructures obtained during the experimental work.

Mr C Coetzee, for his assistance with the scanning electron microscope (SEM).

Eskom for provision of material and financial aid, as well as the opportunity to conduct this task.

The Lord Jesus Christ and my family for supporting me.

Caro-Mé

The rest of my friends

There is no reality, there is only perception

CHAPTER 1

1.1 INTRODUCTION

The main energy supplier, world wide today, for electricity is still fossil fuel power stations. A huge quantity of the construction in these power stations is done by means of fusion welding processes. The wide range of materials used to build these huge constructions all have to meet rigid specifications of high strength, good toughness and often resistance against fatigue, corrosion and creep deformation (high temperature areas like the boilers and main steam pipelines).

However the most important factor in the choice of these materials is essentially that they posses *good weldability*. The question arises then: What is meant by '*good weldability*'? This can be defined as the ability of a material or combination of materials to be welded under fabrication conditions into a specific suitably designed structure and to perform satisfactorily in intended service[1]. As such the concept of good weldability has to be a function of a number of interacting variables, which include [2]:

1. Type of welding process
2. Composition and mechanical properties of weld metal and base metal
3. Welding sequence
4. Energy input
5. Joint design and size
6. Welding consumables
7. Structural constraint
8. Environment

A very simple definition of weldability is more often used. Will the material be free from cracking during fabrication and subsequent use? A clear distinction has been drawn between cracking occurring during the service life of the material and cracking occurring very shortly after welding or during welding.[3]

One such type of the latter mentioned is reheat cracking, also called stress relief cracking.

It has been demonstrated that reheat cracks form by a low ductility creep cavitation mechanism at the prior austenite grain boundaries during post weld heat treatment (PWHT)[4]. Thus reheat cracking usually occurs in the coarse grained heat affected zone (CGHAZ) and by means of intergranular fracture along the prior austenite grain boundaries. A troubling aspect encountered during reheat cracking is heat-to-heat variations, with respect to cracking susceptibility of the material. This indicates dependence on residual elements rather than on the bulk chemistry. The bulk chemistry of the alloys may therefore not necessarily be a reliable predictor of susceptibility to cracking.[5] At present the phenomenon and mechanism responsible for reheat cracking has been well researched and documented. Nevertheless, reheat cracking is still frequently a problem during welding, necessitating expensive repairs and reheat treatment. Some empirical guidelines on how to prevent reheat cracking have been established over the years. A much better understanding of the complex interaction of welding stresses, weld defects, geometrical constraint and material properties are required. This is of particular concern in the repair welding of creep damaged components, which may be at a greater risk of cracking than new material.

1.2 Cr-Mo AND Cr-Mo-V STEELS :

The properties sought after in a steel grade for high temperature applications are the following:

- High hot tensile strength
- Low creep rate
- High stress rupture ductility
- Corrosion and/or oxidation resistance

Cr-Mo and Cr-Mo-V steels are designated for use at elevated temperatures because of their resistance to creep. They are used as construction material for the construction of steam power plants, especially boilers, high pressure pipes and tubes, flanges, forgings, turbine rotors, water boilers, collectors and other highly stressed structural components.[6]

These steels typically contain 0.5 – 9.0% chromium and 0.5 – 2.0% molybdenum, with a carbon content usually less than 0.2%. Vanadium is sometimes added in the range of 0.35 – 0.7% and provides added creep strength due to formation of fine vanadium carbide precipitates. Small additions of nickel also improve the toughness and ductility. Chromium and molybdenum, when used as alloying elements in steel increases the hardenability and strength at elevated temperatures. Chromium further also improves resistance to oxidation and scaling. The most popular grades of Cr-Mo and Cr-Mo-V steels used today are listed in Table 1.1.

German Spec DIN17 715	British Spec BS3604 Grade HFS :	Also known as
15Mo3	-	½Mo
13CrMo4 4	620	1Cr-½Mo
10CrMo9 10	622	2¼Cr-1Mo
14MoV6 3	660	½Cr-½Mo-¼V
X20CrMoV12 1	762	12Cr or X20
X10CrMoVNb91		Steel 91 or P91

Table 1.1: Pipe and tube material chemical composition comparisons

Cr-Mo steels are normally used in a heat-treated condition. The heat treatment is either quenching and tempering or normalising and tempering. Sometimes annealing or isothermal annealing is used to produce a soft, relatively more stable ferritic microstructure. Two of the factors that make Cr-Mo steels so attractive for high temperature applications are transformation hardening, but more important is the fact that low alloy Cr-Mo steels have resistance to softening during post weld heat treatment (PWHT) and creep service. The maximum resistance depends on the degree of precipitate

dispersion. Chromium can form several types of precipitates. Chromium is soluble in cementite-M_3C and it tends to spheroidize these carbides. Three additional carbides can also be formed – $Cr_{23}C_6$ (cubic), Cr_7C_3 (hexagonal) and Cr_3C_2 (orthorhombic), each of which can dissolve considerable amounts of iron. The extent of solid solubility of iron in Cr_7C_3 is significant and thus it prevents the third carbide, Cr_3C_2, from occurring in equilibrium with ferrite.

Molybdenum can form hexagonal M_2C carbides, which are not in thermodynamic equilibrium with ferrite. Therefore, during long exposure times at elevated temperatures, M_6C type carbides evolve [7].

Vanadium carbide, V_4C_3 (cubic), is the most important carbide in Cr-Mo-V steels. The improvement of the creep strength of Cr-Mo-V steels over Cr-Mo steels is due to the presence of very fine vanadium carbides, in the matrix, that are more stable than either chromium and molybdenum carbides [8].

As mentioned before these steels are widely used in the manufacture of components that operate in the creep regime, such as boiler waterwall tubes, headers and main steam pipes, in power stations. The superheated steam (565°C) is transported from the headers to the turbine by the main steam pipeline. These pipes carry large volumes of steam and like the headers are not subjected to the aggressive environment of the boiler itself.

The dimensions of the different pipes are calculated on the basis of a service life in excess of 100 000 h (11½ years). The useful life of these pipes is more often actually determined by the development of creep damage, especially near or in the weldments. The creep damage is often characterised by the development of a number of microcavities in the microstructure of the steel. These microcavities may eventually coalesce into creep cracks. Inspection of replicas of the microstructure is an acceptable method to assess the remnant creep life of boiler pipe structures.

Creep damage is in no way uniform throughout the pipes. Some areas, especially in or around weldments may be severely damaged while the

surrounding base metal may contain very little damage. Therefore it has become practice to replace only the damaged sections. To date the acceptable creep damage in the parent metal has been set at 50 voids/mm^2. Therefore if 50 voids/mm^2 or more are detected, the section is no longer fit for service and has to be replaced. A new section will then be prepared and welded into position. This implies that new material and service exposed material will be welded together.

This raises the following questions:

1. To what extent will the prior creep damage be affected by the welding thermal cycle?
2. What effect will this prior creep damage in the HAZ have on the integrity on the weldment?
3. What effect will the subsequent thermal exposure have on the integrity of the weldment?
4. Will the service-exposed material be more susceptible to reheat cracking during post weld heat treatment (PWHT), after welding?

1.3 REFERENCES

1. "Welding Metallurgy", Welding Handbook, 7th Edition. Vol. 1, Chapter 4, American Welding Society, 1982.
2. Luther, G.G., Jackson, C.E. and Hartbouer, C.E., "A Review of Weldability Test of Carbon and Low Alloy Steels". Welding Journal, Research Supplement, October 1949, pp. 376s-396s.
3. Coe, F.R., "The avoidance of Hydrogen Cracking in Welding", The Welding Institute, 1973.
4. BonisZewski, T., ISI Conference on "Heat Treatment Aspects of Metaljoining Processes", London, 1971, pp. 29-41.
5. McPherson, R., "Compositional effects on Reheat Cracking of Low Alloy Ferritic Steels", Metals Forum, Vol.2(3), 1980, pp. 175-186.
6. Wegmuller, C.R., "Chrome-Moly Steel Builds Big Vessels", Welding Design and Fabrication, July 1983, pp. 47-52.
7. Lundin, C.D. and Khan, K.K., "Fundamental Studies of the Metallurgical Causes and Mitigation of Reheat Cracking in 1¼Cr-½Mo and 2¼Cr-1Mo Steels", WRC Bulletin 409, February 1996.

8. Parker, J.D. and Parsons, A.W.J., "High Temperature Deformation and Fracture Processes in 2¼Cr1Mo-½Cr½Mo¼V Weldments", Int. J. Pres. & Piping 63, pp. 45-54, 1995

CHAPTER 2: LITERATURE SURVEY

2.1 THE HEAT AFFECTED ZONE (HAZ): TRANSFORMATION AND BEHAVIOR

When materials are joined by fusion welding processes, parts of the material have to be heated up to its melting point (T_m). This severe thermal cycle causes transformation of the original microstructure and changes in the properties of the material, in a region close to the weld. This volume of metal, or zone, is usually referred to as the heat affected zone (HAZ).

The metallurgical transformations that occur during welding affect the final microstructure and therefore may influence many of the problems that can develop during and after welding. The coarse grained heat affected zone (CGHAZ) is the location of maximum susceptibility for reheat cracking. It is also the primary region for reduced toughness.

Results from Ito and Nakanishi[1] indicates that in 1Cr-½Mo alloys a HAZ consisting of martensite or lower bainite was more susceptible to reheat cracking than upper bainite. Thus, the HAZ transformation characteristics play a vital role in the weldability of a material. The transformation behaviour may in turn provide the key to reducing or eliminating weld HAZ problems.

Easterling[2] has compared regions in the microstructure in a weld with the iron-carbon (Fe-C) equilibrium phase diagram (Figure 2.1). Accordingly the HAZ can be divided into sub-zones. Each sub-zone has its own distinct microstructure, as well as mechanical properties. A few problems arise with this simple type of representation. The weld thermal cycle differs significantly from conditions used to obtain the phase diagram, especially heating (1600°C/s) and cooling rates (260°C/s). Also, during welding, complete homogenisation never exists. Non-equilibrium constituents such as martensite and bainite are also not taken into consideration.

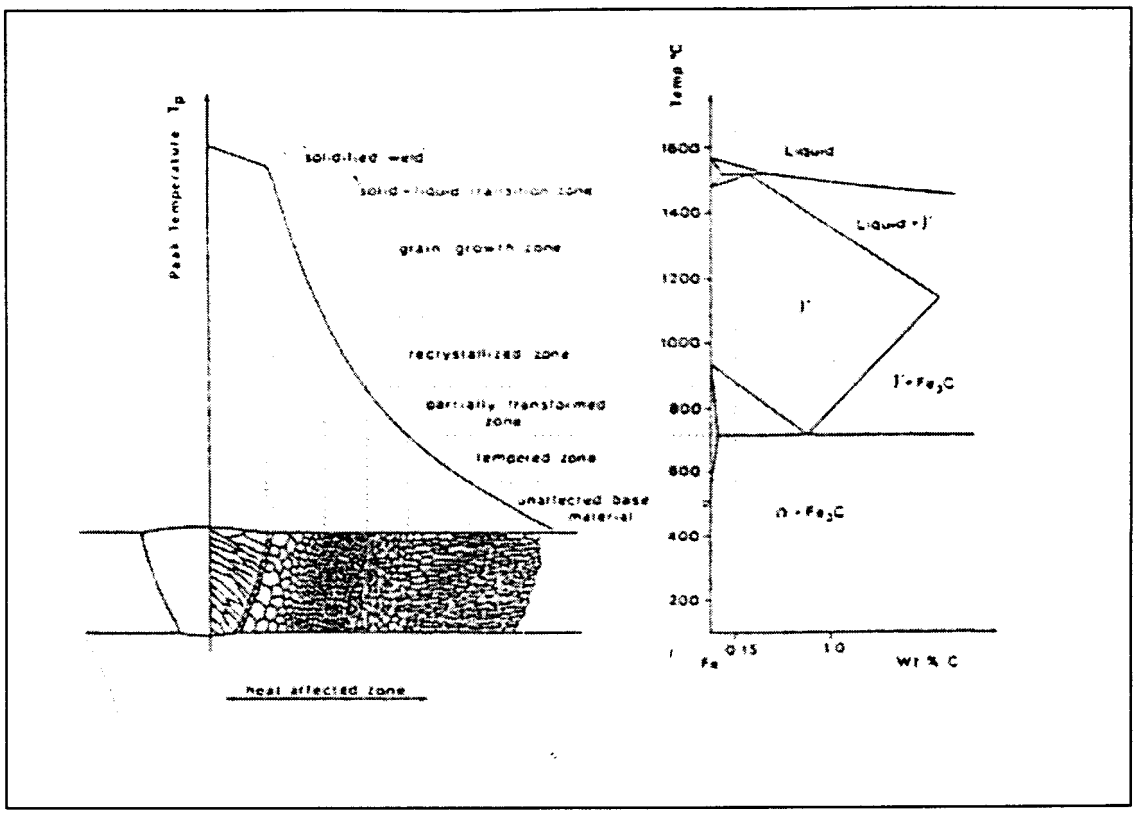

Figure 2.1: A schematic diagram of the various sub-zones of the heat affected zone approximately corresponding to the alloy C_0 (0.15 wt % C) [2].

The same objections to the use of the equilibrium phase diagram, to predict weld HAZ transformations, also extend to the use of standard continuous cooling transformation (CCT) diagrams. The starting base when developing these diagrams is homogeneous austenite. In welding, there is very little to no homogeneity, due to the inability of alloying elements to diffuse uniformly throughout the austenitic phase and the incomplete solution of carbides, nitrides and other constituents. This is due to the rapid heating and cooling rates of the weld thermal cycle and the concomitant short austenitizing times. In order to accurately predict the on-cooling transformation temperatures and microstructures, weld HAZ CCT diagrams must be derived using the heating and cooling conditions relevant for welding. Very few of these CCT diagrams have been developed under welding conditions. Conventional CCT's are however available for most of the commercial grades of Cr-Mo and Cr-Mo-V steels.

When these conventional CCT's are studied it becomes apparent that the resulting microstructure under various welding conditions may be complex.

Depending on the degree of homogenisation and the cooling rate (related to the heat input and preheat for a given process and material thickness), the on-cooling microstructures in the weld HAZ might consist of martensite, mixed martensite and bainite or bainite coupled with retained austenite.

The following have been found when 1¼Cr-½Mo and 2¼Cr-1Mo was studied. In regions containing homogeneous or nearly homogeneous austenite (regions heated above 1100°C) the ferrite reaction is suppressed and only a bainitic reaction occurs. The reaction start temperatures are in the vicinity of 540°C, depending on the peak temperature reached and the grain size of the austenite. The regions heated between 955-1100°C contain undissolved carbides. These carbides can act as nucleating sites for the formation of pro-eutectoid ferrite in addition to the bainite reaction products. In the regions of the HAZ heated in the range 790-955°C, austenitization is limited to only those areas immediately surrounding the grain boundaries. This continuous network of austenite may transform to martensite that can have poor impact properties. These trends are found in general in the Cr-Mo and Cr-Mo-V steels and again shows the complexity of the resulting HAZ microstructure after welding these materials.

2.2 RESIDUAL STRESSES IN A WELDMENT

Residual stresses develop during cooling in the weld HAZ and fusion zone due to restrained shrinkage and transformation volume changes as a result of austenite decomposition. On cooling, those areas of the base metal that experienced thermal expansion due to heating must contract or flow plastically. The bulk of the base metal that has experienced no significant heating (and therefore no decrease in strength) prevents or restrains the contraction of the cooling material. Above approximately 650°C, the weld fusion zone and those areas immediately adjacent to the weld accommodate the thermal contraction by plastic deformation without developing any significant stress. This is the due to the fact that the yield strength is low above this temperature. Cooling below 650°C results in significant increases in yield strength with decreasing temperature. Plastic deformation only occurs

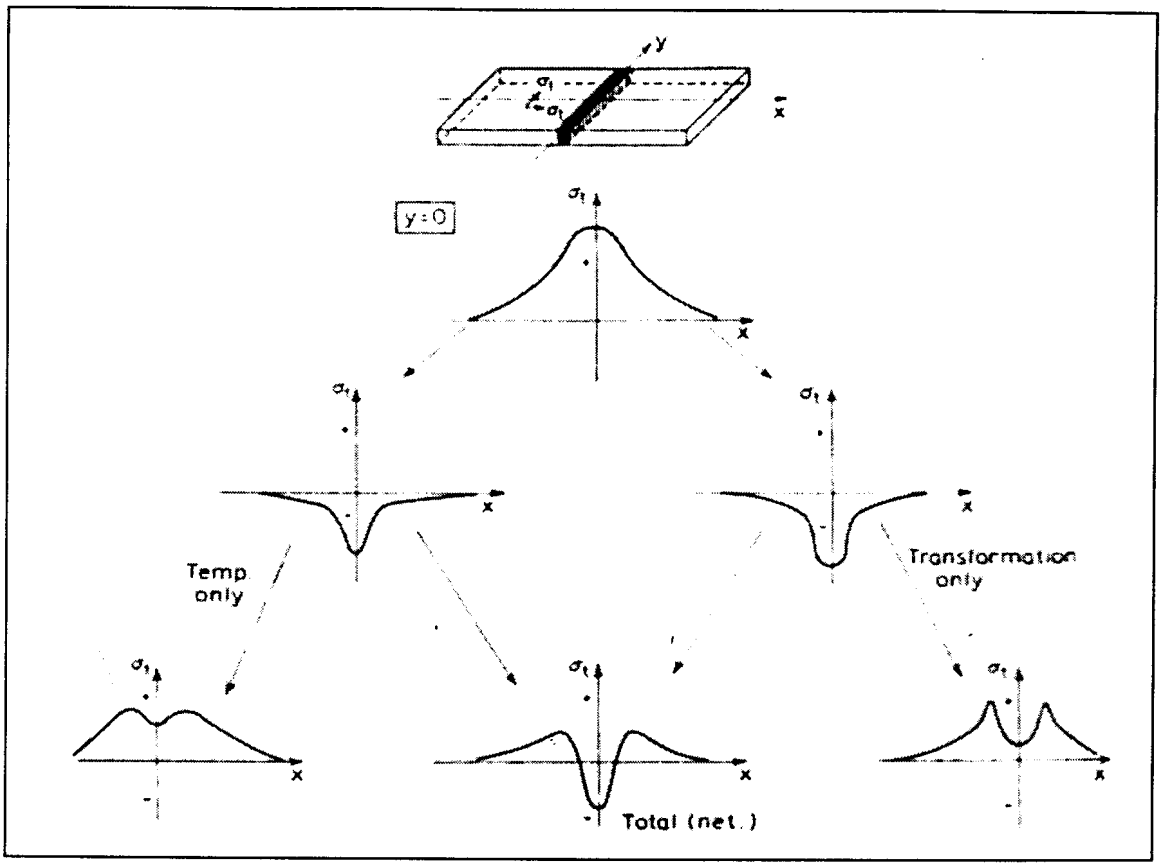

Figure 2.2: Schematic illustration of transverse residual stresses at the weld centre line caused by interaction of shrinkage, quenching and transformation strains[3].

when stresses due to thermal contraction exceed the yield stress. Therefore, cooling to the preheat temperature results in increasing residual tensile stress concomitant with increased yield strength in the fusion zone and HAZ. The resultant residual tensile stresses that occur in the HAZ and fusion zone are in force and moment equilibrium with comprehensive stresses in the bulk of the base material.

Transformational stresses are a result of the volumetric expansion that occurs during decomposition of austenite. The material being transformed attempts to expand but expansion is hindered by the cooler material that is not undergoing transformation. The material being transformed therefore experiences a compressive stress and the cooler material a tensile stress. If the transformation temperature is high, the effects of subsequent bulk shrinkage will override the transformation stresses. However, if the

transformation temperature is low, the transformation stresses will lower the overall tensile stress in the HAZ and fusion zones.

Superposition of the components of the residual stress developed during welding lead to an extremely complex final residual stress state. The CGHAZ, that portion of the HAZ adjacent to the fusion zone, is subjected to a significant tensile stress both in the direction of and perpendicular to the weld. These biaxial residual stress states as well as the unfavourable metallurgical characteristics of the CGHAZ exacerbate the susceptibility of this zone to reheat cracking.

A schematic diagram of transverse residual stresses is shown in Figure 2.2.

2.3 MICROSTRUCTURAL EVOLUTION IN THE HAZ UPON PWHT

A major function of PWHT is to restore ductility in the HAZ and weld metal in Cr-Mo and Cr-Mo-V weldments. In addition, the PWHT also reduces the residual stresses in the weldment by a creep relaxation process.

Detailed recommended practices for welding Cr-Mo and Cr-Mo-V steels are given in ANSI/AWS D10.8-86[4]. In this code the various PWHT temperatures and holding times for different grades of Cr-Mo steels are specified.

During austenitization in a weld thermal cycle, all or part of the carbides are taken up into solution, depending on the peak temperature experienced, the material thickness and energy input. During the subsequent cooling the matrix transforms to bainite/martensite/ferrite. The end product still remains supersaturated with respect to carbon as well as alloying elements that subsequently precipitate as carbides during tempering. The various types of carbides present in Cr-Mo and Cr-Mo-V steels are MC, M_2C, M_3C, M_7C_3 and M_6C. The carbide type, size, distribution and morphology will depend on the chemical composition, microconstituents present at the temperature and time of tempering.

Baker and Nutting[5] have shown that the types of carbides present in 2¼Cr-1Mo base metal are dependant on, starting microstructure, heat treatment (tempering) and time at the tempering temperature. After normalising, the microstructure was found to consist of a mixture of ferrite and bainite whereas after quenching the microstructure was mainly bainitic. They determined that the carbide evolution in the bainitic regions of both quenched and normalised material was similar as shown below:

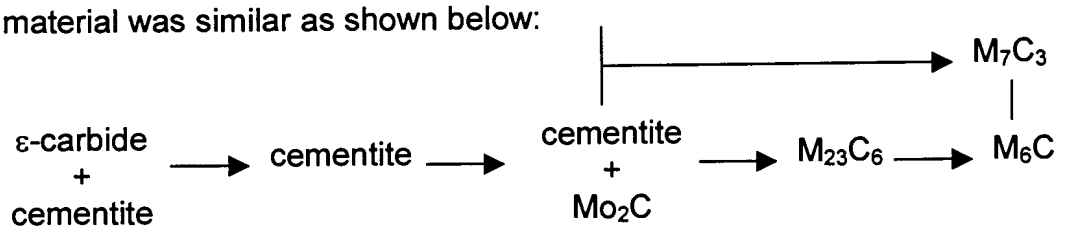

In the ferritic regions the M_2C type carbides do not go through all the transition carbides and transform directly to M_6C carbides. The M_2C carbides were found to be more stable in the ferrite than in the initial microstructures consisting of martensite or bainite. In the martensitic and bainitic microstructures $M_{23}C_6$ grew at the expense of Mo_2C, degrading the creep properties with increasing tempering temperature or time at tempering temperature. This has led some researches to recommend using materials in the normalised and tempered condition rather than in the quenched and tempered condition. The presence of pro-eutectoid ferrite is however generally regarded as unfavourable, due to its poor toughness and low strength. Current alloy development reflects the need to avoid the formation to primary ferrite in the microstructure during cooling by making increased hardenability one of the principal criteria in alloy design.

Modification of Cr-Mo alloys by the addition of vanadium results in the precipitation of finely dispersed, slow growing V_4C_3 upon tempering or post weld heat treatment. The precipitation occurs directly inside the matrix and unlike the precipitation of Mo_2C, is not dependent on the formation of any other carbides. In alloys containing more than 0.1% V, the Mo_2C carbides can have a metal atom ratio of up to 0.3 of Vanadium present. Vanadium in Mo_2C results in the stabilisation of Mo_2C. The combined effects of precipitation and

stabilisation result in vanadium being one of the most potent elements in promoting creep resistance.

One is inclined to believe that the carbide evolutionary sequence in the CGHAZ may be similar to that in the base metal. The situation is however complicated by the fact that some of the more stable carbides such as TiC, NbC and V_4C_3, although finer than the chromium, molybdenum or iron containing carbides, may not dissolve. Lundin *et al.*[6] have found that in the 2¼Cr and 3Cr alloys that contain modifying elements such as vanadium, niobium and titanium, the carbides do not completely dissolve during a coarse grain HAZ simulation thermal cycle. However, in standard alloys, all the carbides dissolve upon CGHAZ simulation. Thus the subsequent precipitation of carbides during PWHT will be affected. The investigation further revealed that in steels modified with vanadium, titanium and boron, the Mo_2C type carbides persist for longer times when compared to other alloys at a PWHT temperature of 675°C. The carbide evolution sequence in the CGHAZ of 1CrMoV steel is shown in Figure 2.3. It can be seen from Figure 2.2 that the carbides present in the CGHAZ on tempering will depend on the PWHT temperature.

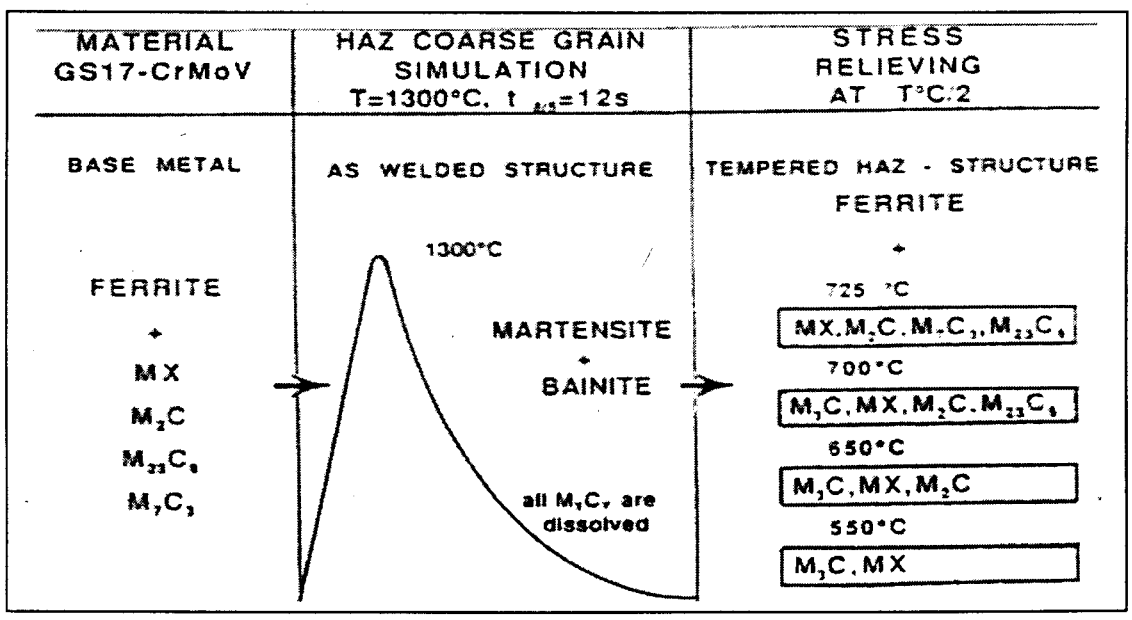

Figure 2.3: Carbides in the CGHAZ of 1CrMoV steel upon PWHT.[7]

2.4 REHEAT CRACKING

Several reasons may exist to reheat the weld metal after welding; to relieve residual stresses in the weld and to obtain the best possible microstructure in the HAZ and the weld metal. The principal problem to be studied here is reheating of the weld in the range 500-650°C in order to obtain stress relieving, and the type of cracking that may result from this treatment. Cracking is manifested by low rupture ductility and intergranular fracture along the prior austenite grain boundaries. An example of reheat cracking in a multi-run butt weld in Cr-Mo-V steel is shown in Figure 2.4.

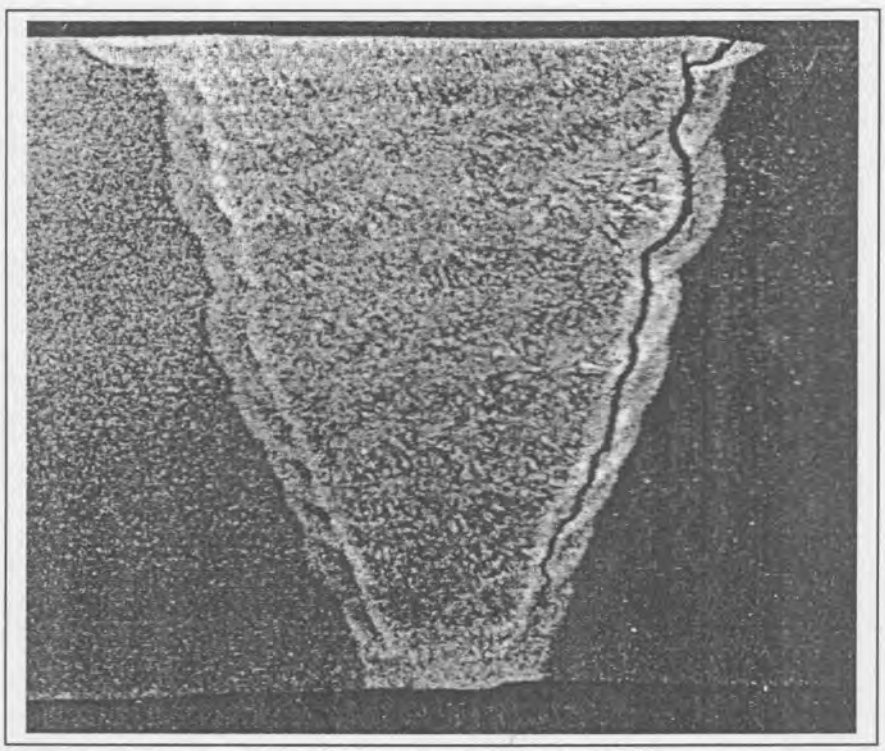

Figure 2.4: Reheat crack in Cr-Mo-V butt weld. After Branah, G.D., High temperature mechanical properties as design parameters.

During the post weld heat treatment (PWHT), the residual stresses are relaxed by localised creep deformation. Any part of the weld, like notches and sharp transitions, which are in a state of high tensile residual stress, will act as strain raisers, when the stresses are relaxing at high temperatures. Cracking and fissuring can then easily nucleate in a susceptible material.

As stated above the reheat cracks form on the prior austenite grain boundaries, in that part of the HAZ that has experienced temperatures well above ~1100°C, and subsequently has undergone plastic deformation. Sometimes the cracks are well developed (optically visible and extending along several grain boundaries), and other cases the damage appears only as a row of small voids on the grain boundaries.

It is now believed that several conditions must be present for reheat cracking:

1. The microstructure must be susceptible – a coarse prior austenite size like the CGHAZ of welds.
2. Residual stresses must be present.
3. Stress concentrators, like notches or discontinuities – weld configuration, slag inclusions, lack of fusion and cracks.

It has been shown that if a material containing a CGHAZ, undergoes a post weld heat treatment, without any plastic strain occurring during this heat treatment, no loss in elevated temperature bend or tensile ductility is shown. Simulated HAZ microstructures do show an increase in impact transition temperature, even without plastic strain. Reheat and stress rupture cracks form because the relaxation strains exceed the creep ductility of the CGHAZ at the applicable temperatures.

A brief overview of some of the theories regarding reheat cracking will now follow:

2.4.1 When the temperature exceeds 1200°C, carbides like chromium, molybdenum and vanadium are taken into solution in the HAZ. Coinciding with this high temperature interval, grain growth occurs in the HAZ. The rapid cooling from these high temperatures and the low transformation temperatures of these steels suppresses the reprecipitation of the carbides. The final microstructure, after welding, is usually martensitic or even lower bainite. During the PWHT and/or the service life the carbide forming elements precipitate out of the supersaturated solid solution as carbides. The manner in which the

precipitation occurs is similar to that encountered during normal tempering. The precipitates form in the grain interior and although initially small in size (a few Angstroms in diameter), cause 'stiffening' of the grain interior. Secondary hardening occurs depending on the temperature. At the grain boundaries there are not precipitates of a sufficient size to prevent grain boundary sliding. It has also been observed that some areas next to the grain boundaries may contain no precipitates (denuded zone)[8]. Plastic deformation imposed on a microstructure in this condition will be restricted by the strong (hard) grain interiors and subsequently most of the deformation will take place along the weaker grain boundaries or denuded zones, causing grain boundary sliding. During the stress relieving, the overall strains may be small, but with a large grain size (like the CGHAZ) there is less grain boundary area, and local high shear and tensile strains develop at the grain boundaries. The resulting significant deformations lead to formation of voids at discontinuities on the grain boundary interfaces and these cavities when linked up, form the final grain boundary cracks.

2.4.2 Trace elements or impurities play a very important role in reheat cracking. It has been shown that high purity heats of the same bulk chemistry do not show a ductility loss in simulated CGHAZ microstructures. However various interactions exist among the alloying elements and the trace elements can affect ductility. This is most likely due to the segregation of trace impurities to the grain boundaries at high temperatures and this can cause embrittlement. Several researchers have found that segregation of residual elements (sulphur, phosphorus, tin and antimony) cause severe problems by embrittling the grain boundaries.[9,10,11] In work done by Hippsley *et al.*[12] it was noted that the segregation of impurities at the grain boundaries can be due to equilibrium segregation from the grain matrix or solute rejection from grain boundary carbides. It has been stated that although the segregation of trace elements at elevated temperature plays a major role in the loss of ductility, the closest to the true mechanism is most

likely a combination of the two ideas – precipitation strengthening and segregation.[9,10]

The necessary factors for reheat cracking was summarised by Ito and Nakanishi: [1]

1. The material must have undergone a thermal cycle that results in solution of alloying elements and retains the elements in solid solution after cooling.
2. Grain growth must have occurred as a result of thermal cycling.
3. Heat treatment within the temperature range 450-700°C, resulting in significant precipitation strengthening.
4. Grain strength and internal stress must exceed the strength of the grain boundaries.
5. A stress riser must be present to initiate cracking.

The complexity of reheat cracking is illustrated in Figure 2.5.

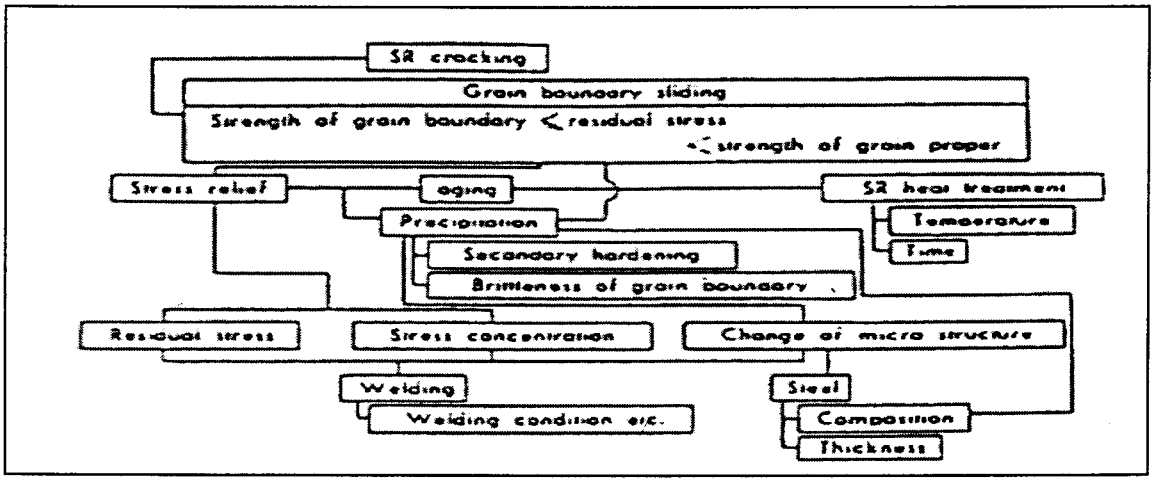

Figure 2.5: Block diagram showing factors involved in stress relief cracking [1].

2.5 MICROSTRUCTURAL EFFECTS

Researchers have shown that a martensitic or lower bainitic microstructure is more susceptible to reheat cracking than upper bainite. However, they state that this difference is related to the precipitation processes, rather than the optically resolved microstructure. The martensitic and lower bainitic structures

are supersaturated with alloying elements and carbon. During the PWHT this leads to severe secondary hardening (precipitation of carbides).[1,13]

2.6 COMPOSITIONAL EFFECTS (ALLOY CHEMISTRY)

The composition of these high temperature application steels plays a vital role with regard to the susceptibility to reheat cracking. For the high temperature application steels these alloying elements are usually chromium, molybdenum and vanadium. They increase the tensile and creep strength due to carbides or carbonitride precipitates in the ferrite matrix. Unfortunately according to many researchers these elements also greatly enhance the susceptibility to reheat cracking. To restrict these elements to very low alloy additions is not practical because their presence is important for the hardenability, strength and creep resistance of these steels.

The following elements were found to be detrimental to cracking: carbon, vanadium, molybdenum (individually and in concert with vanadium), niobium, aluminium, and copper. With regards to residual elements: phosphorus, sulphur, tin, antimony and arsenic. Chromium, boron and titanium's effects are not as clearly defined. Nickel was found to have no effect on cracking. To simplify, the elements that form or promote the M_2C or M_4C_3 type carbides, or enhance grain boundary embrittling are deleterious.

Over the years many researchers have attempted to quantify the effect of the alloying elements in different alloys on susceptibility to reheat cracking. Nakamura *el al.*[14] made such an attempt to determine the effect of the alloying elements in Cr-Mo steels. Their work resulted in the ΔG parameter relationship.

$$\Delta G = Cr + 3.3Mo + 8.1V - 2 \qquad (6\text{-}1)$$

If $\Delta G > 0$, then the material is considered susceptible to reheat cracking.

Ito and Nakanishi[1] extended Nakamura's work, by including additional alloying elements like nickel, copper, niobium and titanium. Their work resulted in cracking parameter P_{SR} :

$$P_{SR} = Cr + Cu + 2Mo + 10V + 7Nb + 5Ti - 2 \quad (6\text{-}2)$$

If $P_{SR} > 0$, the material is considered susceptible to reheat cracking. However, the P_{SR} parameter is only applicable to alloys containing less than 1.5%Cr, 2%Mo, 1%Cu and 0.15%V, Ti and Nb. They also claimed that a chromium content larger than 2% eliminated cracking. The amounts of Ni and Cu added seemed to have no effect on susceptibility and do not appear in the parameter.

However, many researchers have found a poor correlation between these parameters and actual susceptibility to reheat cracking, of different alloys.[15,16] It has also been found by researchers that 2¼Cr-1Mo alloys are susceptible to reheat cracking although Ito and Nankanishi[1] claimed that a chromium content of 2% or greater eliminated cracking.

McMahon *et al.*[16] suggested another parameter:

$$CERL + Cr = Cr + 0.2Cu + 0.44S + P + 1.8As + 1.9Sn + 2.7Sb \quad (6\text{-}3)$$

It is quite clear that trace elements and not carbide formers are the detrimental elements in this parameter; trace elements causing embrittling of the grain boundaries. The greater the CERL + Cr value, the higher the susceptibility to reheat cracking.

Boniszewski[17] suggested the use of a metal composition factor (MCF) :

$$MCF = Si + 2Cu + 2P + 10As + 15Sn + 20Sb \quad (6\text{-}4)$$

The MCF also focuses on the grain boundary embrittling elements. An increase in the MCF correlates with a decrease in rupture ductility as measured by elongation in hot tensile tests.

ΔG_1 was also reconstructed to take into account the effect of carbon where:

$$\Delta G_1 = Cr + 3.3Mo + 8.1V + 10C - 2 \quad (6\text{-}5)$$

If $\Delta G_1 > 2$, the material is considered susceptible to reheat cracking.

Considering the effects for trace elements alone, the R-value was developed for 0.5CrMoV steels:

$$R = P + 2.43As + 3.57Sn + 8.16Sb \quad (6\text{-}6)$$

Susceptibility to reheat cracking increases with an increase in R-value.

Bruscato[18] devised an embrittling factor relating to weight percent of impurity elements (in ppm.):

$$X = \frac{10\ P + 5\ Sb + 4\ Sn + As}{100} \quad (6\text{-}7)$$

Susceptibility increases with X values.

In the subsequent section the effect of some alloying elements individually and in combination with other elements are reviewed.

2.6.1 Effect of Chromium and Molybdenum (Cr & Mo):

As seen by its appearance in the ΔG and P_{SR} parameters, chromium increases the susceptibility of a material to reheat cracking. However, according to Ito and Nakamura a chromium content of larger than 2% should eliminate reheat cracking. The published literature does not agree with this as reheat cracking has been found in material with up to 3% chromium. This could be due to the effect of other elements such as molybdenum, vanadium, titanium and niobium in the steels. Some results show that chromium between 0 and 2% decreases the high temperature ductility and values above 2% increases it markedly.

Molybdenum also appears in the ΔG and P_{SR} parameters and it is clear from these parameters that it has a greater effect on susceptibility to reheat cracking than chromium. During the PWHT (tempering), in the early stages, coherent Mo_2C type carbides precipitate first and the grain interiors become harder (stronger). In the presence of other carbide formers like vanadium, niobium, and titanium, that have a greater affinity for carbon, there is a tendency to form more stable carbides. Even in such circumstances,

molybdenum leads to a large amount of solid solution hardening. Mo_2C is also the carbide that gives great resistance to creep deformation.

Tamaki[19-24] attempted to determine the separate and combined effects of chromium and molybdenum on reheat cracking. A modified implant test was used during these studies. The test was employed to determine the minimum stress that would cause fracture within a 20hr period, while post weld heat treating the sample at 600°C. Cracking susceptibility was related to the magnitude of the critical stress for rupture ($\sigma_{Aw\text{-}crit}$). The lower the stress the higher the susceptibility. The results from these studies are shown in Figure 2.6.

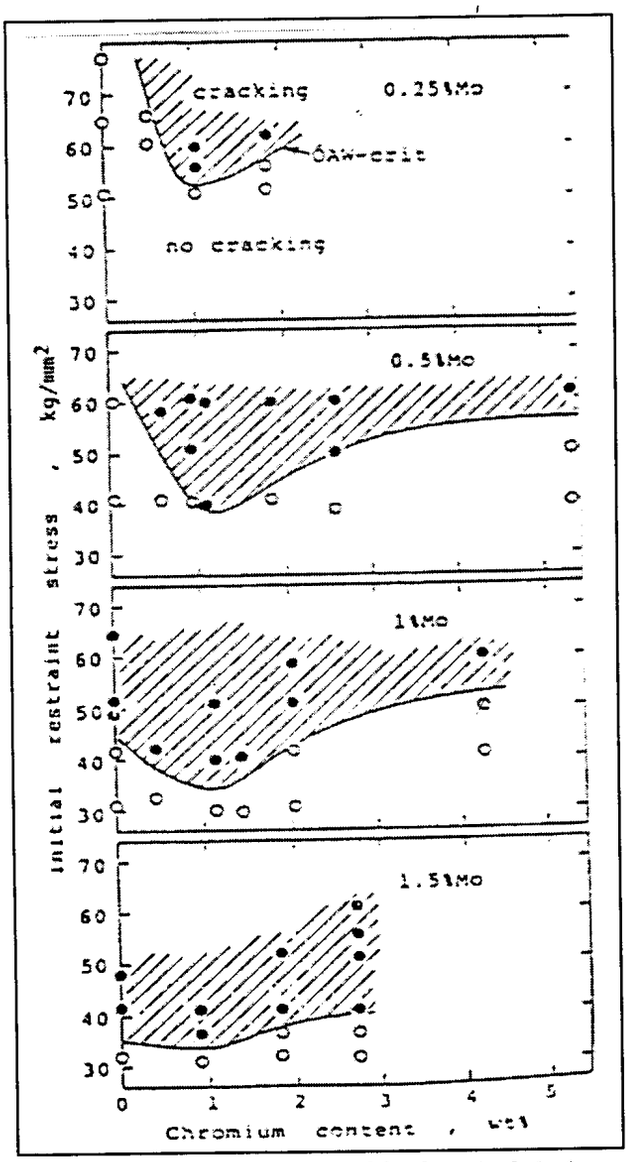

Figure 2.6: Effect of chromium on the critical restraint stress, $\sigma_{Aw\text{-}crit}$ [19].

Figure 2.7 shows the influence of the chromium and molybdenum content, for different stress levels. Susceptibility to reheat cracking with changing alloying content is greatest in these diagrams where the stress contours are closest together.

The plotted data can be divided into four regions:

- I : Alloy < 1% Cr and < 0.5% Mo. Relatively insensitive to cracking.
- IIa : Alloy 0-1% Cr and 0.5-1% Mo. Sensitivity increases with increasing chromium and molybdenum content.
- IIb : Alloy > 2% Cr and 0.5-1% Mo. Sensitivity decreases with increasing chromium content.
- III : Alloy ± 1% Cr and > 1% Mo. Highest sensitivity to cracking.

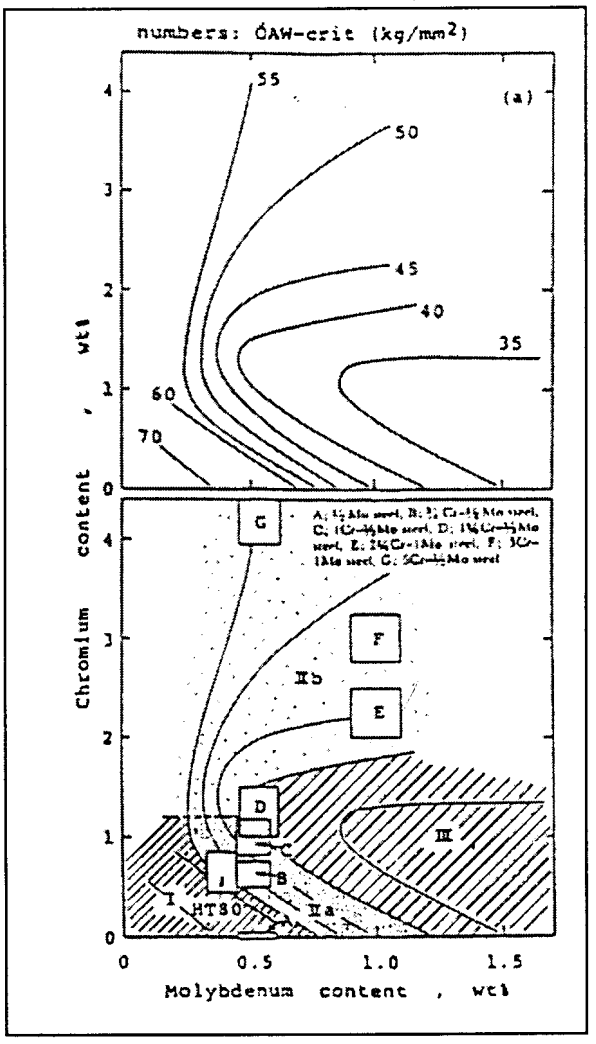

Figure 2.7: Contour lines of critical restraint stress ($\sigma_{AW\text{-}crit}$) shown on the Cr-Mo content diagram [19].

A study on the carbides in the alloy system was also undertaken in order to better understand the microstructural causes for differences in reheat cracking susceptibility.[20] The results showed that materials with the highest fraction of M_2C type carbides, had the greatest tendency to crack. With a smaller amount of M_2C (or larger amount of M_7C_3 or $M_{23}C_6$), the susceptibility to reheat cracking decreased. Figure 2.8 (a) and (b) depict these results graphically.

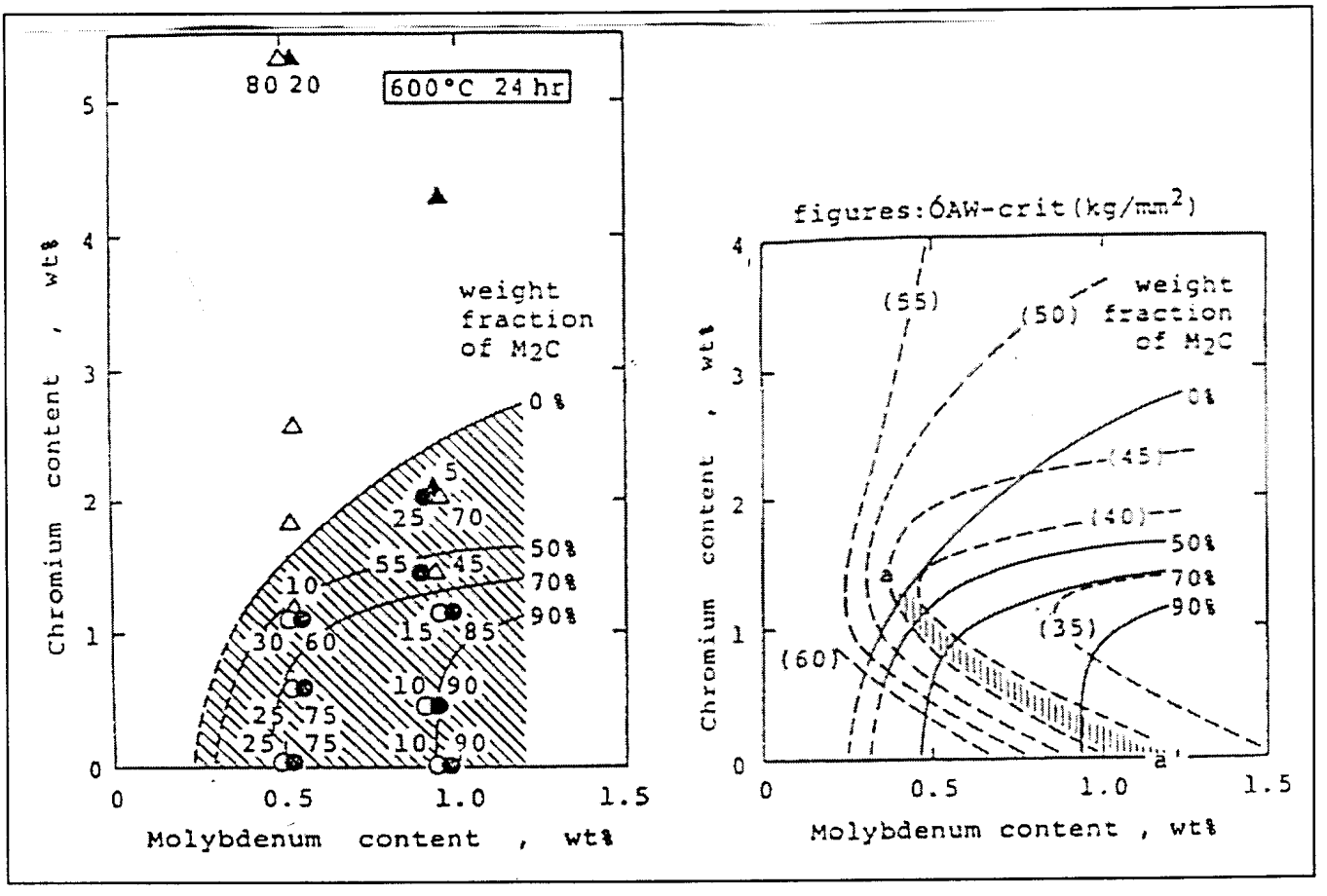

Figure 2.8: (a) Carbides present in Cr-Mo steels tempered at 600°C for 24 h. ○M_3C, ●MC_2, △M_7C_3, ▲$M_{23}C_6$. (b) Weight fraction of M_2C shown on the $\sigma_{AW\text{-}crit}$ diagram [23].

Tamaki also undertook a study on secondary hardening and high temperature hardness, because M_2C and M_7C_3 strengthen the matrix by means of precipitation. The samples were held at temperature for one hour both at the holding temperature and at room temperature after cooling. At room temperature the samples showed an increase in hardness, while at elevated temperature the precipitation of the carbides resulted only in a delay in softening (softening continues to occur but at a lower rate than that which

occurs at lower temperatures). The results of these tests are shown in Figure 2.9.

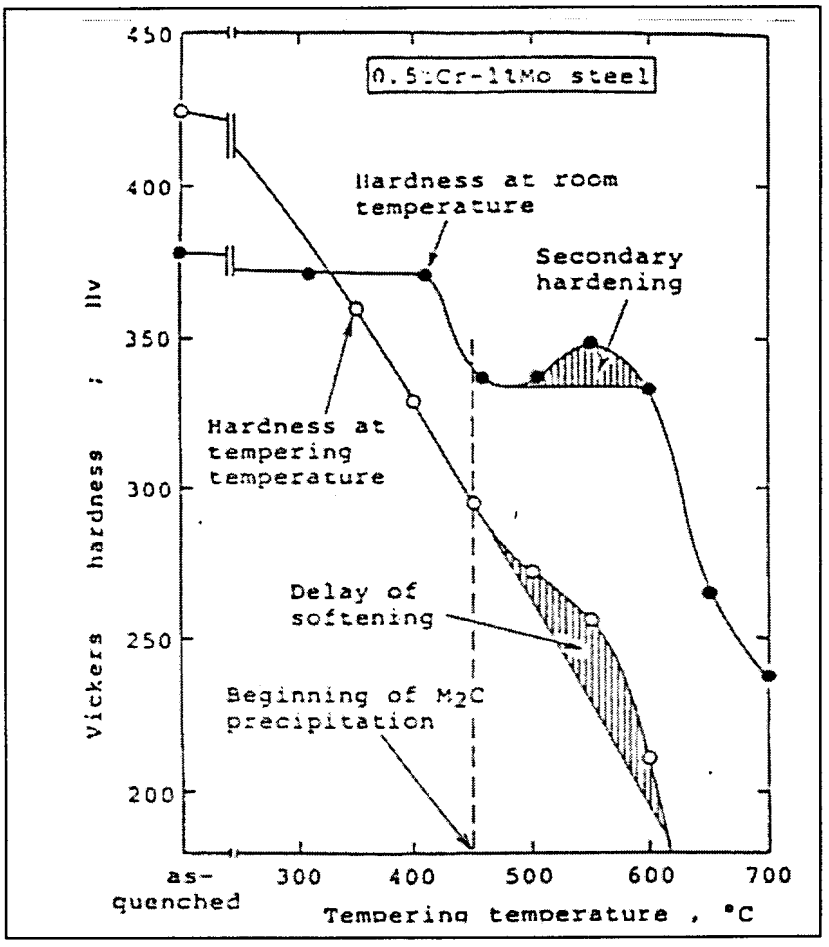

Figure 2.9: Hot hardness and hardness at room temperature versus tempering temperature [23].

When the principal precipitate in the structure was M_2C, the delay in softening occurred at a higher temperature than when the largest fraction of precipitates was M_7C_3. Tamaki postulated that the grain boundary embrittlement would be of a similar nature in either type of alloy and therefore embrittlement of the grain boundaries would initiate at the same temperature and proceed in similar fashion for both types of alloys. This is shown schematically in Figure 2.10. According to this postulation a delay in softening of the matrix which occurs at higher temperatures (large fractions of M_2C carbide), the embrittling of the grain boundaries may cause the intercrystalline flow stress to be less than the intracrystalline flow stress and consequently intercrystalline fracture can occur. If a delay in softening occurs at lower temperatures (large fraction of M_7C_3 carbide precipitates), then the intracrystalline flow stress remains

lower than the intercrystalline flow stress over the whole temperature range and intercrystalline fracture does not occur (Figure 2.10 (b)).

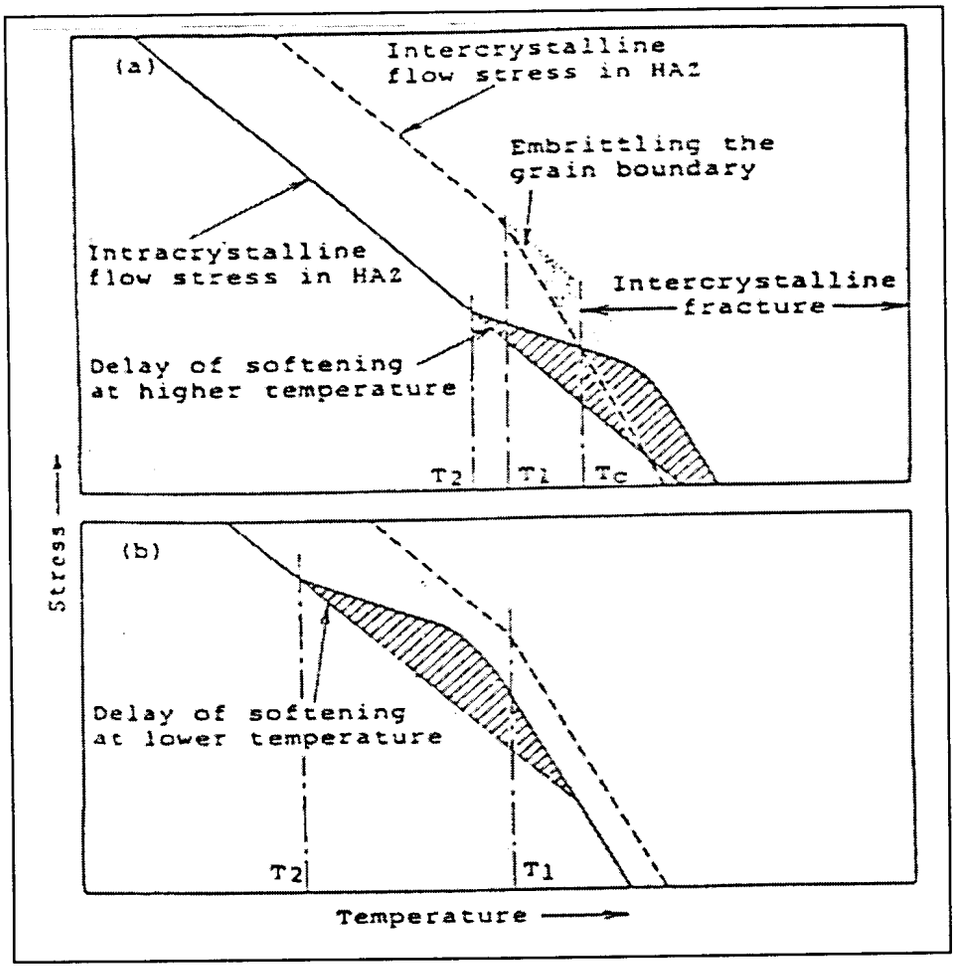

Figure 2.10: Schematic representation of Tamaki's mechanism of reheat cracking [23].

2.6.2 The effect of Vanadium (V):

Vanadium is added to Cr-Mo steels, because vanadium additions dramatically increase elevated temperature strength. This is accomplished by the fine precipitates of V_4C_3 throughout the matrix. When considering the ΔG and P_{SR} parameters vanadium unfortunately increases the susceptibility to reheat cracking drastically (multipliers for vanadium are the greatest).

The fine V_4C_3 precipitates throughout the matrix cause matrix strengthening. This in turn leads to the accumulation of strain in the 'weaker' grain boundaries[25]. It has been reported that early in the heat treatment cycle, intense V_4C_3 precipitation takes place at the ferrite-bainite interfaces due to

segregation effects. At temperatures of 500-550°C, coherent precipitation occurs in the ferrite lattice similar to Mo_2C precipitation. This leads to the maximum hardness and strength.

A few researchers studied the vanadium-to-carbon ratio. Jones[26] studied welds in 1Cr-½Mo-½V materials and found that a vanadium-to-carbon ratio of 3.5-4.5 showed a high susceptibility to cracking. Stone and Murray[27] noted that vanadium-to-carbon ratios of 3-4 induced a minimum in creep ductility. When the ratio was reduced to 1.5 it increased ductility. Thus, a vanadium-to-carbon ratio of 1.5-2 was recommended to mitigate reheat cracking.

Results obtained by Tamaki[24] are shown in Figure 2.11. It is apparent that even small additions of vanadium reduce the critical restraint stress, where the maximum effect is found in low chromium, low to high molybdenum alloys.

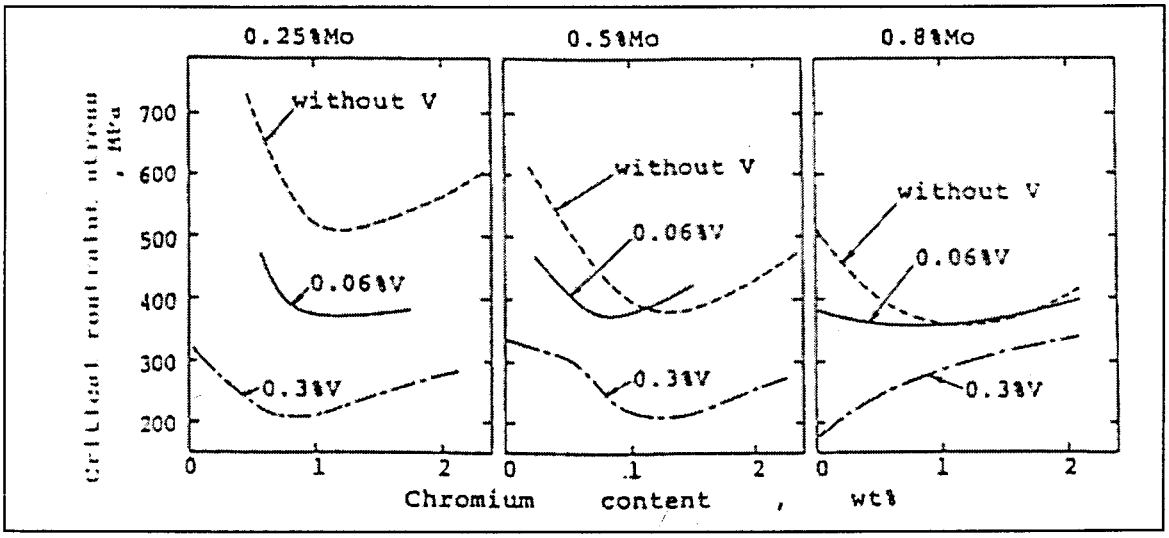

Figure 2.11: Effect of vanadium additions on the critical restraint stress, $\sigma_{AW\text{-}crit}$ of Cr-Mo steels [24].

The increase in cracking susceptibility was said to be related to a decrease in the rate of stress relaxation in a similar fashion to that experienced in the Cr-Mo alloys mentioned in the previous section. It has been suggested that the decrease in the rate of stress relaxation due to a vanadium addition is brought about by the precipitation of V_4C_3 in addition to Mo_2C.

2.6.3 The effect of carbon (C):

Carbon obviously plays an important role in elevated temperature steels, since carbide precipitation is involved in elevated temperature phenomena. In the beginning the researchers overlooked the effect of carbon on reheat cracking susceptibility, since it does not appear in the ΔG or P_{SR} parameters. Some years later, carbon was included in the ΔG_i parameter and the multiplier for carbon in that parameter is quite large. Ito and Nakanichi[1] also studied the effect of carbon in alloys with two vanadium levels. They found that cracking increased as carbon was increased from 0.05-0.10%, but was not changed by a further increase to 0.25%. Other work showed that an increase in carbon content also resulted in larger amounts of segregation of phosphorus at the grain boundaries.[28,29]

2.6.4 The effect of Nickel (Ni):

Nickel does not appear in the ΔG or P_{SR} parameters and appears to have no effect on cracking susceptibility. This was due to the small additions of Nickel. In subsequent research work nickel contents above 1.5% increased the cracking susceptibilty.[21]

2.6.5 The effect of Manganese and Silicon (Mn & Si):

A high manganese to silicon ratio was found to decrease susceptibility to reheat cracking in 2¼Cr-1Mo SA welds.[30] An increase in manganese also showed lower susceptibility in CrMoV steels.[25] Other researchers state that manganese cosegregates with phosphorus to prior austenite grain boundaries and can act as a potent embrittling element.[31,32]

According to Ratliff and Brown[33] an increase in silicon appears to enhance the rate of cementite dissolution and thereby promotes the precipitation of chromium, molybdenum and vanadium carbides. This results in increased

secondary hardening. It appears that silicon accelerates the precipitation of the Mo_2C carbide the most.

2.6.6 The effect of Titanium (Ti):

Harris stated that while small amounts of titanium might appear beneficial (as deoxidiser or grain refiner), large amounts as deliberate alloying additions can increase cracking susceptibility due to matrix strengthening.[34]

2.6.7 The effect of trace elements -- Phosphorus (P), Sulphur (S):

Phosphorus is the most potent, among the residual elements, in embrittling the grain boundaries and thereby increases the susceptibility of the alloy to reheat cracking. By adding the alloying elements chromium and molybdenum, it was found that the solubility of phosphorus in both ferrite and austenite decreased markedly.[30] Segregation of phosphorus to the grain boundaries is thus enhanced by chromium and molybdenum. Phosphide precipitation may even occur at the grain boundaries.

When molybdenum is in solid solution, it ties up phosphorus in Mo-P clusters, thus preventing phosphorus segregation to the grain boundaries. Subsequently, during PWHT, Mo_2C carbides are formed and the phosphorus is released and segregation can take place. It has been suggested that the change in phosphorus concentration in ferrite is closely related to the formation of M_2C carbides.

Wilkenson *et al.*[35] have suggested that phosphorus, when segregated to prior austenite grain boundaries, enhances nucleation of cavities.

Several notable results were obtained by Tamaki in his study of the effect of phosphorus in Cr-Mo steels :[20,22,29,36]

1. Plots were made for alloys low in phosphorus (0.010-0.013%) and high in phosphorus (0.016-0.020%). It showed that increased phosphorus levels moved the critical stress curves to lower molybdenum contents.

2. Phosphorus had already segregated to some extent in the HAZ during the weld thermal cycle. This has to do with the ferrite to austenite phase transformation. The welding cycle thus initiates the segregation and embrittling process.
3. For a particular alloy, there exists a critical phosphorus level below which embrittlement is not apparent. The minimum critical value of phosphorus of 0.008% coincides with the 1Cr-½Mo composition.
4. For the range of alloys tested (0-2%Cr, 0.5%Mo), as long as the phosphorus content was below a critical value for a particular alloy, the critical stress level remained approximately the same.

Auger analysis has shown that sulphur also segregates to the fracture surfaces. Sulphur segregation is associated with dislocation tangles along the boundaries generated by impurity penetration. A grain boundary in this state will be conducive to sliding and will inhibit migration. Cavity nucleation at suitable particles may become possible. Sulphur in the form of grain boundary sulphides has also been linked to the initiation of cavitation on the grain boundaries.[37,38]

Stress-induced segregation of sulphur to the grain boundaries, has also been suggested.[39,40] The sulphur segregates to the grain boundaries, by means of grain boundary diffusion, ahead of the crack tip region during stress relief. This in turn would lead to low crack growth energy requirements.

2.7 WAYS TO MITIGATE REHEAT CRACKING

The most obvious way to avoid reheat cracking is to avoid using susceptible materials. This in practice is not always easily conceivable and some changes to the manufacturing/welding process may be beneficial:

- Use of a low-strength weld metal with high-strength base metals to allow deformation to occur in the fusion zone rather than in the HAZ.

- Increasing heat input or preheat temperature. Higher energy inputs and preheating result in slower cooling rates and softer transformation products.
- Multiple-pass welds. This increases the amount of grain refinement due to overlapping of the HAZ's. There is a limit on the amount of grain refinement one wants to achieve as a too fine a grain size will reduce the creep properties of certain components during operation. This is frequently encountered during remnant life estimation where in-service creep damage first appears and accumulates in the fine grained heat affected zone (FGHAZ).
- Temper beads. In essence it is the same as multi-pass welds, where a final run is made over the last weld bead in order to refine the microstructure of the HAZ. It was found to be very beneficial.
- Complete austenitization after welding or normalising has been found to increase the HAZ toughness and prevent cracking.
- Weld dressing to remove any surface discontinuities at the weld toes effectively reduces cracking by eliminating crack initiation sites.
- Peening, to remove some of the residual tensile stresses at the surface of the weld. Other processes to reduce the weld stresses such as backstepping, interstage PWHT and simplifying the design and geometry of the weldments can also be employed.

2.8 REFERENCES

1. Ito, Y. and Nakanishi, M., "Study of Stress Relief Cracking in Welding Low Alloy Steels", The Sumitomo Search, No. 7, May 1972, pp. 27-36.
2. Easterling, K., "Introduction to the Physical Metallurgy of Welding", Butterworths, Boston, 1983
3. Macherauch, E. and Wohlfahrt, H., "Different sources of residual stress as a result of welding", Conference on Residual Stresses in Welded Construction and Their Effects", pp. 267, The Welding Institute, London, November 1977.
4. American Welding Society, Recommended Practices for Welding Cr-Mo Steels, ANSI/AWS D.10.8-86, AWS, Approved November 18, 1995.
5. Baker, R.G. and Nutting, J., "The Tempering of 2¼Cr-1Mo Steel After Quenching and Normalizing", Journal of Iron and Steel Institute, July 1959, pp. 257-267.

6. Lundin, C.D., Henning, J.A., Menon, R. and Khan, K.K., "Transformation, Metallurgical Response and Behaviour of the Weld Fusion Zone in Cr-Mo Steels for Fossil Energy Application", Final Technical Report No. ORNL/sub.81-7685/02&77, September 1987.
7. Buchmayr, B., Cerjak, H. and Fauland, H.P., "The Effect of the Precipitation Behaviour on the HAZ-Properties of 1Cr-Mo-V Steel", 2nd International Conference on Trends in Welding Research, Gatlinburg, Tennessee, May 1989.
8. Boniszewski, T. and Eaton, N.F., " Electron Fractography of Weld Reheat Cracking in CrMoV Steel", Metal Science, Vol. 3, 1969, pp. 103-110.
9. Vinckier, A. and Dhooge, A., "Reheat Cracking in Welded Structures during Stress-Relief Heat Treatments", Journal of Heat Treating, Vol. 1(1), ASM, 1979, pp. 72-80.
10. Dhooge, A., Dolby, R.E., Sebille, J., Steinmetz, R. and Vinckier, A.G., "A Review of Work Related to Reheat Cracking in Nuclear Reactor Pressure Vessel Steels", International Journal of Pressure Vessels and Piping, Vol.6(5), September 1978, pp. 329-409.
11. Presser, R.I., McPherson, R., "The Role of Trace Elements in Reheat Cracking", Conference on Residual Stresses in Welded Construction and Their Effects", pp. 387-398, The Welding Institute, London, November 1977.
12. Hipsley, C.A., King, J.E. and Knott, J.F., "Toughness Variations and Intergranular Fracture during the Tempering of Simulated HAZ Structures in a Mn-Mo-Ni Steel", Proceedings of International Conference on Advances in the Physical Metallurgy and Application of Steels, University of Liverpool, 21-24 September, 1981, Metals Society, London, England, pp. 147-155.
13. Meitzner, C.F. and Pense, A.W., "Stress-Relief Cracking in Low Alloy Steel Weldments', Welding Journal, Research Supplement, Vol.48(10), 1969, pp. 431s-440s.
14. Nakamura, H., Naiki, T. and Okabayaski, H., "Fracture in the Process of Stress-Relaxation Under Constant Strain", 1st International Conference on Fracture, September 1965, Vol2. Sendai, Japan, pp. 863-878.
15. Pense, A.W., Galda, e.J, Powell, G.T., "Stress Relief Cracking in Pressure Vessel Steels", Welding Journal, Research Supplement, August 1971, pp. 374s-378s.
16. McMahon, C.J. Jr., Dobbs, R.J. and Gentner, D.H., "Stress Relief Cracking in MnMoNi and MnMoNiCr Pressure Vessel Steels", Materials Science and Engineering, Vol. 37, 1979, pp. 179-186.
17. Boniszewski, T., "Reheat Cracking in 2¼Cr-1Mo SA Weld Metal", Metal Construction, 14(9), 1982, pp. 495-496.
18. Bruscato, R., "Temper Embrittlement and Creep Embrittlement of 2¼Cr-1Mo Shielded Metal Arc Welding Deposits", Welding Journal, Research Supplement, April 1970, pp. 148s-156s.
19. Tamaki, K., Suzuki, J., "Effect of Chromium and Molybdenum on Reheat Cracking Sensitivity of Steels", Transactions on the Japan Welding Society, Vol. 14(2), October 1983, pp. 39-43.

20. Tamaki, K., Suzuki, J., "Assesment of Reheat Cracking Sensitivity of Steels from their Chemical Composition", Metals/Materials Technical Series, 85 ASM's International Welding Congress, Toronto, Canada, 14-17 October, 1985, pp. 1-8.
21. Tamaki, K., Suzuki, J., "Reheat Cracking Test on High Strength Steels by a Modified Implant Test", Transactions on the Japan Welding Society, Vol. 14(2), October 1983, pp. 33-38.
22. Tamaki, K., Suzuki, J., "Assesment of the Reheat Cracking Sensitivity of Cr-Mo Steels", The 4th International Symposium of the Japan Welding Society, November 1982, Osaka, 4JWS-II-17, pp. 467-472.
23. Tamaki, K., Suzuki, J., Nakaseko, Y. and Tajiri, M., "Effect of Carbides on Reheat Cracking Sensitivity", Transactions of the Japan Welding Society, Vol. 15(1), April, 1984.
24. Tamaki, K., Suzuki, J. and Kojima, M., "Combined Influence of Chromium, Molybdenum and Vanadium on Reheat Carcking of Steels", IIW Document IX-1518-88.
25. Mullery, F. and Cadman, R.O.L., "Cracking of Welded Joints in Ferritic Heat-Resisting Steels", British Welding Journal, April 1962, pp. 212-220.
26. Jones, K.E., "Stress-Relief Cracking of Welded Pipe/Casting Joints in Cr-Mo-V Steels", Paper 5 in Proceedings of Conference on Welding Creep Resistant Steels, The Welding Institute, Cambridge, 17-18 February, 1970, pp. 66-78.
27. Stone, P.G. and Murray. J.D., "Creep Ductility of Cr-Mo-V Steels", Journal of Iron and Steel Institute. Vol. 203, November, 1965, pp. 1094-1107.
28. Ehart, H., Grabke, H.J. and Onel, K., "Grain Boundary Segregation of Phosphorous in Iron Base Alloys: Effects of Carbon, Chromium and Titanium", Proceedings of Conference on Advances in Physical Metallurgy and Application of Steels, London, 21-24 September, 1981, pp. 282-285.
29. Tamaki, K., Suzuki, J., "Effect of Phosphorous on Reheat Cracking in Cr-Mo Steels", Research Reports of the Faculty of Engineering, Mie University, Vol. 9, December 1984, pp. 8-16.
30. Anonymous, "Testing Techniques to Study the Susceptibility to Reheat Cracking of Carbon-Manganese and Low Alloy Steels", Welding in the World, Vol. 12(11/12), 1974.
31. Bodnar, R.L., Ohhashi, T. and Jaffee, R.I., "Effects of Mn, Si and Purity on the design of 3.5 NiCrMoV, 1CrMoV and 2.25Cr-1Mo Bainitic Alloys", Metallurgical Transactions A, Vol. 20A, August 1989, pp. 1445-1460.
32. Weng, Y.Q. and McMahon, C.J. Jr., "Interaction of Phosphorous, Carbon, Manganese and Chromium in Intergranular Embrittlement of Iron", Materials Science and Technology, Vol. 3, March 1987, pp. 2207-216.
33. Ratliff, J.L. and Brown, R.M., "The Deleterious Effect of Small Quantities of Aluminium on the Stress-Rupture Properties of a Cr-Mo-V Steel", Transactions of the American Society of Metals, Vol. 60, 1967, pp. 176-186.
34. Harris, P. and Jones, K.E., "The Effect of Composition and Deoxidation Practice on the Reheat Cracking Tendencies of ½Cr-½Mo-¼V Steel", Proceedings of International

Conference on Welding Research Related to Power Plants", England, 17-21 September, 1972, pp. 369-380.

35. Wilkenson, D.S., Abiko, K., Thyagarajan, N. and Pope, D.P., "Compositional effects on the Creep Ductility of a Low Alloy Steel", Metallurgical Transactions A, Vol. 11A, November 1980, pp. 1827-1836.
36. Tamaki, K., Suzuki, J., "Recent Studies on Reheat Cracking of Cr-Mo Steels", Proceedings of International Conference on Stress Relieving Heat Treatments of Welded Steel Constructions, 6-7 July, 1987, Bulgaria, pp. 325-326.
37. You, C.P., Hippsley, C.A. and Knott, J.F., "Stress Relief Cracking Phenomena in High Strength Structural Steels", Metal Science, Vol. 18, August 1984, pp. 387-394.
38. Dolby, R.E., "Advances in the Welding Metallurgy of Steels", Proceedings of International Conference on Advances in the Physical Metallurgy and Application of Steels, 21-24 September 1981, The Metals Society, London, pp. 111-125.
39. Shin, J. and McMahon, C.J. Jr., "Mechanisms of Stress-Relief Cracking in Ferritic Steel", Acta Metallurgica, Vol. 32(9), 1984, pp. 1535-1552.
40. Hippsley, C.A., "Brittle Intergranular Fracture at Elevated Temperatures in Low Alloy Steels", Materials Science and Technology, June 1985, Vol. 1, pp. 475-479.
41. Lundin, C.D. and Khan, K.K., "Fundamental Studies of the Metallurgical Causes and Mitigation of Reheat Cracking in 1¼Cr-½Mo and 2¼Cr-1Mo Steels", WRC Bulletin 409, February 1996.

CHAPTER 3: EXPERIMENTAL PROCEDURE

To determine a certain steel grade's susceptibility towards reheat cracking a suitable test method must be selected or developed. The specimen should if possible incorporate a welded joint similar to the joint used in the components like headers and main steam pipes. The joint should also be manufactured with the same heat inputs, welding processes, consumables, pre-heating, etc. Furthermore, the thermal treatment during testing should aim to duplicate as closely as possible the prescribed PWHT thermal cycle.

When reviewing the many papers that studied the phenomenon of reheat cracking it becomes quite clear that a multitude of tests exists and has been employed. Comparing the test results is complex and sometimes lead to confusion. In order to simplify the overall number of tests, three categories were proposed to classify the tests[1]:

A. Tests on complete weldments
    1. Lehigh restraint test
    2. Restrained fillet weld test
    3. Y-groove test
    4. Stellite bead test
    5. BWRA ring test
    6. Steampipe butt weld test
    7. H-type restraint test
    8. Circular patch restraint test
    9. Strained root bead test
    10. Restrained butt weld test
    11. MRT test
    12. NRC Regulatory Guide cladding test
B. Tests on specimens containing a weld
    1. Jigged stress relaxation test
    2. Isothermal constant load rupture test
    3. Implant test
    4. Controlled heating rate, constant load test
    5. Vinckier test – Stainless backing bar test

C. Tests on specimens containing a thermally simulated HAZ
    1. Isothermal stress relaxation test
    2. Isothermal constant load rupture test
    3. Isothermal slow strain-rate tensile test
    4. Controlled heating rate stress relaxation test
    5. Controlled heating rate constant load test
    6. Stainless sleeve test
    7. Pre-cracked bend test
    8. Slit tube test
    9. Jigged stress relaxation test

The use of tests on complete weldments has the advantage of being related to actual weld and PWHT conditions. It has been found however that reproducibility is a significant problem. Results show considerable scatter with one sample cracking and another showing no cracking. The complex interactions of residual stress and strain, their distribution and magnitude, relaxation and triaxiality, together with progressively changing microstructures during PWHT are difficult to incorporate in a small weld sample. A small test specimen will also experience a significantly smaller amount of creep strain than a large welded structure.

Weld simulation tests have the advantage of reproducibility, known stress level and control of the microstructure in the test area. It is also possible to accurately locate or place a notch in a well-defined microstructure. The disadvantages are that strains associated with weld contractional stresses are not duplicated and in general only one area of the HAZ is tested and the effects of the adjacent weld metal and base metal are not present.

The existing tests mentioned above all suffer from one or more of the following disadvantages:

1. Difficulty in quantifying susceptibility
2. Poor correlation with field experience
3. Poor reproducibility
4. Lack of one or more of the factors necessary for reheat cracking

5. Requirement of expensive instrumentation or elaborate testing facility
6. Only one region of the HAZ is tested and the effects of weld metal, other HAZ regions and base metal are not accounted for in the test

To overcome the deficiencies of these tests a test method developed by Lundin[1] was used in this program for studying the susceptibility of service-exposed material towards reheat cracking. This test has the capability of simultaneous evaluation of reheat cracking in various regions of the weldment. It also incorporates all the necessary factors for reheat cracking to occur as listed in the literature survey as summarised by Ito and Nakanishi[2].

The test is called the 'Spiral Notch Test'. The use of a notch is important, as many researchers have noted that the effect of a stress raiser is very important in the mechanism of reheat cracking. The sample is exposed to a simulated weld thermal cycle with a peak temperature (T_M) of 1300°C in the centre of the sample. Lower temperature transformation products as well as the unaffected base metal are also incorporated into the test length of the sample. A schematic diagram of such a sample is given in Figure 3.1. It can be seen from the figure that every metallurgically different region of the weld is notched similarly and thus the stress concentration experienced by every region will be virtually identical because the notch extends through the base metal and weld HAZ. The sample is then inserted into a creep frame at a constant load. A protective gas atmosphere protects the sample from excessive oxidation during testing. The gas consisted of 5% Hydrogen (H_2) and the balance Argon (Ar). The region and mode of fracture for a specific stress, during the PWHT thermal cycle can then be determined. A schematic representation of the test procedure is shown in Figure 3.2. It was decided to conduct isochronous rather than isothermal tests. Thus the full effect of the PWHT thermal cycle could be evaluated as well as the specific failure temperature for a given load applied. Due to time constraints it was decided to use a heating rate of 400°C/h for the first hour up to 400°C and afterwards 100°C/h until failure. The peak temperature of the PWHT was set at 750°C.

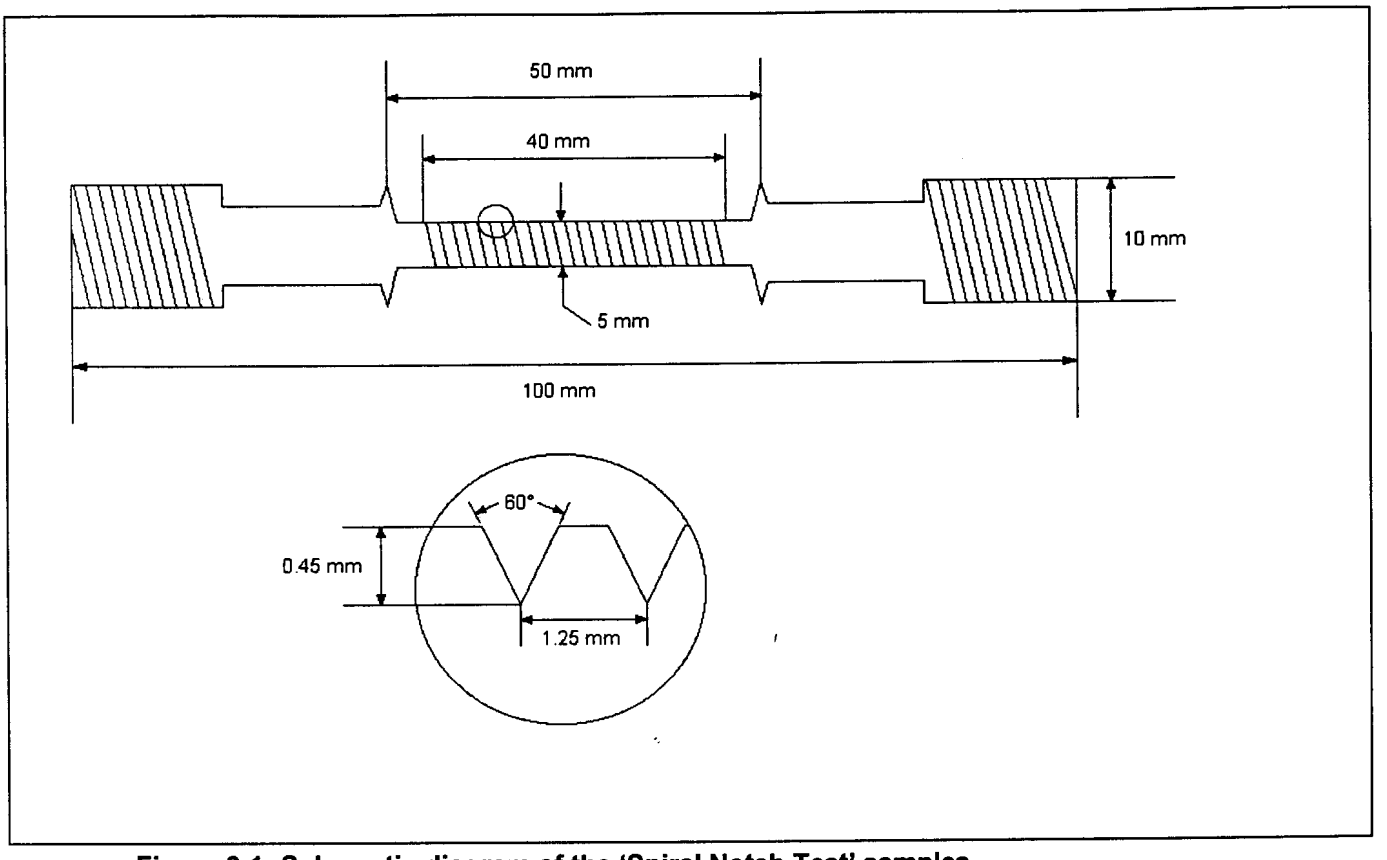

Figure 3.1: Schematic diagram of the 'Spiral Notch Test' samples

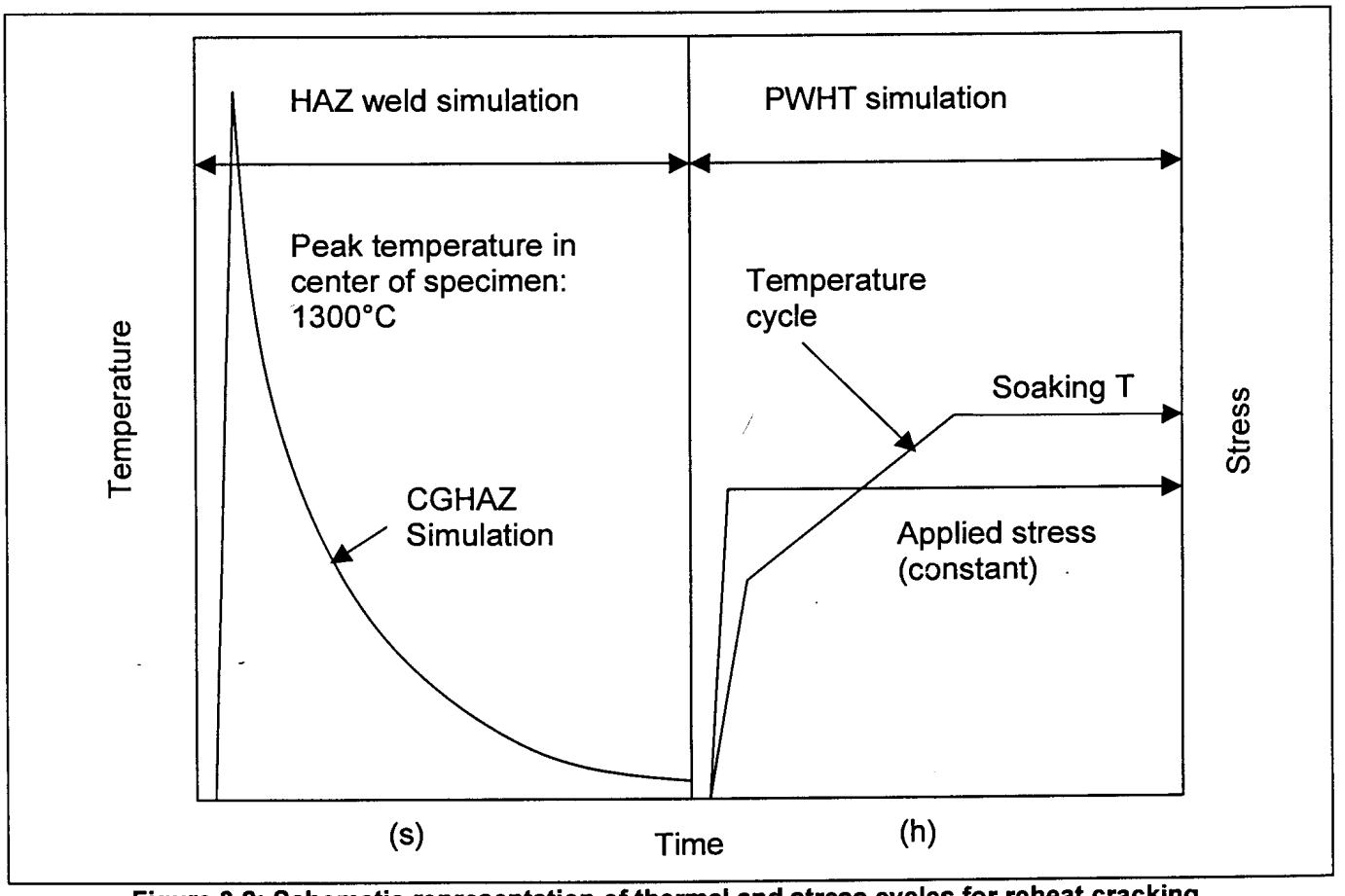

Figure 3.2: Schematic representation of thermal and stress cycles for reheat cracking studies

The materials received were analysed to confirm the grade. Eskom accredited methods 106 (alloying elements) and 119 (carbon) were used. The tests were conducted at Technology Services International (TSI). TSI is company that forms part of the Eskom group.

3.2 CGHAZ SIMULATION

As indicated, the spiral notch test method makes use thermally simulated test samples. A peak temperature of 1300°C was selected as this closely relates the peak temperature during welding for the CGHAZ. The weld simulator heats the sample by means of electrical current flowing through the sample. An S-type thermocouple in conjunction with a REX P-200 controller unit regulates the thermal cycle. Due to the size of the sample and the limitation of the simulator the heating rates of actual welding could not be replicated accurately. Heating rates of around 250°C/s were achievable. To more closely simulate actual welding conditions with a heat input of 1kJ/mm, it was decided to control the cooling down time from 800°C to 500°C ($\Delta t_{8\text{-}5}$). This region is critical for the type of transformation products that will form when welding is performed. When $\Delta t_{8\text{-}5}$ is properly controlled the effect of pre-heating as described in the welding procedure specification (WPS) is taken into account. Thus it is possible to closely simulate actual welding conditions. As an example the conditions during simulation of the X20 material is shown.

$$\Delta t_{8-5} = \frac{q/v}{2\pi\lambda\theta_1} \qquad (3\text{-}1)$$

$$\frac{1}{\theta_1} = \frac{1}{773 - T_0} - \frac{1}{1073 - T_0} \qquad (3\text{-}2)$$

q/v = heat input (kJ/mm)

λ = Thermal conductivity ($Jm^{-1}s^{-1}K^{-1}$)

Equations 3-1[3] and 3-2[3] are used to calculate the amount of time that it will take to cool down from 800°C to 500°C for a certain preheat temperature. For X20 at a preheat or interpass temperature of 300°C (λ = 26 $Jm^{-1}s^{-1}K^{-1}$) a Δt_{8-5} of 18 s was calculated. During actual simulation the recorded time was 16 s. Thus for all four grades of steel tested the simulated HAZ represented the HAZ of welded material with a heat input of 1kJ/mm. The total length of the HAZ was 20 mm.

3.3 SAMPLE MANUFACTURE

The CGHAZ simulated samples were then machined according the dimensions as shown in Figure 3.1.

3.4 ARTIFICIAL AGING OF P91 MATERIAL

Due to the fact that no service-exposed P91 material was available from power plants, it was decided to artificially age some of the available new material.

Blank samples for CGHAZ simulation were placed in a stainless steel tube with some zirconium chips. The tube was welded shut and heated in a furnace at 650°C for around 860h. This corresponds to a service exposure at 550°C of more than 150 000 hours.

3.5 INSTRUMENTS AND MEASUREMENTS DURING TESTING

The creep frame used was a Denison machine, model T.48. It has a capacity of 1000 kg. A REX P-250 controller and three K-type thermocouples controlled the furnace.

The knife-edges visible on the sample were used to attach the elongation rig of the creep frame. Two LVDT's (Linear Variable Differential Transducers) were attached to the elongation rig. The displacement of the LVDT's was

used to measure the elongation of the sample during testing. The type of LVDT used was Schaevitz PCA 116-300.

A K-type thermocouple was spot welded to the sample during testing. Thus the thermal cycle and failure temperature experienced by the sample could be accurately recorded.

The sample temperature and elongation was measured and logged using a computer with a data logging card as well as a Yokagawa HR 1300 Recorder.

3.6 SCANNING ELECTRON MICROSCOPY

One half of a fractured sample was used for metallography and the other for fractography. The fracture surfaces were studied by scanning electron microscopy (SEM), to assess the fracture mechanism. The fracture surfaces are represented in the following sections for each steel grade.

3.7 METALLOGRAPHY

Certain samples were taken to study the microstructure of the four different steel grades, in the new and service exposed condition, as well as in the as-simulated and after testing (PWHT) condition. The samples were sectioned longitudinally so that a full transverse view ranging from the HAZ to base metal was possible. The samples were mounted and ground and polished to a 1μm finish. The ½Cr-½Mo-¼V and 2¼Cr-1Mo grades were etched with 2% Nital. The X20 and P91 grades were etched with Vilella's etchant. The etched samples were then studied using an optical microscope to determine the various microstructures of the different regions in each sample. The different microstructures are represented in the following sections for each steel grade.

3.8 HARDNESS SURVEY

The metallographic samples were used for the hardness survey. Vickers microhardness with a load of 300g was taken. The results for the hardness survey are represented in the following sections for each steel grade.

3.9 REFERENCES

1. Lundin, C.D. and Khan, K.K., "Fundamental Studies of the Metallurgical Causes and Mitigation of Reheat Cracking in 1¼Cr-½Mo and 2¼Cr-1Mo Steels", WRC Bulletin 409, February 1996.
2. Ito, Y. and Nakanishi, M., "Study of Stress Relief Cracking in Welding Low Alloy Steels", The Sumitomo Search, No. 7, May 1972, pp. 27-36.
3. Easterling, K., "Introduction to the Physical Metallurgy of Welding", Butterworths, Boston, 1983.

4.1 INTRODUCTION

One of the most widely used creep resistant low alloy steels is ½Cr-½Mo-¼V. The material is supplied in the tempered condition with a ferritic and pearlitic structure. The presence of vanadium is the primary reason for the creep strength of the material. Some of the more common properties of this grade are listed below[1]. The service-exposed material was obtained from Hendrina power station and operated at 540°C for 150 000 hours.

4.1.1 General Chemical Composition

ELEMENT	min %	max %
C	0.10	0.18
Si	0.10	0.35
Mn	0.40	0.70
P	0	0.035
S	0	0.035
Cr	0.30	0.60
Mo	0.50	0.70
V	0.22	0.32

4.1.2 Mechanical Properties

PROPERTY	VALUE
Yield stress	>= 345 MPa
Tensile Strength	490 – 640 MPa
Elongation	>= 20 %
Impact value (DVM)	>= 41 J
Hardness Brinell	145 – 190 HB_{30}

Mechanical Properties at ambient temperature (Values for longitudinal sample bars <= 60mm ∅

4.2 CHEMICAL ANALYSIS

Eskom accredited methods No 106 (Alloying elements) and 119 (Carbon) were used on the new and service-exposed material. The results are shown in Table 4.1. The original result sheets are attached in Appendix 1.

Element	New Material	Service-exposed Material (± 150 000 h at 540°C)
Carbon	0.14	0.19
Chromium	0.46	0.53
Nickel	0.08	0.16
Manganese	0.51	0.54
Molybdenum	0.51	0.54
Vanadium	0.28	0.31
Sulphur	0.01	0.012
Phosphorus	0.008	0.014
Silicon	0.12	0.24
Titanium	0.01	0.01
Copper	0.09	0.15
Cobalt	0.01	0.02
Niobium	0.005	0.005
Tin	0.01	0.02
Tungsten	0.005	0.005

Table 4.1: Chemical analysis for new and service-exposed ½Cr-½Mo-¼V material

The chemical composition of the test material was within specified range for ½Cr-½Mo-¼V material.

4.3 SPIRAL NOTCH TEST RESULTS (Constant load, PWHT Thermal Cycle)

The results from the spiral notch tests on the new and service-exposed ½Cr-½Mo-¼V are shown in Table 4.2 and Graphs 4.1 and 4.2.

Table 4.2: Position of final fracture for ½Cr-½Mo-¼V steel

Nominal Stress (MPa)	½Cr-½Mo-¼V New Material	½Cr-½Mo-¼V Service-exposed Material
356	CGHAZ	Base Metal
305	CGHAZ	Base Metal
204	CGHAZ	Base Metal
153	-	Base Metal

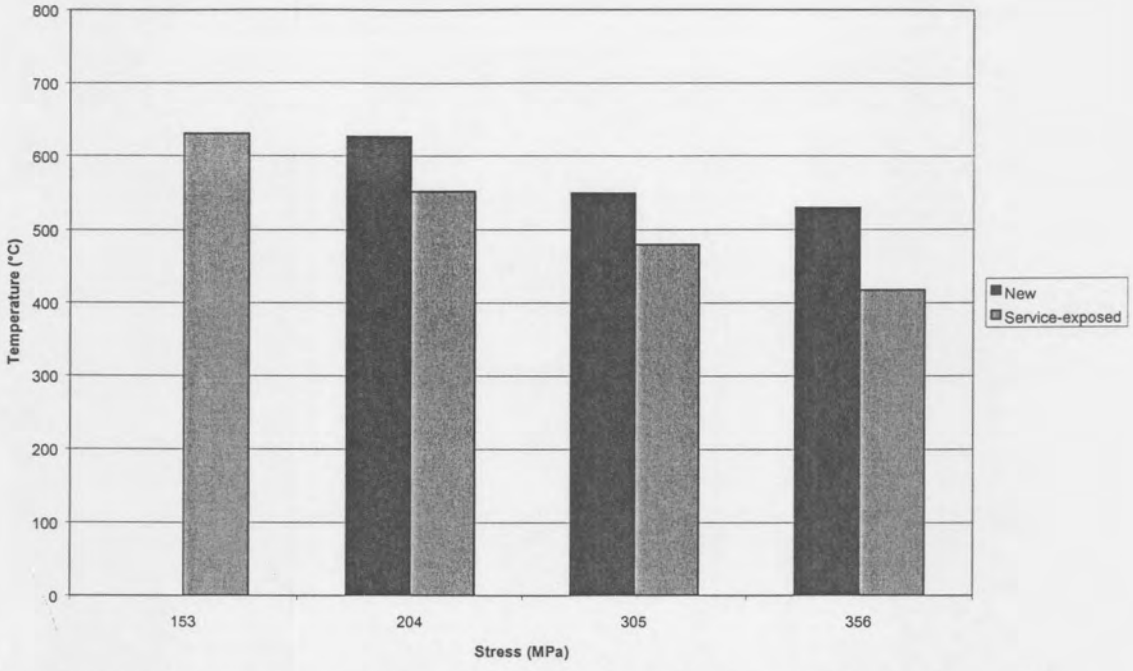

Graph 4.1: Temperature of final fracture for ½Cr-½Mo-¼V steel samples

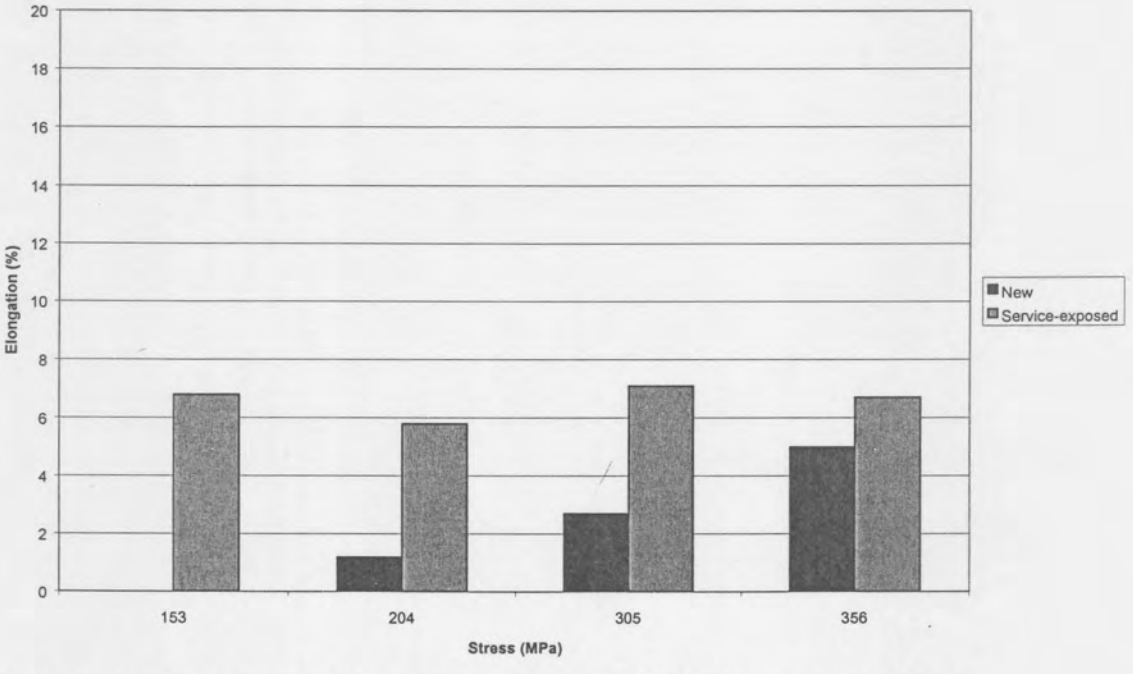

Graph 4.2: Amount of elongation for ½Cr-½Mo-¼V steel samples

The experimental graphs compiled during these tests are attached in Appendix 2.

4.4 SEM FRACTOGRAPHY

The fracture surfaces of the samples tested at 204 MPa for both new and service-exposed material were studied in the SEM to confirm the mechanism of fracture. The fracture surfaces are shown in Figures 4.1 to 4.5.

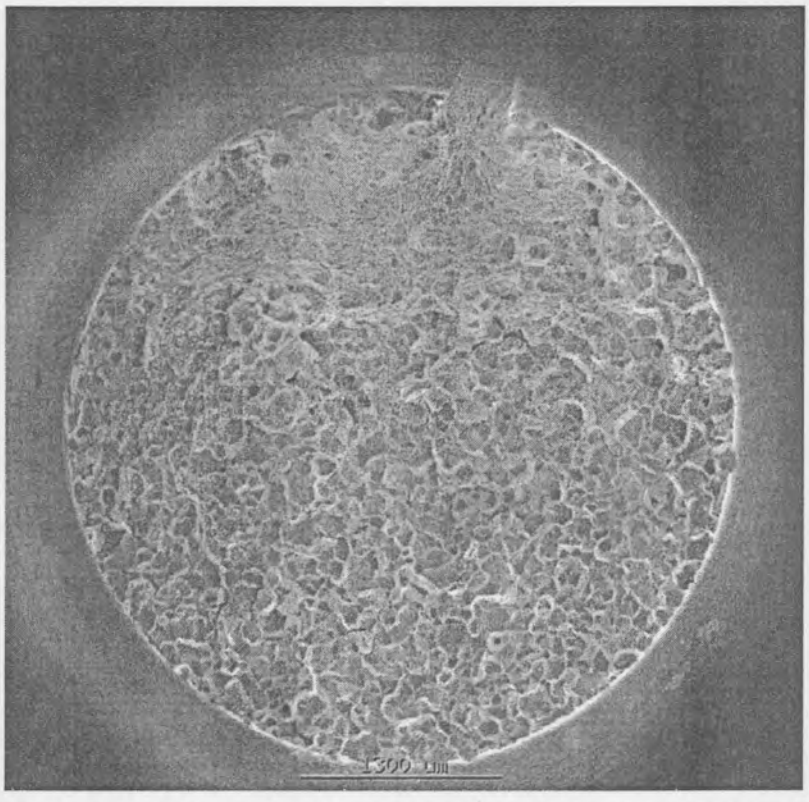

Figure 4.1: ½Cr-½Mo-¼V New material – Intergranular fracture surface, 204 MPa

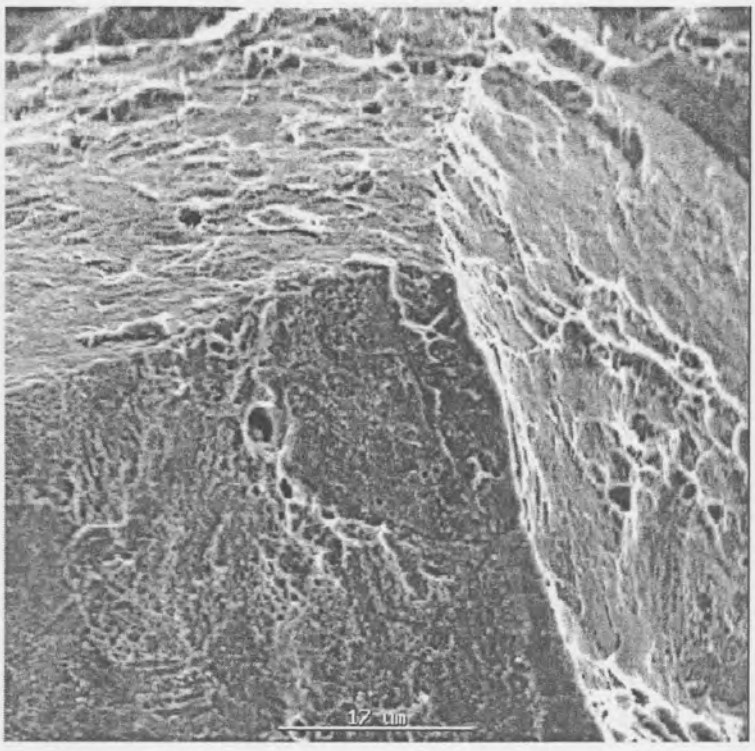

Figure 4.2: High Magnification of Figure 4.1. Some microductility on prior austenite grain boundaries

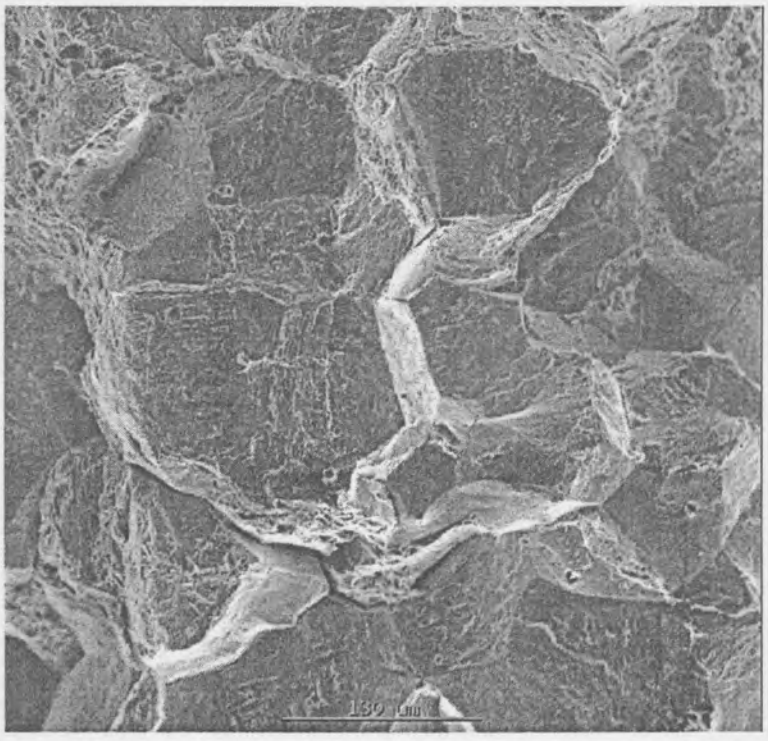

Figure 4.3: Intergranular fracture along prior austenite grain boundaries, area of higher magnification than Figure 4.1

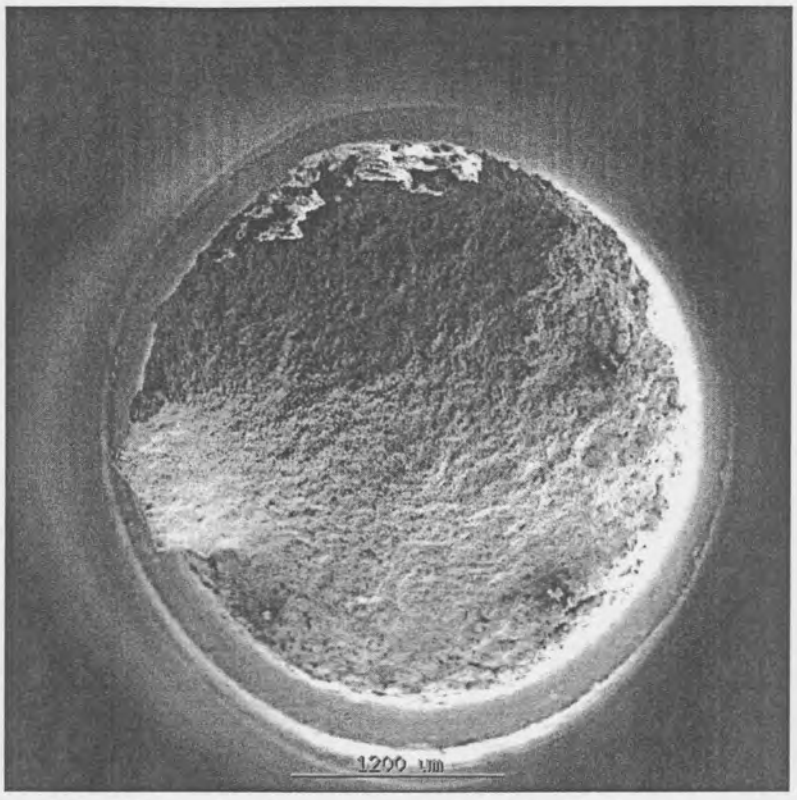

Figure 4.4: ½Cr-½Mo-¼V Service-Exposed material – Ductile fracture surface, 204 MPa

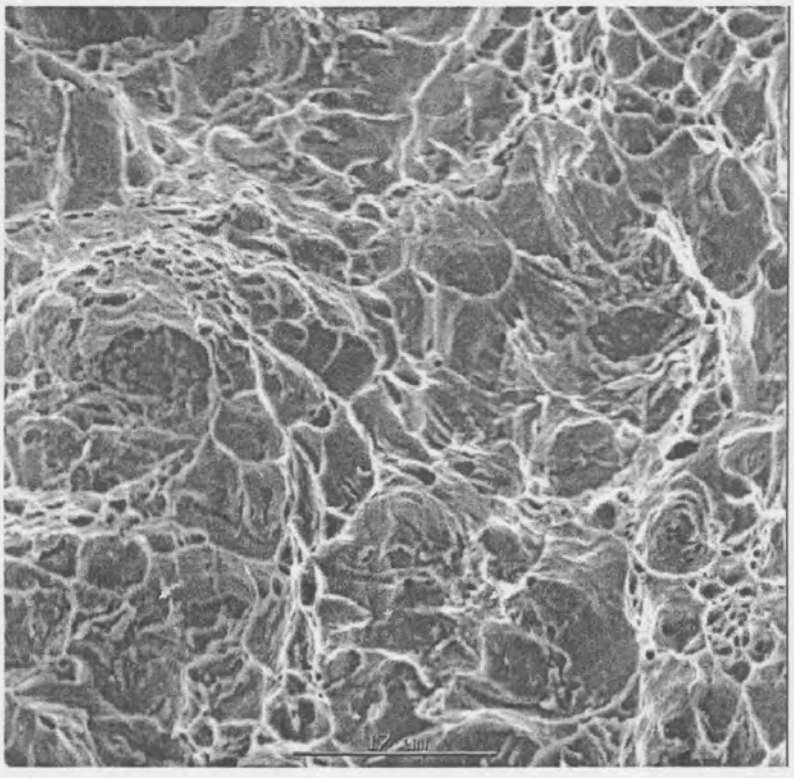

Figure 4.5: High magnification of Figure 4.4 – Microvoid coalescence (MVC)

4.5 METALLOGRAPHY

Metallographic samples were prepared from new and service-exposed material after the CGHAZ thermal simulation. The samples tested at 204 MPa (new and service-exposed) were also taken and metallographic samples were prepared. The resulting microstructures are shown in Figures 4.6 to 4.13. Descriptions of the structures are given in Table 4.3.

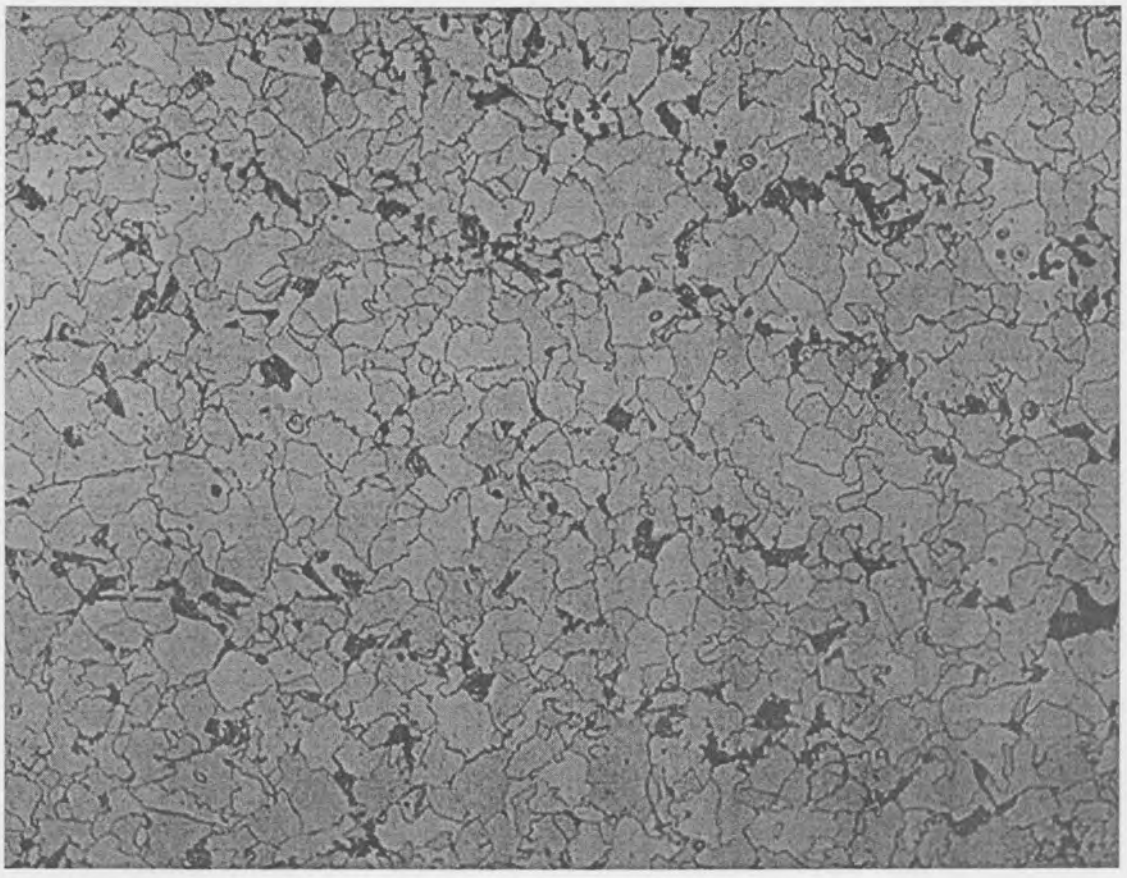

Figure 4.6 Base metal of new material – 200x (After thermal simulation)

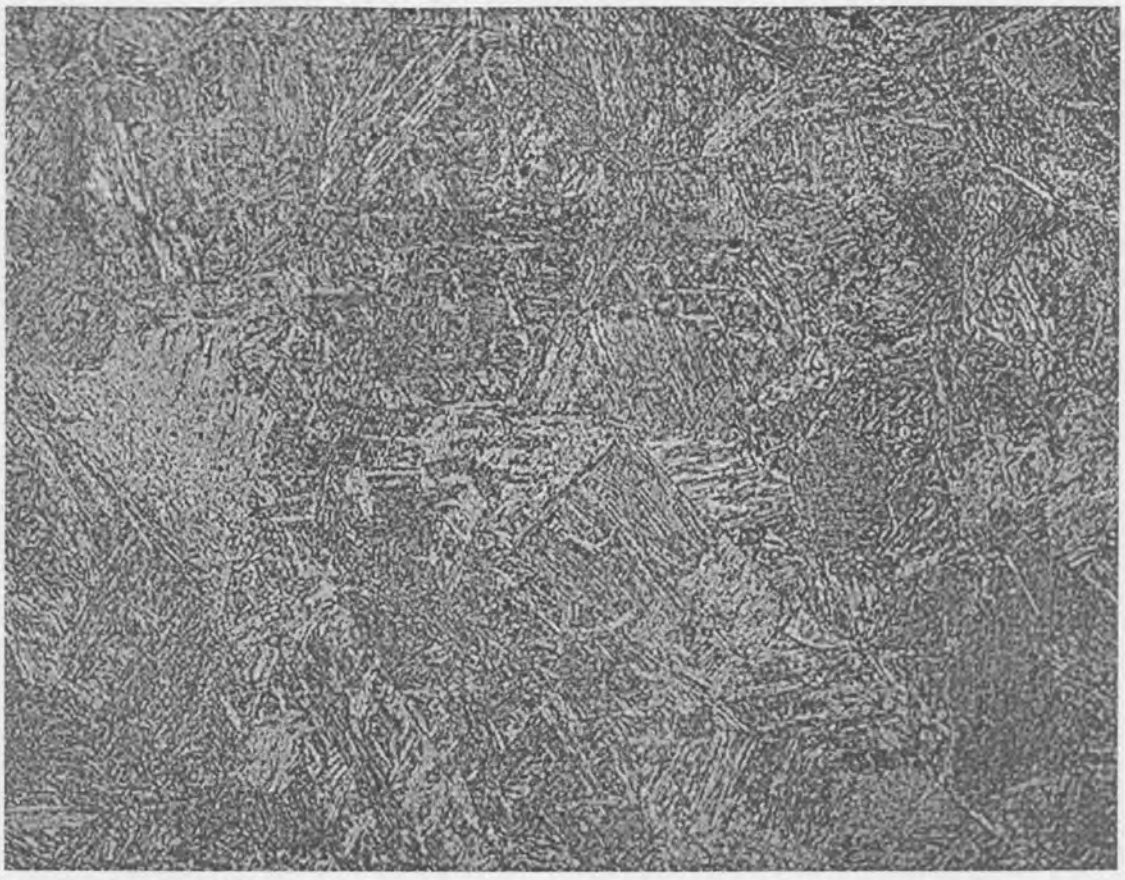

Figure 4.7: CGHAZ of new material – 200x (After thermal simulation)

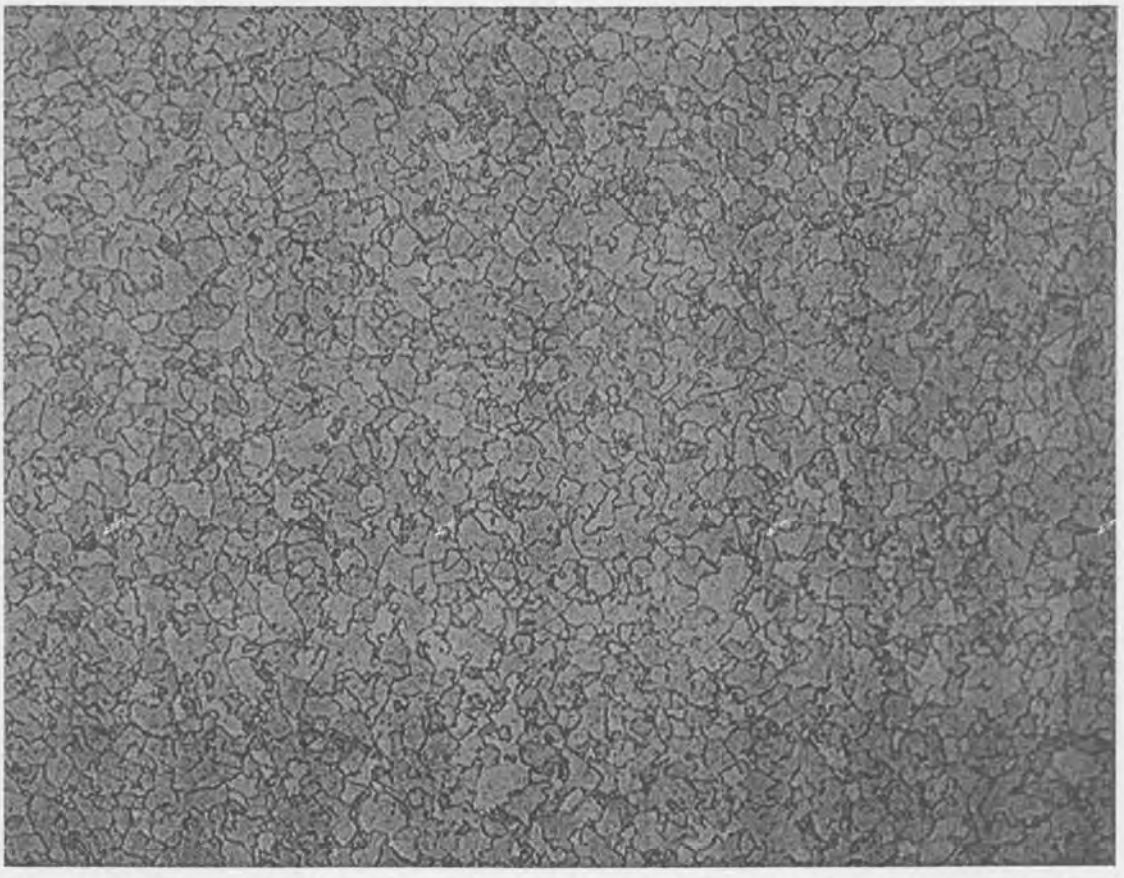

Figure 4.8: Base metal of service-exposed material – 200x (After thermal simulation)

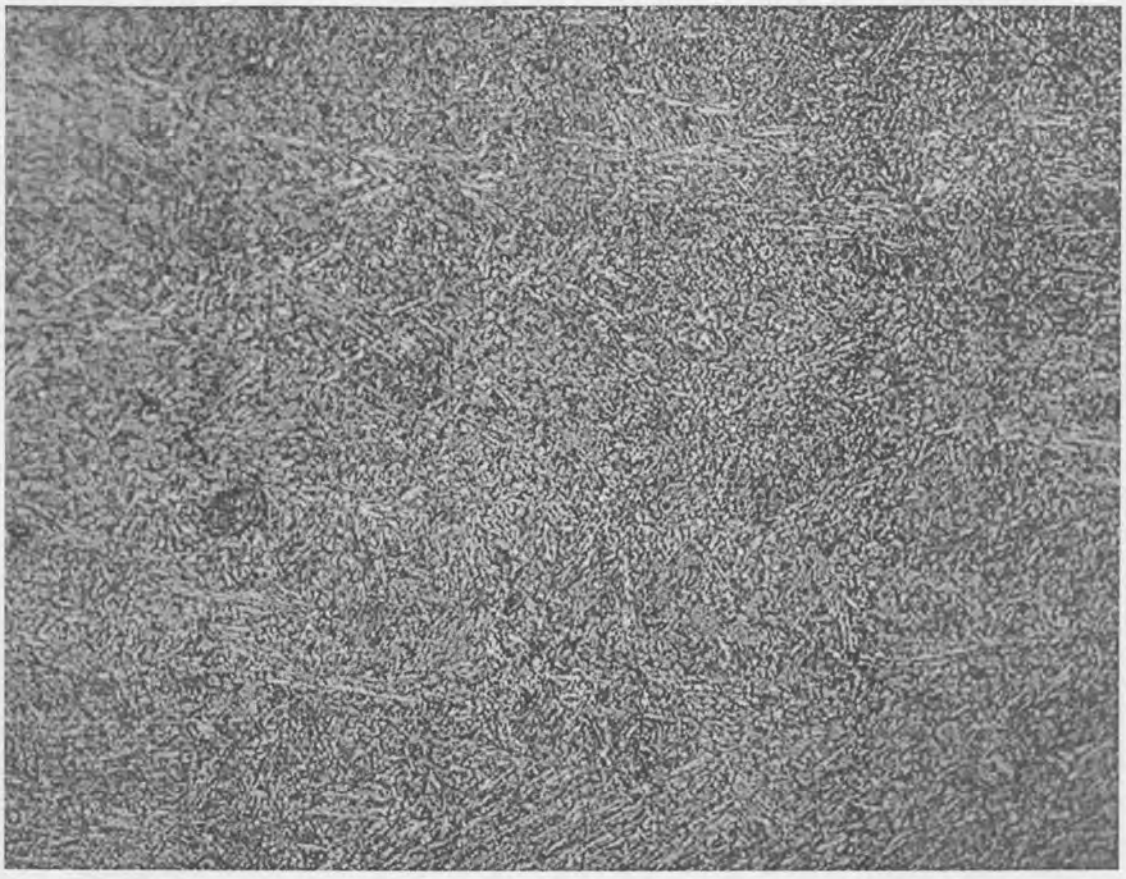

Figure 4.9: CGHAZ of service-exposed material – 200x (After thermal simulation)

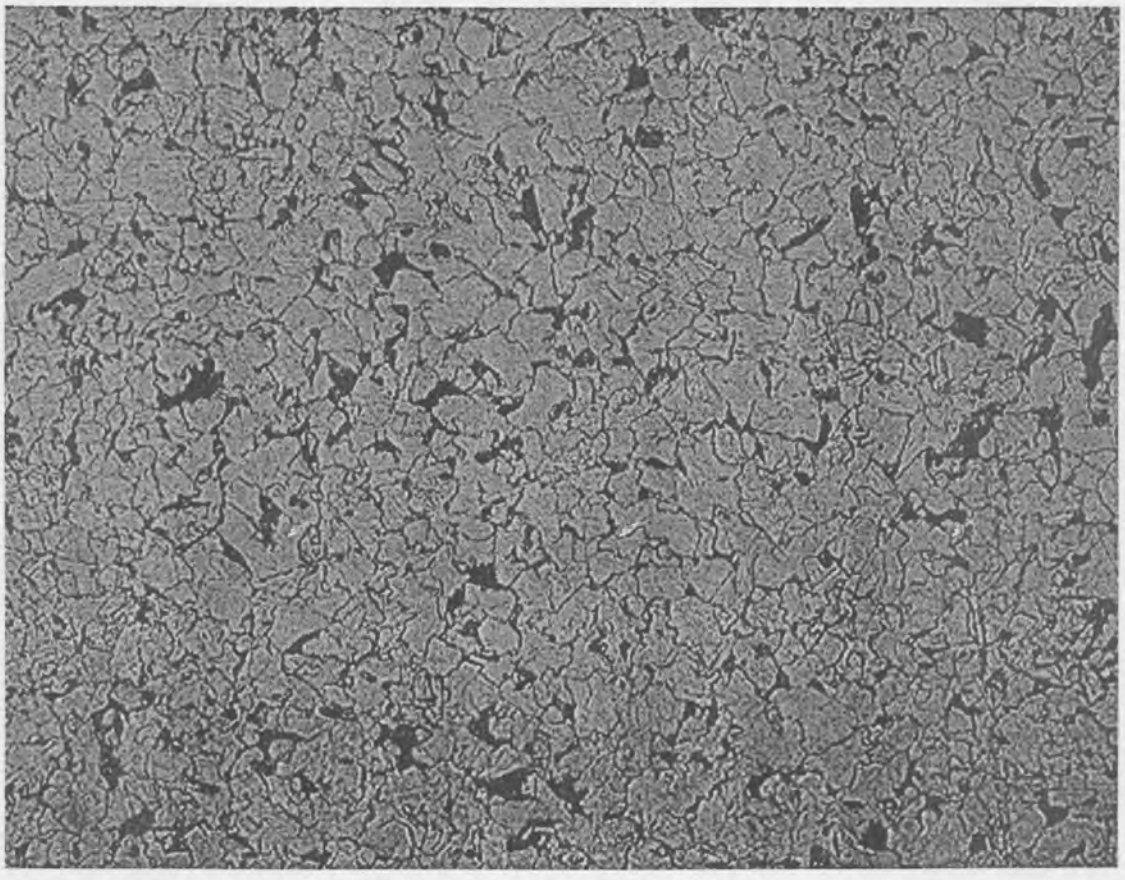

Figure 4.10: Base metal of new material – 200x (After PWHT)

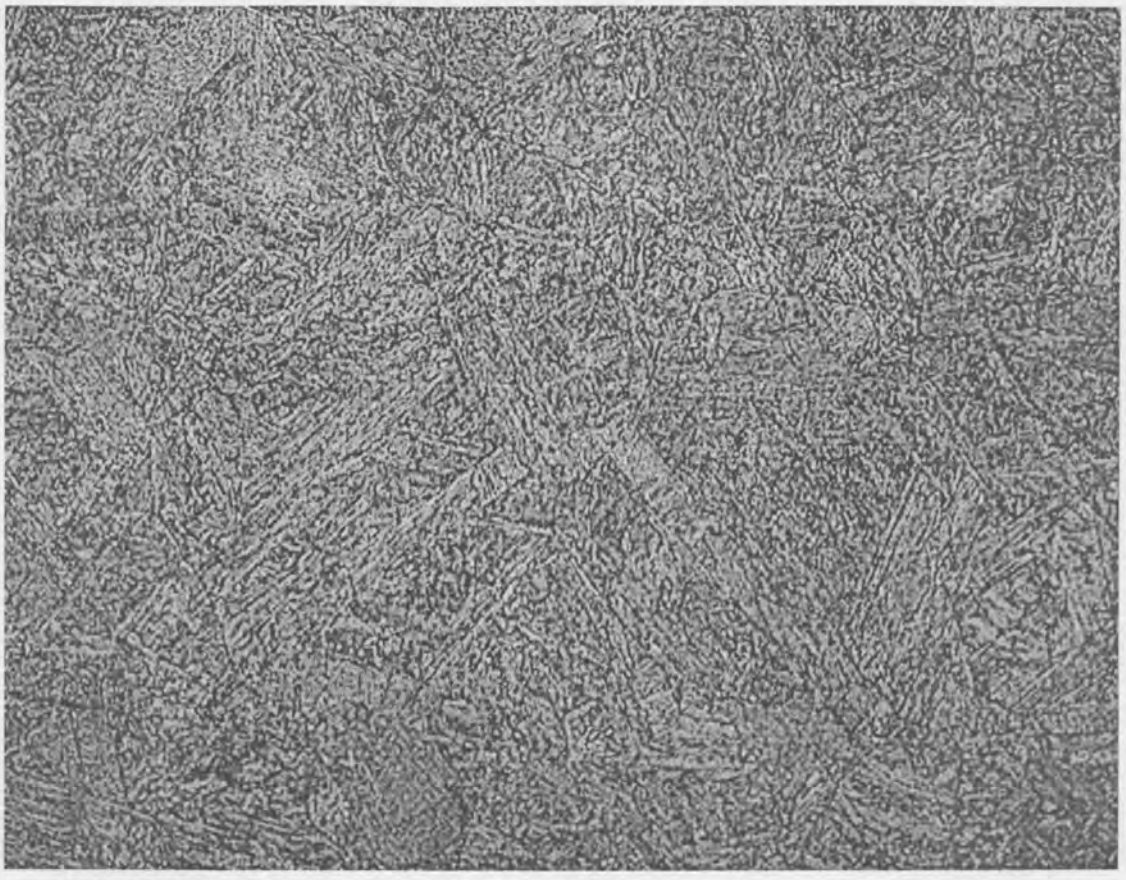

Figure 4.11: CGHAZ of new material – 200x (After PWHT)

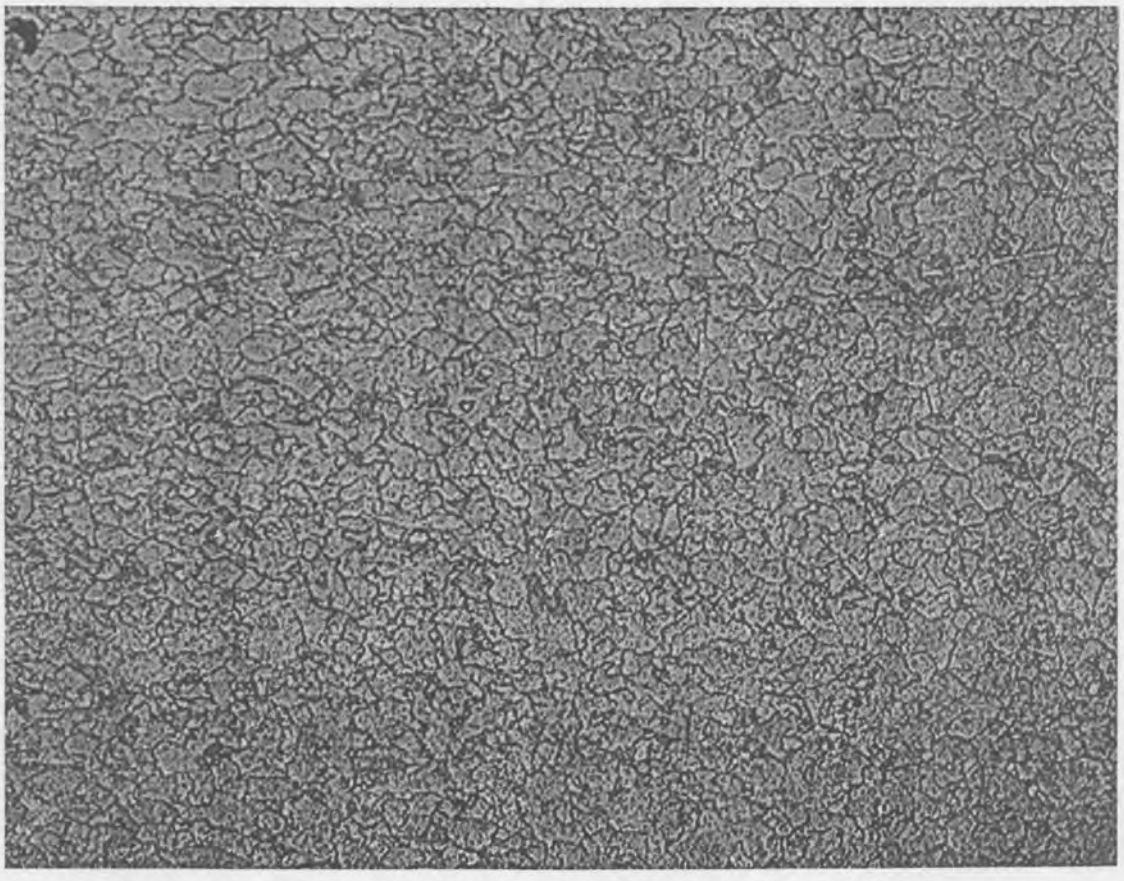

Figure 4.12: Base metal of service-exposed material – 200x (After PWHT)

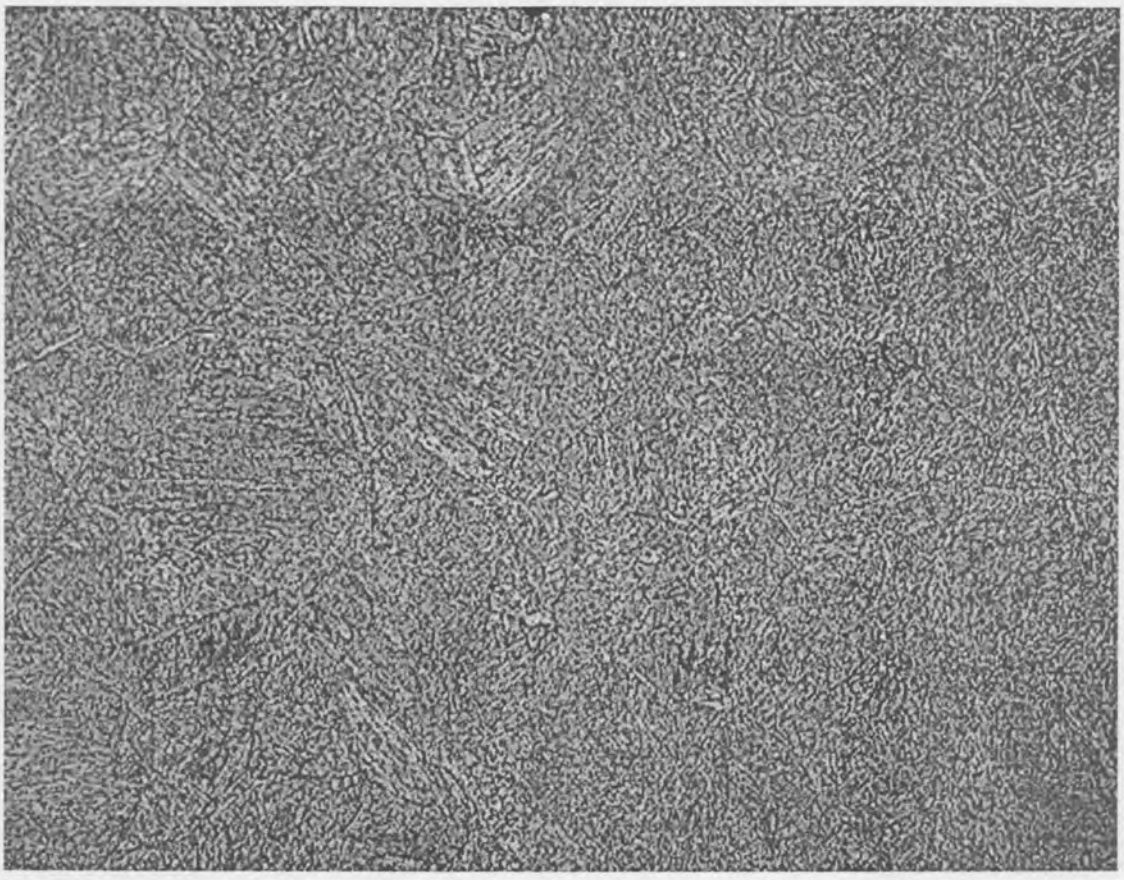

Figure 4.13: CGHAZ of service-exposed material – 200x (After PWHT)

Table 4.3: Description of metallographic sample microstructures

Condition	State	Figure No.	Description
As-simulated	New	4.6	Base metal. Ferritic matrix with partially spheroidised pearlite. There is a dispersion of fine carbides on the grain boundaries. ASTM grain size of around 7.
		4.7	CGHAZ. Untempered bainitic microstructure. Might be upper bainite. FGHAZ will have the same structure as Fig4.7 with smaller grains.
	Service-exposed	4.8	Base metal. Ferritic matrix with a dispersion of coarse and continuous carbides on the grain boundaries. Still some signs of the decomposed secondary phase (Pearlite). Ferrite has an ASTM grain size of about 9.
		4.9	CGHAZ. Untempered bainitic microstructure. In essence the same as the condition of the CGHAZ of the new material.
PWHT	New	4.10	Base metal. Ferritic matrix with partially spheroidised pearlite. There is a dispersion of fine carbides on the grain boundaries. ASTM grain size of around 7. Some areas that appear overtempered.
		4.11	Tempered Bainite. Inside of the needles have broken apart. Fine carbides throughout the matrix
	Service-exposed	4.12	Base metal. Ferritic matrix with a dispersion of coarse and continuous carbides on the grain boundaries. Still some signs of the decomposed secondary phase (Pearlite).
		4.13	CGHAZ. The structure consists of tempered bainite.

Hardness profiles were determined from the same samples used for metallography. A Vickers microhardness-testing machine with a load of 300g was used. The profiles start at the centre of the HAZ and extend through to the base metal. The profiles are shown in Graph 4.3.

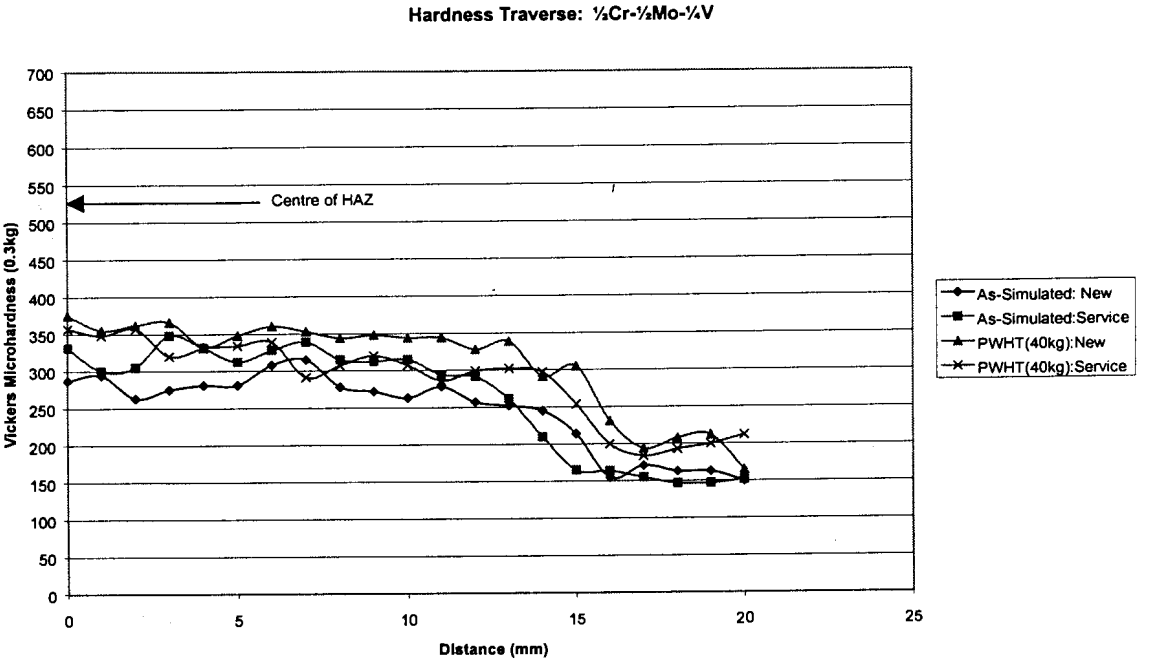

Graph 4.3: Hardness profile of ½Cr-½Mo-¼V – New and Service exposed

4.7 DISCUSSION

From the spiral notch tests it is quite clear that there is a distinct difference between the behaviour of the new and service-exposed material. The new material underwent less elongation than the service-exposed material and all samples tested fractured in the CGHAZ area of the sample. All the service-exposed samples fractured in the base metal area of the samples and at lower temperatures than the corresponding new material.

The fracture surfaces studied under the SEM clearly shows two different fracture mechanisms that lead to failure during testing. The new material

failed by a brittle, intergranular failure mechanism at all loads tested. The service-exposed material all failed in a ductile manner at all loads tested. Some microductility along the prior austenite grains boundaries of the new material were observed. The fractography shows that the new material failed due to a reheat cracking mechanism.

The state of the microstructures shows that the CGHAZ simulation for new and service-exposed material delivers almost an identical HAZ in the material. Grain sizes were larger than expected during actual welding but this is a common occurrance when weld simulation is performed. After PWHT (spiral notch test) the HAZ's of both states showed tempering of the bainite. Very minor changes were observed in the base metal areas. In the new and service-exposed material, the carbides were taken up into solution during the CGHAZ simulation. The cooling rate from the peak temperature is to high for these carbides to re-precipitate thus they remain in solid solution. During the subsequent PWHT these carbides re-precipitate adding strength to the matrix. The base metal carbides did not go through significant changes during PWHT. These carbides, in the new material, are still in the meta-stable state that contributes to creep strength. The carbides in the service-exposed material have already either mostly or all transformed to the more stable carbide type with a lower creep strength.

The hardness profiles also showed that after CGHAZ simulation the hardness for new and service-exposed materials are similar in the HAZ. After PWHT an increase in hardness was found in the HAZ; due to secondary hardening for both the new and service-exposed material. The re-precipitation of carbides took place during the PWHT. In general the hardness of the service-exposed material is however lower than that of the new material.

4.8 CONCLUSION

It was found that ½Cr-½Mo-¼V material in the unexposed condition is susceptible for reheat cracking after welding. Referring to Figure 4.2 the microductility observed on the grain boundaries indicates reheat cracking but

that the mechanism is not wholly a brittle mechanism. Some precipitate free or denuded zones in close proximity to the grain boundaries play a role in the cracking mechanism.

The service-exposed material fractured in the base metal and was consequently not susceptible to reheat cracking, for the test conditions used. The carbides in the base metal of the service-exposed are in the stable state and have lower creep strength. The softer base metal of the service-exposed state protected the HAZ during PWHT by being the primary area to undergo deformation under the influence of tensile stress due to the fact that there is little or no meta-stable carbides that add creep strength. The starting microstructure of the material before welding apparently plays a significant role in the susceptibility of the material with regards to reheat cracking.

4.9 REFERENCES

1. Stahlschlüssel – Key to Steel, 1998

CHAPTER 5: 2¼Cr-1Mo (10CrMo9-10)

5.1 INTRODUCTION

Another commonly Cr-Mo creep resistant alloy used is 2¼Cr-1Mo. Up to the 1950's it was highest ferritic alloy used in boiler applications. The material is supplied in the quenched and tempered condition with a ferritic and bainitic structure. Some of the more common properties of this grade are listed below[1]. The service-exposed material was obtained from Kriel power station and operated at 510°C for 130 000 hours.

5.1.1 General Chemical Composition

ELEMENT	min %	max %
C	0.08	0.14
Si	0	0.50
Mn	0.40	0.80
P	0	0.030
S	0	0.025
Cr	2.00	2.50
Mo	0.90	1.10
Cu	0	0.30

5.1.2 Mechanical Properties

PROPERTY	VALUE
Yield stress	>= 290 MPa
Tensile Strength	480 – 660 MPa
Elongation	>= 18 %
Impact value (DVM)	>= 55 J
Hardness Brinell	130 – 175 HB_{30}

Mechanical Properties at ambient temperature (Values for longitudinal sample bars <= 60mm ∅

5.2 CHEMICAL ANALYSIS

Eskom accredited methods No 106 (Alloying elements) and 119 (Carbon) were used on the new and service-exposed material. The results are shown in Table 5.1. The original result sheets are attached in Appendix 1.

Element	New Material	Service-exposed Material (± 130 000 h at 510°C)
Carbon	0.11	0.10
Chromium	2.41	2.57
Nickel	0.05	0.17
Manganese	0.49	0.54
Molybdenum	0.87	0.91
Vanadium	0.01	0.02
Sulphur	0.001	0.003
Phosphorus	0.018	0.021
Silicon	0.11	0.04
Titanium	0.01	0.01
Copper	0.04	0.12
Cobalt	0.01	0.03
Niobium	0.005	0.005
Tin	0.01	0.01
Tungsten	0.005	0.02

Table 5.1: Chemical analysis for new and service-exposed 2¼Cr-1Mo material

The chemical composition of the test material was within specified range for 2¼Cr-1Mo material.

5.3 SPIRAL NOTCH TEST RESULTS (Constant load, PWHT Thermal Cycle)

The results from the spiral notch tests on the new and service-exposed 2¼Cr-1Mo are listed in Table 5.2 and Graphs 5.1 and 5.2.

Table 5.2: Position of final fracture for 2¼Cr-1Mo steel samples

Nominal Stress (MPa)	2¼Cr-1Mo New Material	2¼Cr-1Mo Service-exposed Material
356	Base Metal	Base Metal
305	Base Metal	Base Metal
204	CGHAZ	Base Metal
153	Base Metal	Base Metal

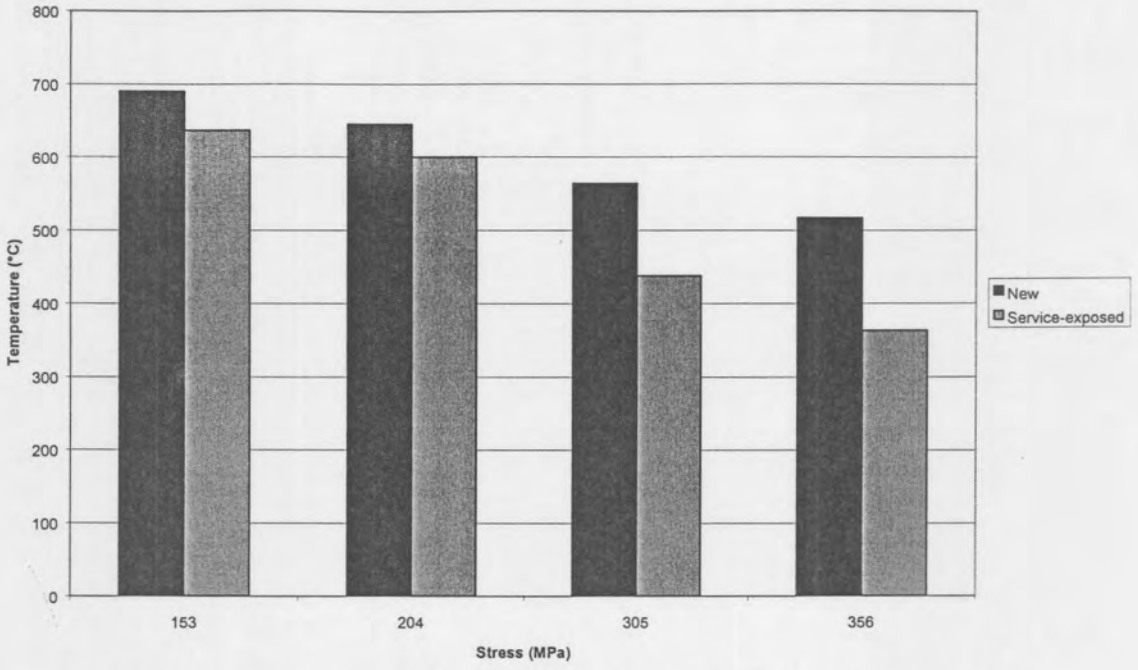

Graph 5.1: Temperature of final fracture for 2¼Cr-1Mo steel samples

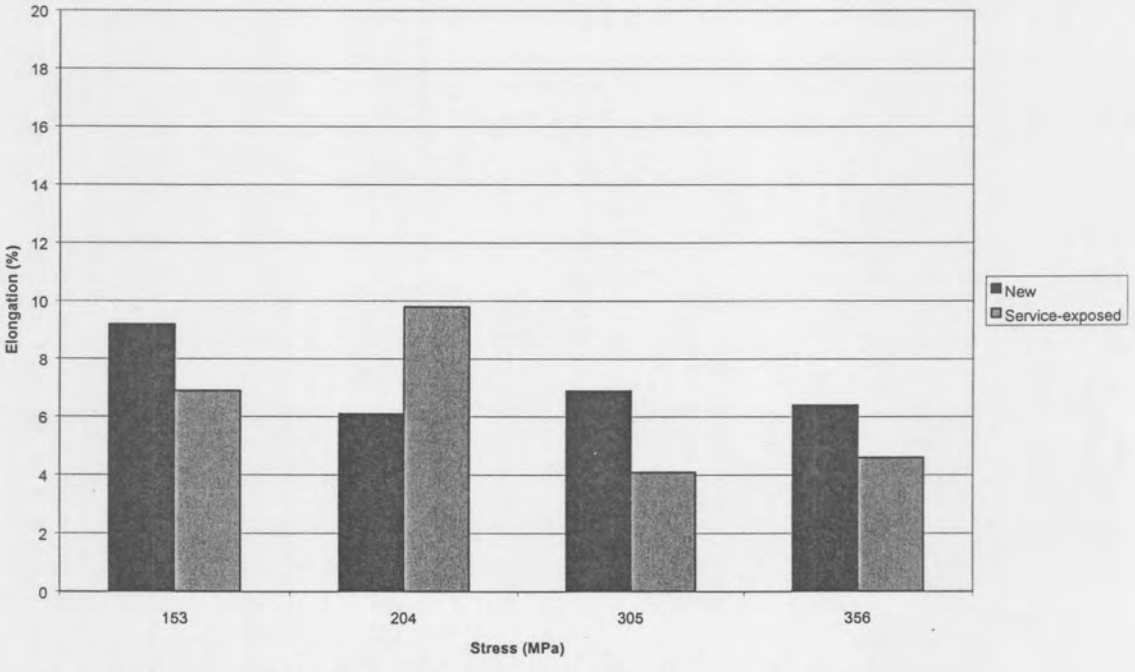

Graph 5.2: Amount of elongation for 2¼Cr-1Mo steel samples

The experimental graphs compiled during these tests are attached in Appendix 2.

5.4 SEM FRACTOGRAPHY

The fracture surfaces of the samples tested at 204 MPa for both new and service-exposed material was studied in the SEM to confirm the mechanism of fracture. The fracture surfaces are shown in Figures 5.1 to 5.5.

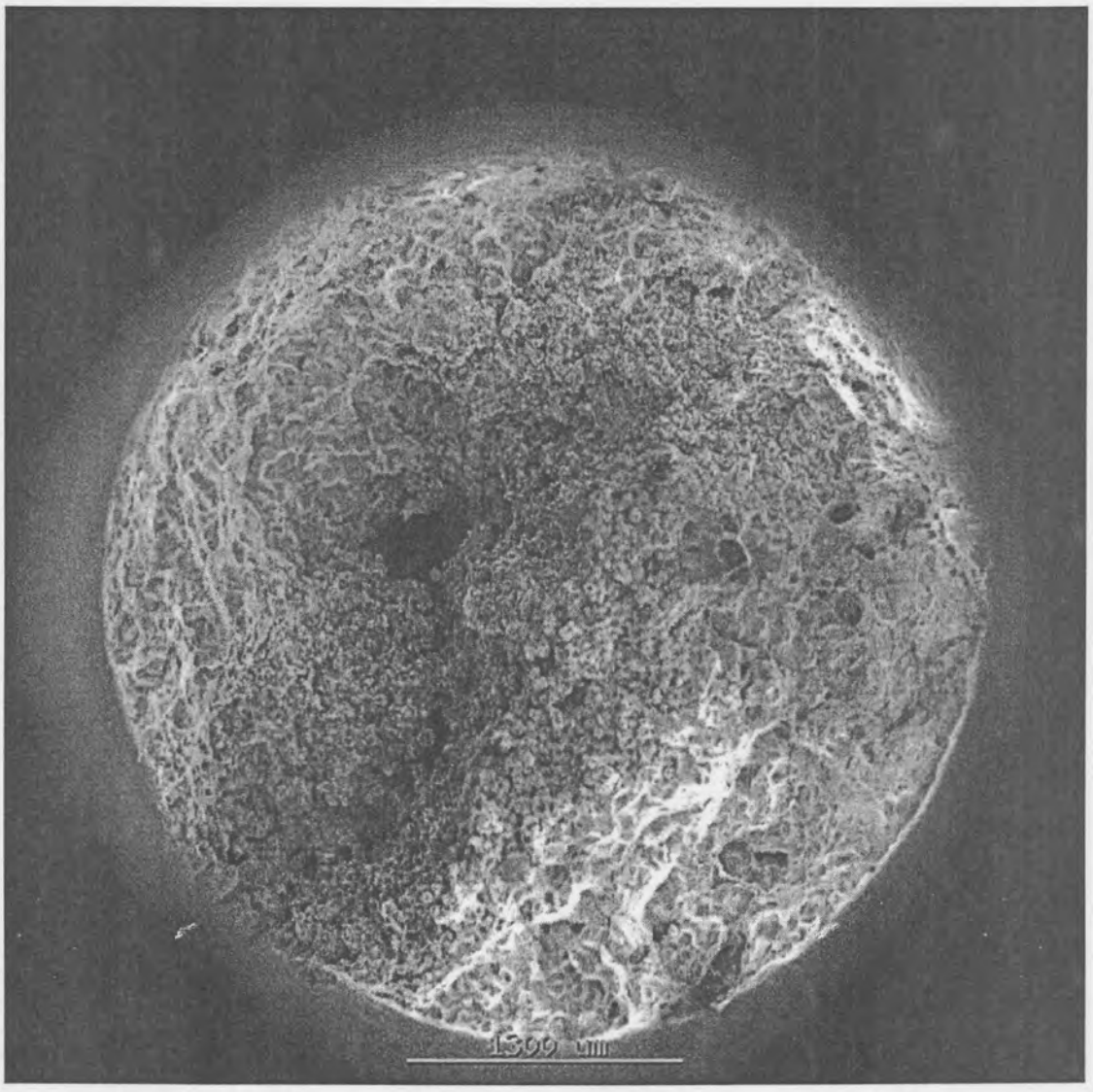

Figure 5.1: 2¼Cr-1Mo New material – Intergranular fracture surface, 204 MPa

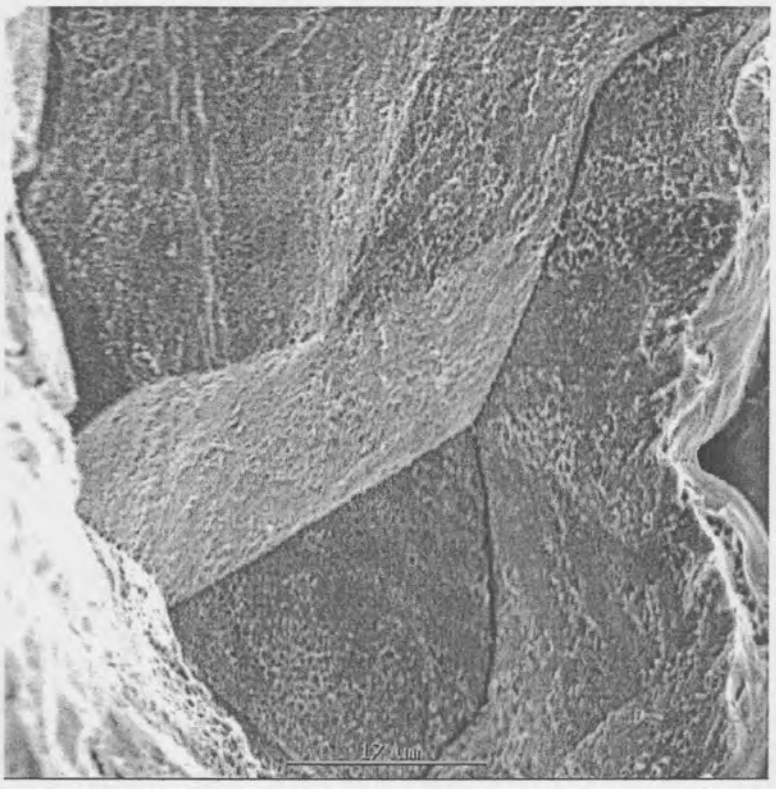

Figure 5.2: High Magnification of Figure 5.1. Some microductility on prior austenite grain boundaries

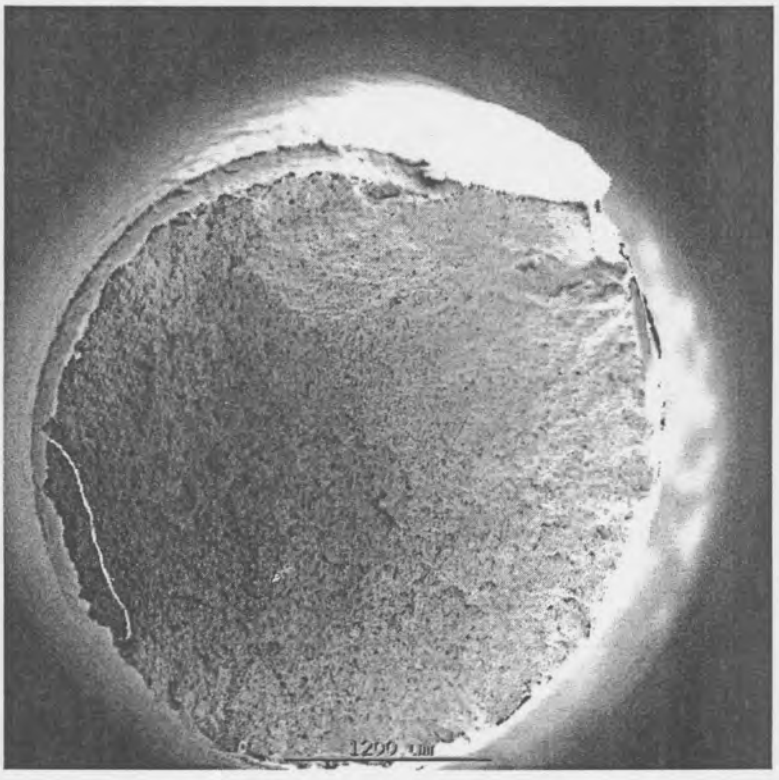

Figure 5.3: 2¼Cr-1Mo Service-exposed material – Ductile fracture surface, 204 MPa

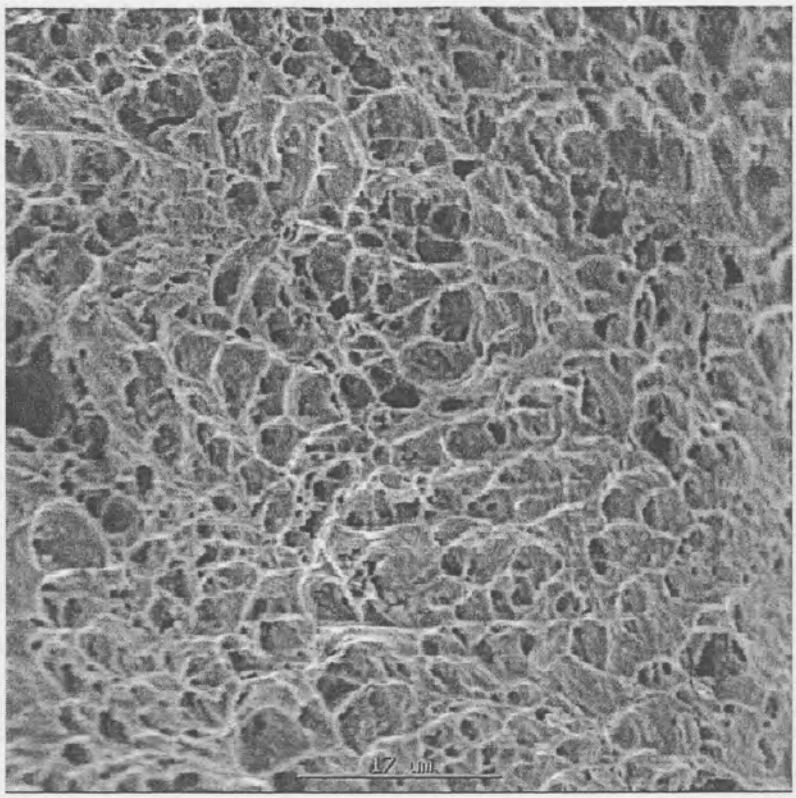

Figure 5.4: High magnification of Figure 5.3 – Microvoid coalescence (MVC)

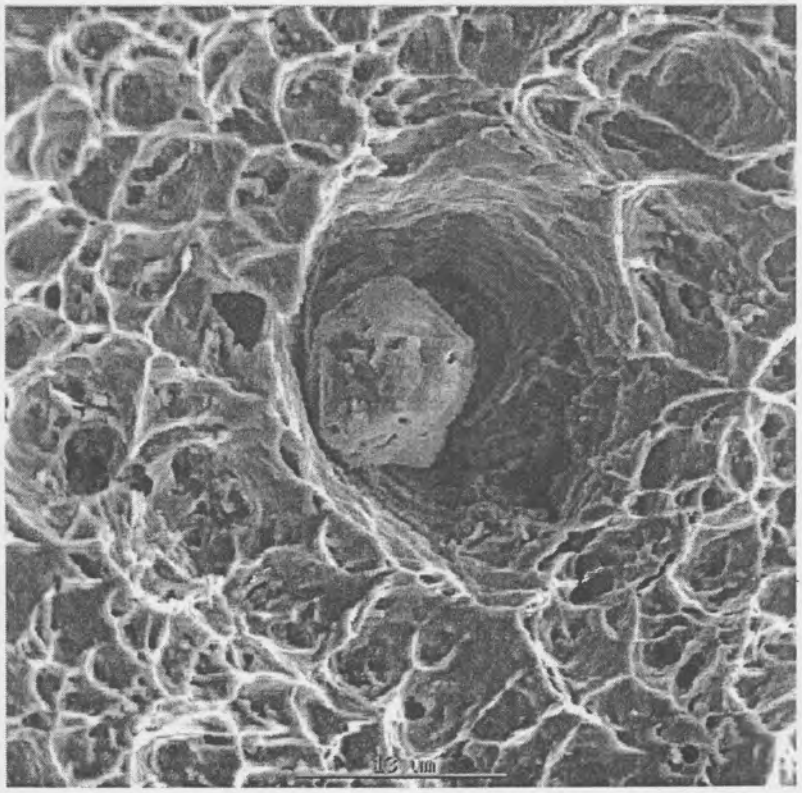

Figure 5.5: Inclusion particle trapped in the ductile fracture.

5.5 METALLOGRAPHY

Metallographic samples were prepared from new and service-exposed material after the CGHAZ simulation. The samples tested at 204 MPa (new and service-exposed) were also taken and metallographic samples were prepared. The resulting microstructures are shown in Figures 5.6 to 5.13. Descriptions of the structures are given in Table 5.3.

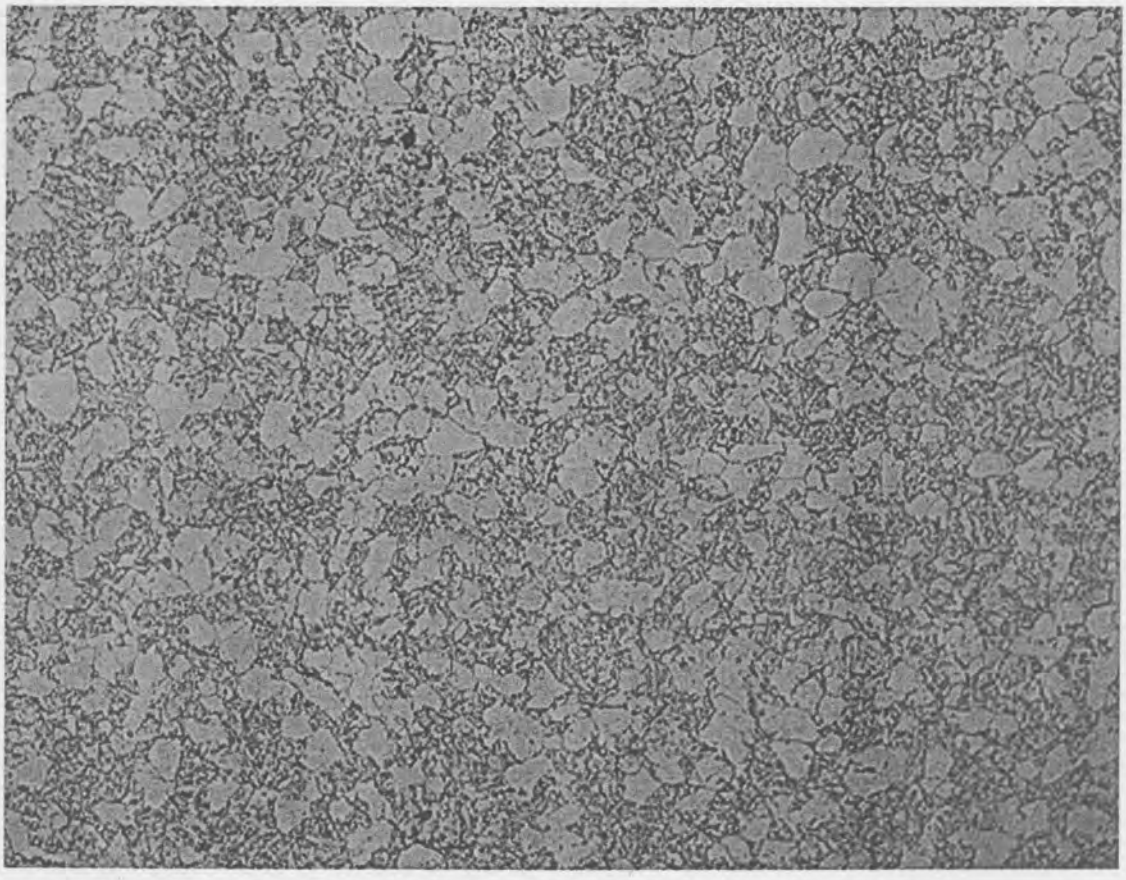

Figure 5.6: Base metal of new material – 200x (After thermal simulation)

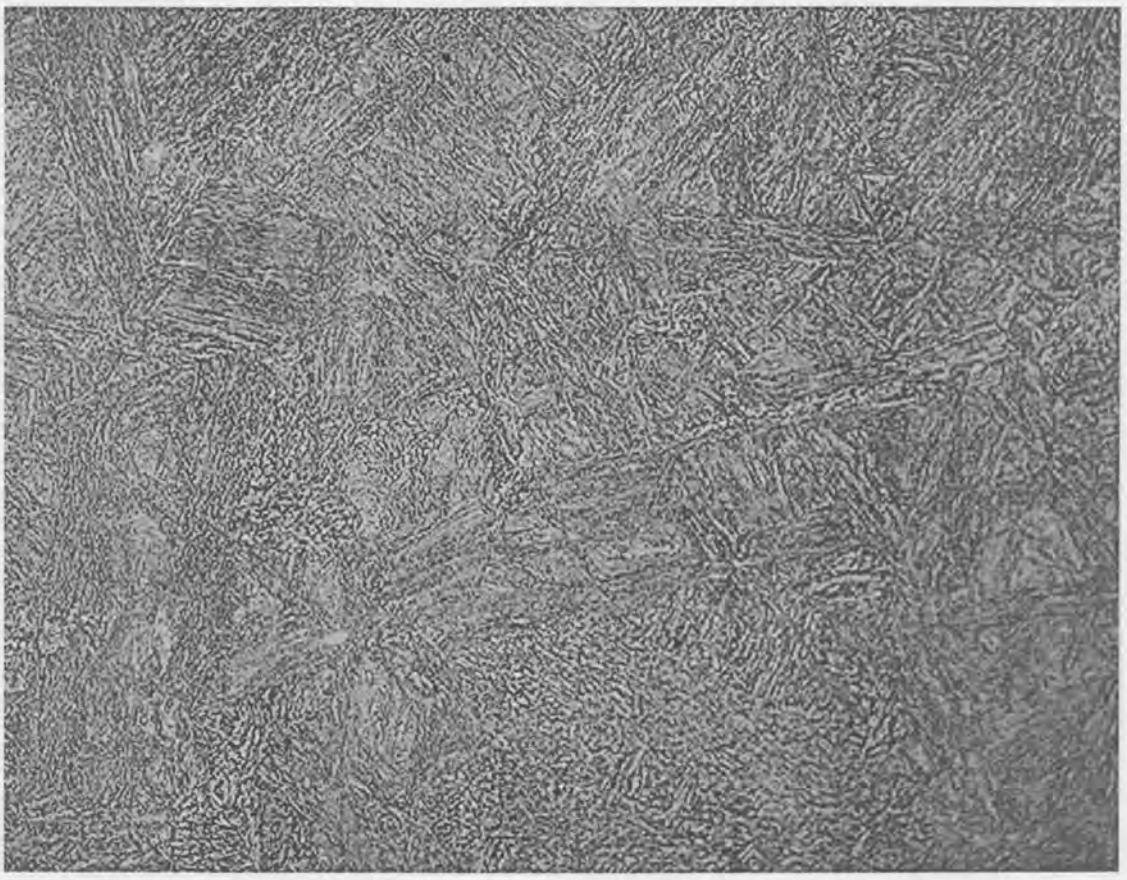

Figure 5.7: CGHAZ of new material – 200x (After thermal simulation)

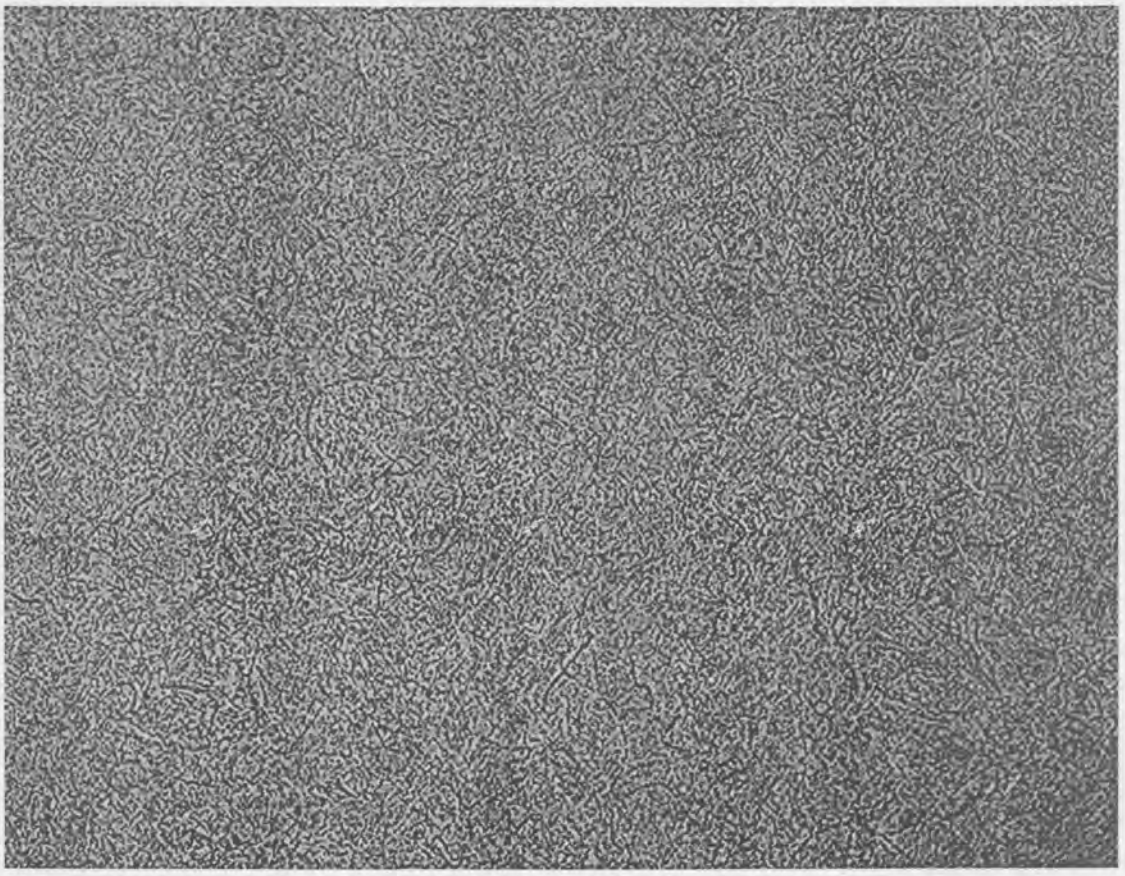

Figure 5.8: Base metal of service-exposed material – 200x (After thermal simulation)

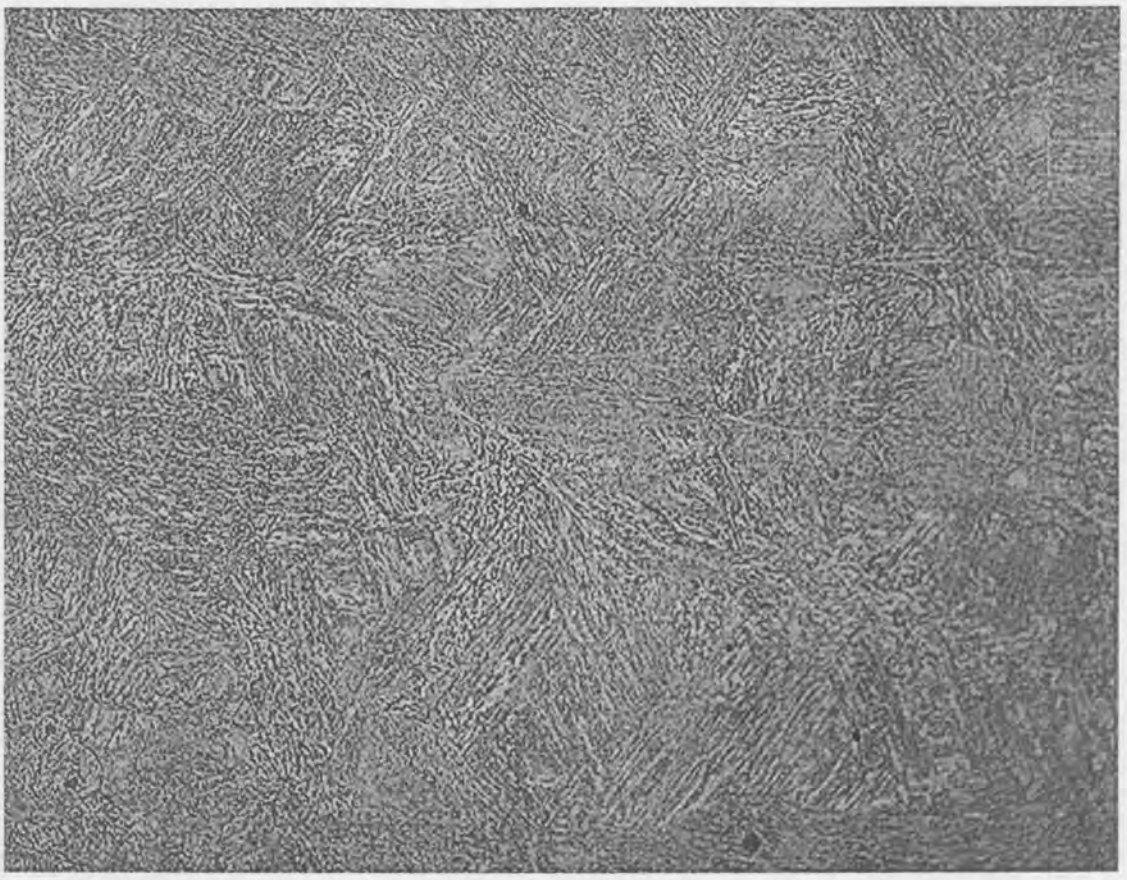

Figure 5.9: CGHAZ of service-exposed material – 200x (After thermal simulation)

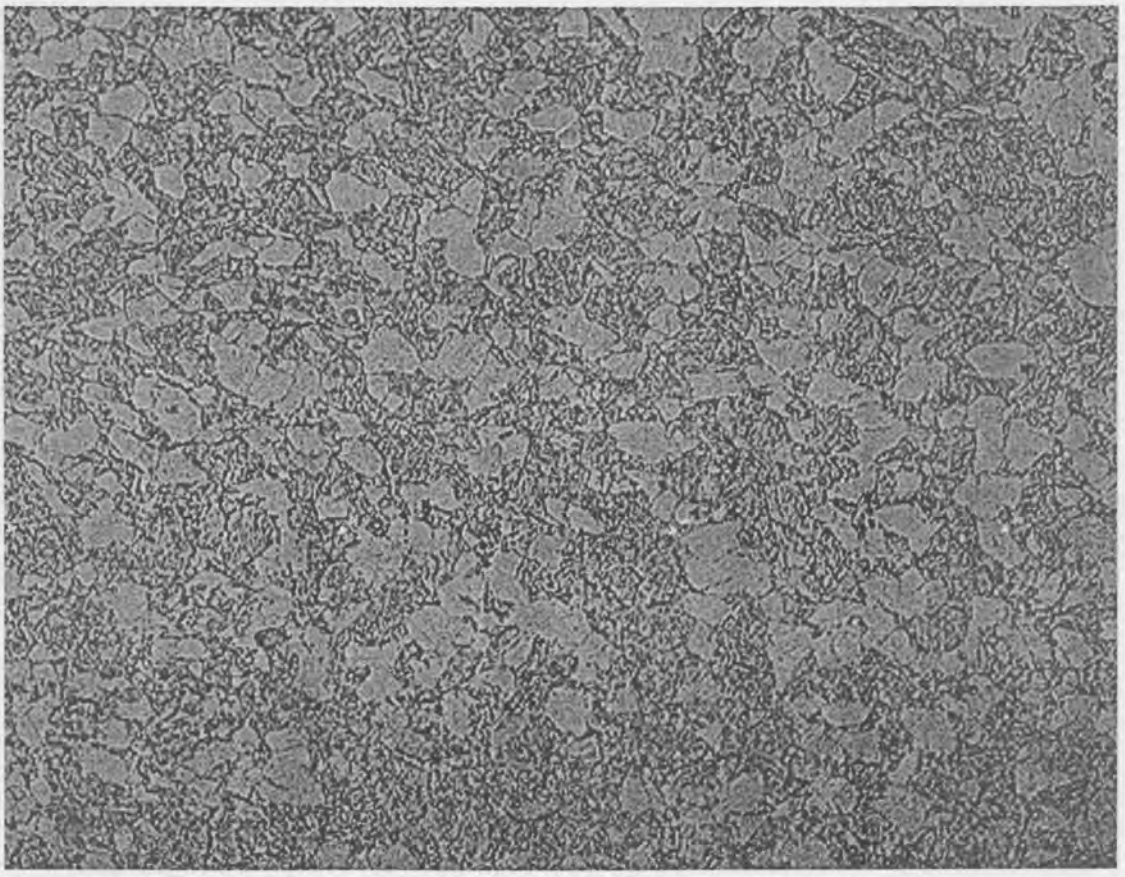

Figure 5.10: Base metal of new material – 200x (After PWHT)

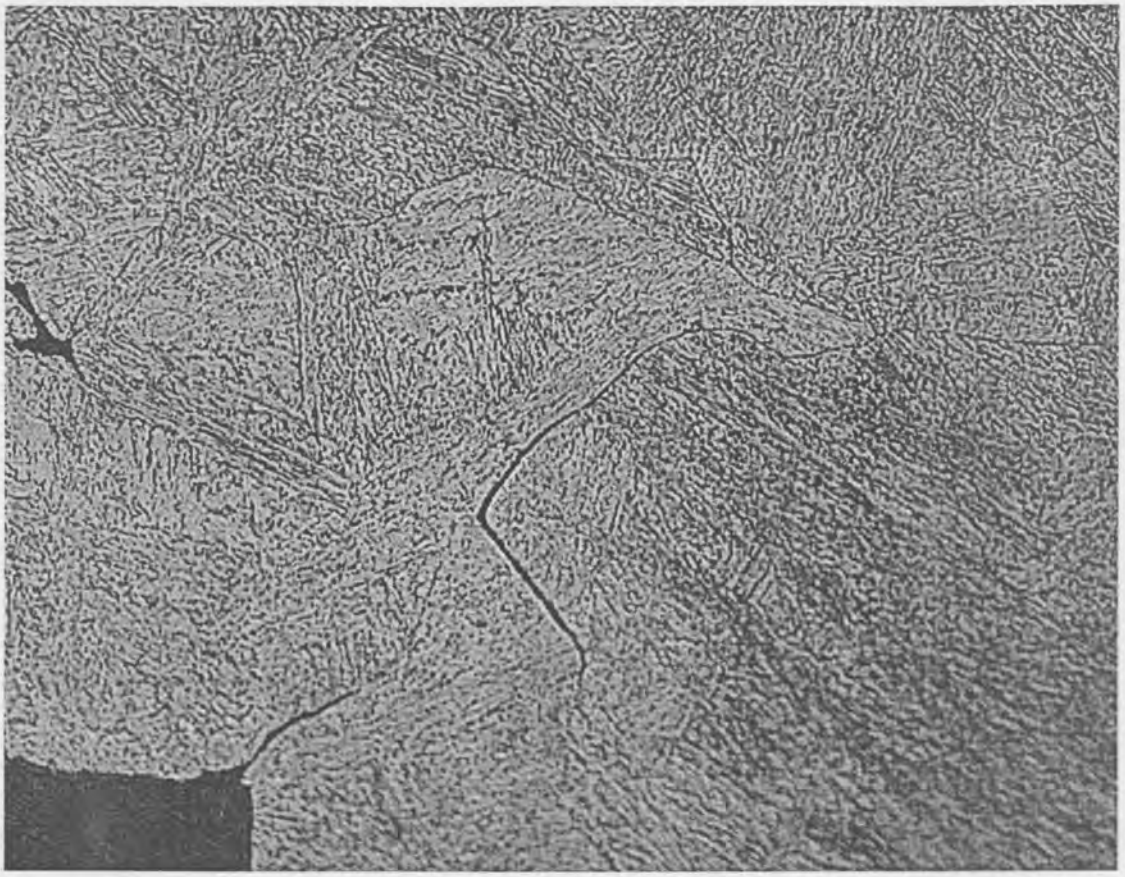

Figure 5.11: CGHAZ of new material – 500x (After PWHT). Secondary intergranular crack visible

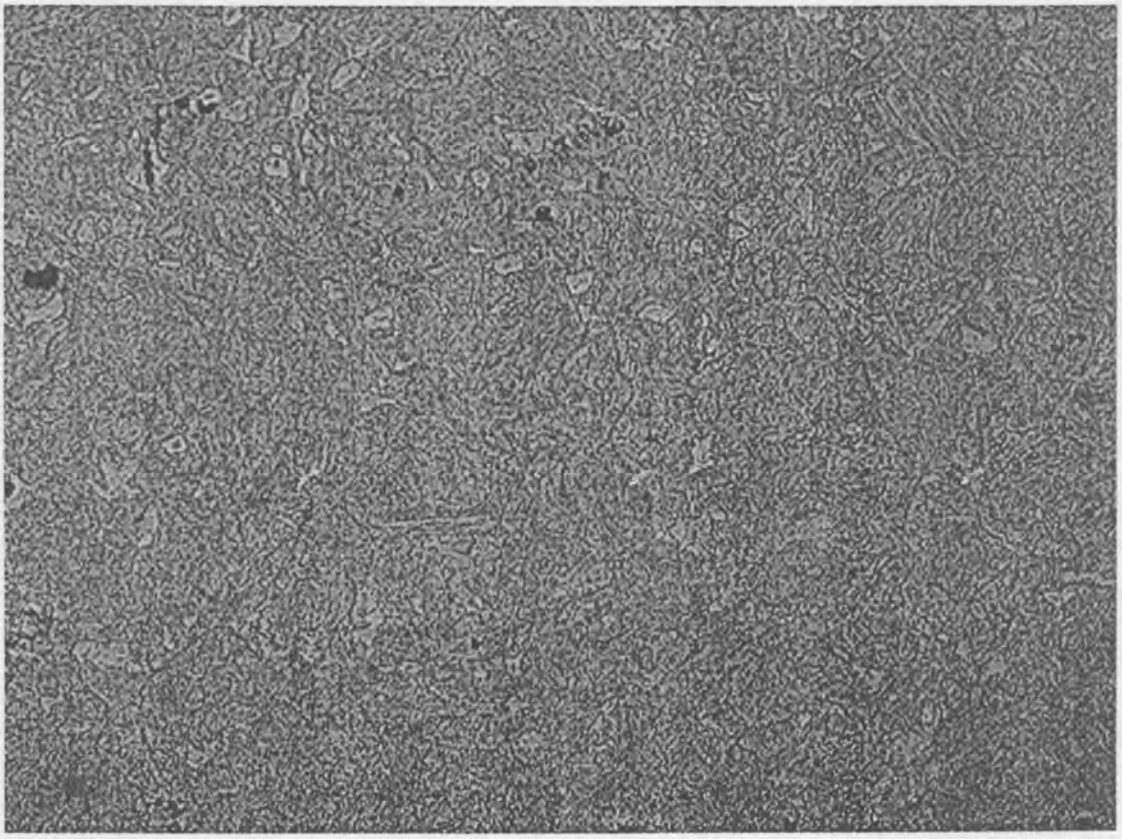

Figure 5.12: Base metal of service-exposed material – 200x (After PWHT)

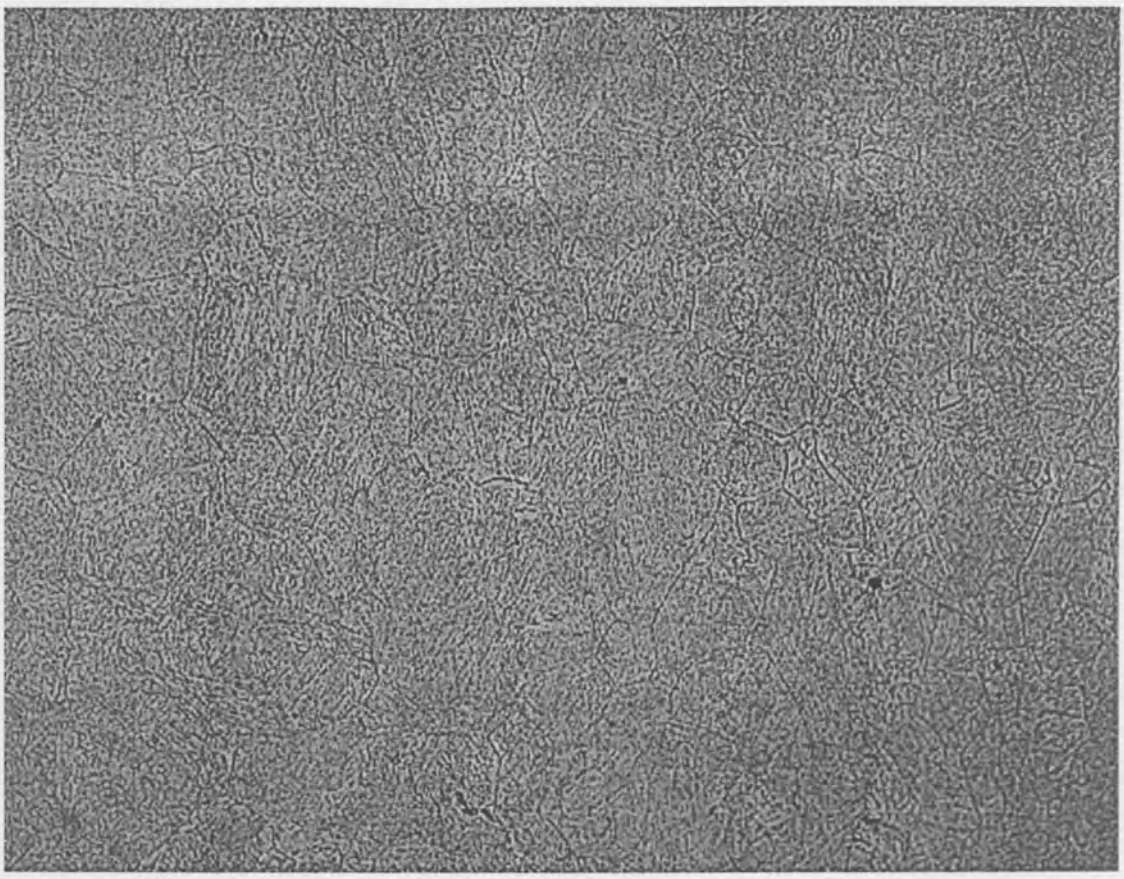

Figure 5.13: CGHAZ of service-exposed material – 200x (After PWHT)

Table 5.3: Description of metallographic sample microstructures

Condition	State	Figure No.	Description
As-simulated	New	5.6	Base Metal: Ferritic matrix coupled with partly decomposed tempered Bainite. There is also a dispersion of fine carbides on the grain boundaries. ASTM grain size of approximately 8.
		5.7	CGHAZ: Bainite. In the FGHAZ the structure is the same although grains are smaller. The FGHAZ appeared to be more tempered than The CGHAZ.
	Service-exposed	5.8	Base Metal: No ferritic matrix left. Tempered, partly decomposed Bainite with a dispersion of fine carbides throughout the structure.
		5.9	CGHAZ: Bainite. In the FGHAZ the structure is the same although grains are smaller. The FGHAZ appeared to be more tempered than The CGHAZ.
PWHT	New	5.10	Base Metal: Ferritic matrix coupled with partly decomposed tempered Bainite. There is also a dispersion of fine carbides on the grain boundaries. The amount of carbides present seem to be greater that in the As-simulated condition.
		5.11	CGHAZ: Partly tempered Bainite with a dispersion of fine carbides throughout.
	Service-exposed	5.12	Base Metal: Islands of ferrite are visible. Coarse carbides present on the grain boundaries. Tempered partly decomposed Bainite with a dispersion of fine carbides is also present.
		5.13	CGHAZ: Tempered Bainite (needles broken apart). There is also a dispersion of fine carbides on the prior austenite boundaries.

5.6 HARDNESS SURVEY

Hardness profiles were determined from the same samples used in the metallography. A Vickers microhardness-testing machine with a load of 300g was used. The profiles start at the centre of the HAZ and extend through to the base metal. The profiles are shown in Graph 5.3.

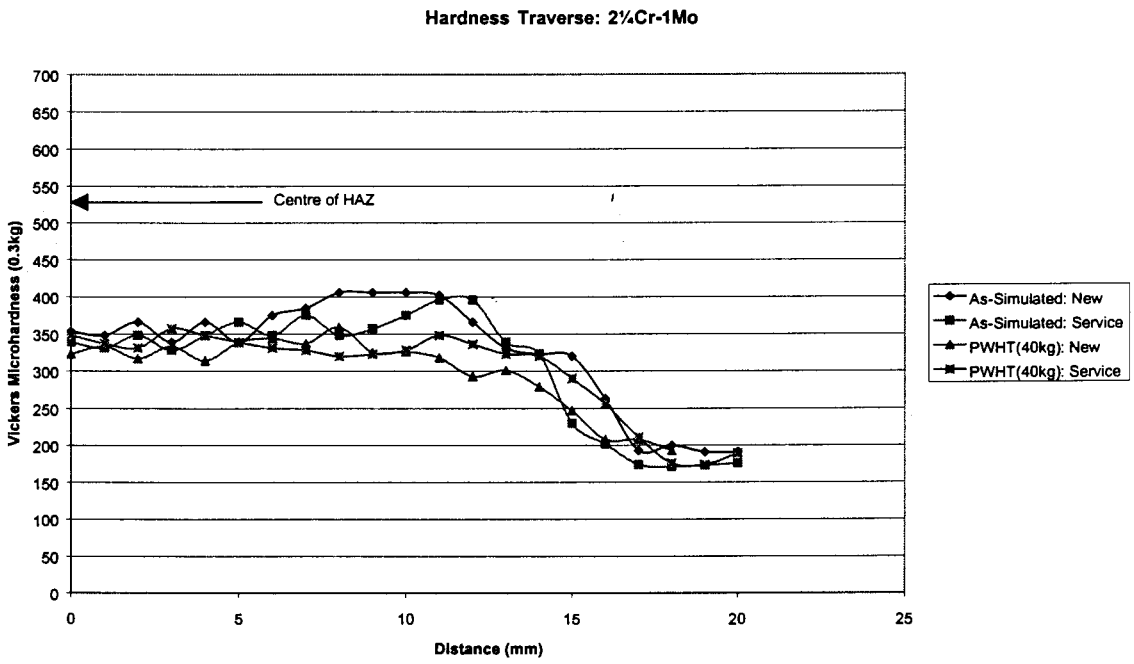

Graph 5.3: Hardness profile of 2¼Cr-1Mo material – New and Service exposed

5.7 DISCUSSION

From the spiral notch tests only one sample of the new material, tested at 204 MPa, failed in the CGHAZ. The rest of the samples all failed in the base metal area. The service-exposed material all failed in the base metal region, for all loads applied during the spiral notch test. For all loads applied the amount of elongation was higher for new material in comparison with service-exposed material, except for the tests conducted at 204 MPa, where the new material failed in a brittle manner in the CGHAZ, with lower elongation than the

service-exposed material. Failure of the service-exposed material took place at lower temperatures than the comparative new material for all loads applied.

The fracture surfaces studied by SEM clearly show two different fracture mechanisms that lead to failure during testing (204 MPa new and service-exposed). The new material failed with a brittle, intergranular failure mechanism. The service-exposed material all failed in a ductile manner at all loads tested. Some microductility along the prior austenite grains boundaries were observed. The fractography shows that the new material, tested at 204 MPa failed due to a reheat cracking mechanism.

The state of the microstructures shows that the CGHAZ simulation for new and service-exposed material resulted in almost an identical HAZ in the material. Grain sizes were larger than expected during actual welding but this is common when weld simulation is performed. After PWHT (spiral notch test) the HAZ's of both states showed tempering of the bainite. A real difference was observed in the base metal microstructure of the two different states of 2¼Cr-1Mo. For new material it was ferrite and tempered bainite. For the service-exposed material no ferritic structure was present; it only consisted of decomposed bainite with carbides dispersed throughout the matrix. The creep properties of the service-exposed material were thus lower than that of the new material during the PWHT (spiral notch test). This is due to the fact that the structure is decomposed and that the meta-stable carbides that add creep strength have transformed to the stable carbide type, with a lower creep strength.

The hardness profiles also showed that after CGHAZ simulation, the hardness for new and service-exposed materials are fairly similar in the HAZ. The base metal hardness of the service-exposed material was mostly lower than that of the new material. No significant hardening of the HAZ took place during PWHT, probably due to the lack of vanadium. No significant changes took place in the base metal of the new and service-exposed material during PWHT.

5.8 CONCLUSION

Unexposed (new) 2¼Cr-1Mo material can be susceptible for reheat cracking after welding, though not as severely as new ½Cr-½Mo-¼V. The lack of vanadium as alloying element probably leads to 2¼Cr-1Mo material being less susceptible. No severe secondary hardening can take place, only chrome and molybdenum carbides add to creep strength. The service-exposed material showed no susceptibility for reheat cracking, for the test conditions employed. The softer base metal of the service-exposed state protected the HAZ during PWHT by being the primary area to undergo deformation under the influence of tensile stress due to the fact that there is little or no meta-stable carbides that add creep strength. It seems that starting microstructure (state of the carbides) before welding can play a role with regards to reheat cracking.

5.9 REFERENCES

1. Stahlschlüssel – Key to Steel, 1998

CHAPTER 6: X20CrMoV12-1

6.1. INTRODUCTION

X20CrMoV12-1 (X20) material was developed during the sixties and seventies to enhance the properties of creep resistant steels for elevated temperature use to improve boiler efficiency. In South African power stations the material was first used on wide scale during the late 1970's and during the 1980's. The steel is normally used in the quenched and tempered condition and the starting microstructure is tempered martensite. The service-exposed material was obtained from Duvha power station and operated at 540°C for 150 000 hours.

6.1.1 General Chemical Composition[1]

ELEMENT	min %	max %
C	0.17	0.23
Si	0	0.50
Mn	0	1.00
P	0	0.030
S	0	0.030
Cr	10.0	12.5
Mo	0.80	1.20
Ni	0.30	0.80
V	0.25	0.35

6.1.2 Mechanical Properties[1]

PROPERTY	VALUE
Yield stress	>= 490 MPa
Tensile Strength	690 – 830 MPa
Elongation	>= 16 %
Impact value (DVM)	>= 41 J
Hardness Brinell	205 – 250 HB_{30}

Mechanical Properties at ambient temperature (Values for longitudinal sample bars <= 60mm ∅.

6.2 CHEMICAL ANALYSIS

Eskom accredited methods No 106 (Alloying elements) and 119 (Carbon) were used on the new and service exposed material. The results are shown in Table 6.1. The original result sheets are attached in Appendix 1.

Element	New Material	Service Exposed Material (± 150 000 h at 540°C)
Carbon	0.22	0.19
Chromium	12.05	12.29
Nickel	0.75	0.48
Manganese	0.59	0.45
Molybdenum	0.82	0.78
Vanadium	0.26	0.30
Sulphur	0.004	0.013
Phosphorus	0.016	0.020
Silicon	0.07	0.013
Titanium	0.01	0.01
Copper	0.11	0.09
Cobalt	0.01	0.01
Niobium	0.01	0.005
Tin	0.01	0.01
Tungsten	0.005	0.005

Table 6.1: Chemical analysis for new and service exposed X20CrMoV121 material

The chemical composition of the test material was within specified range for X20 material.

6.3 SPIRAL NOTCH TEST RESULTS (Constant load, PWHT Thermal Cycle)

The results from the spiral notch tests on the new and service exposed X20 are listed in Table 6.2 and Graphs 6.1 and 6.2.

Table 6.2: Position of final fracture for X20 steel samples

Nominal Stress (MPa)	X20 New Material	X20 Service-exposed Material
407	Base Metal	Base Metal
356	Base Metal	Base Metal
305	Base Metal	Base Metal
254	Base Metal	Base Metal

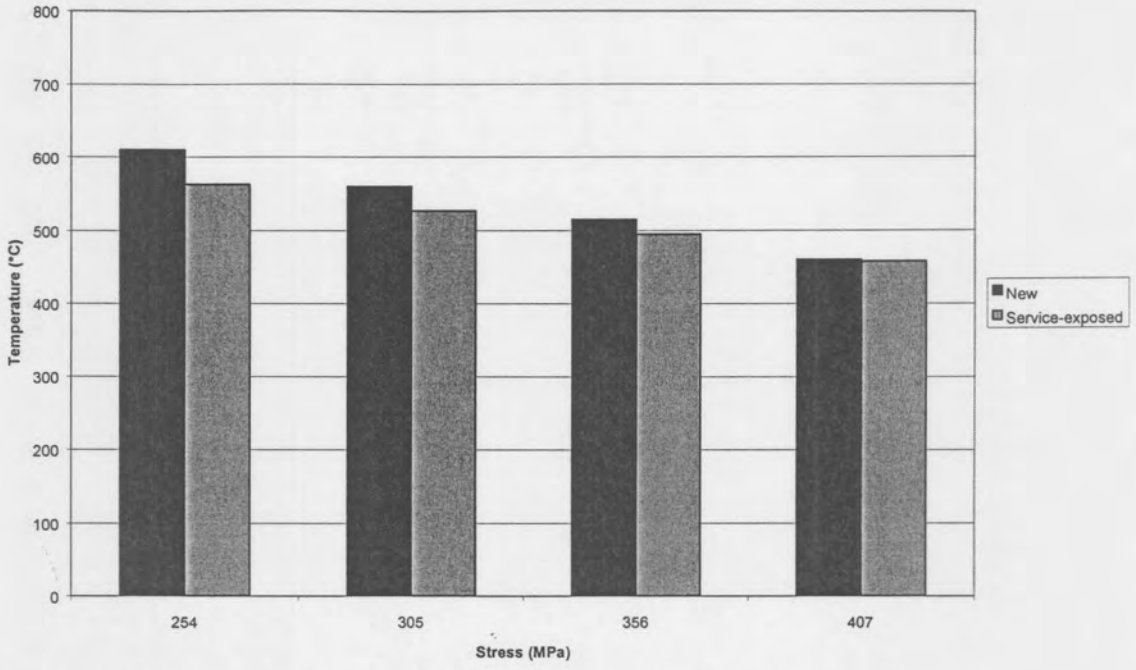

Graph 6.1: Temperature of final fracture for X20 steel samples

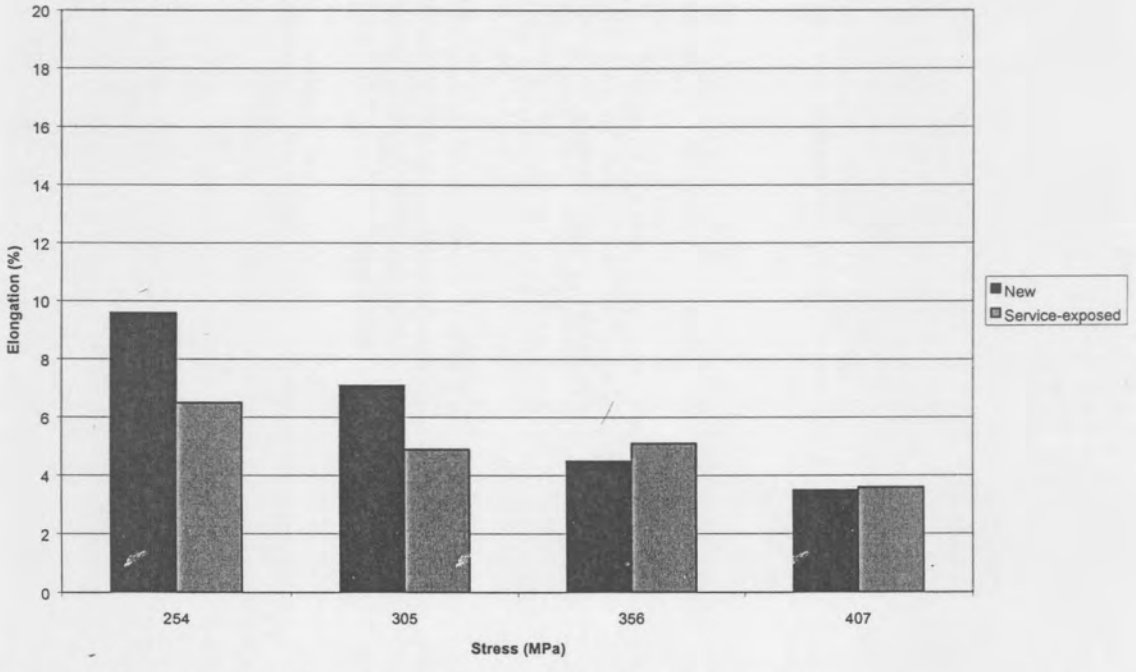

Graph 6.2: Amount of elongation for X20 steel samples

The experimental graphs compiled during these tests are attached in Appendix 2.

6.4 SEM FRACTOGRAPHY

The fracture surfaces of the samples tested at 254 MPa for both new and service exposed material was studied by SEM to confirm the mechanism of fracture. The fracture surfaces are shown in Figures 6.1 to 6.4.

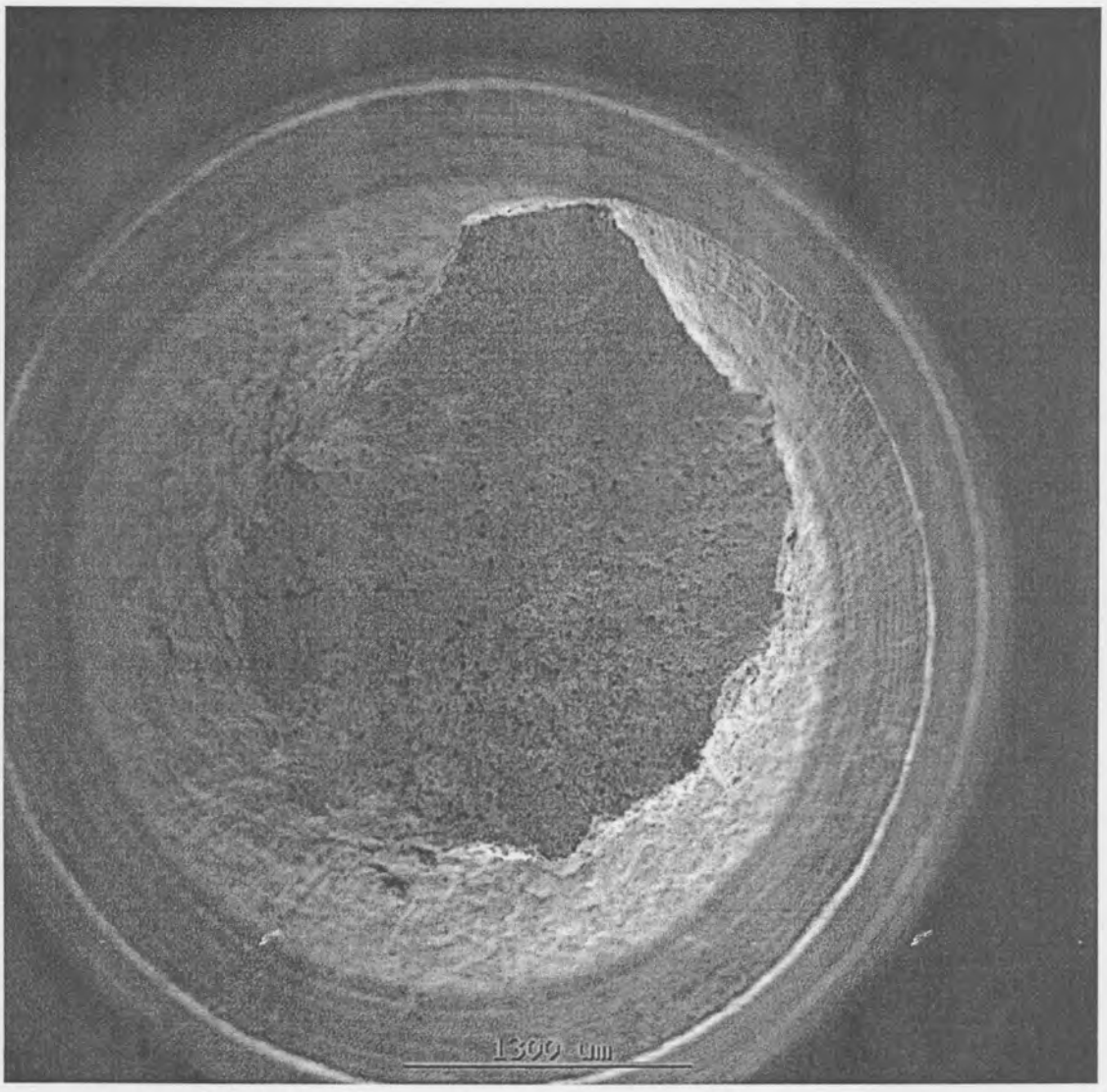

Figure 6.1: X20 New Material – Ductile fracture surface, 254 MPa

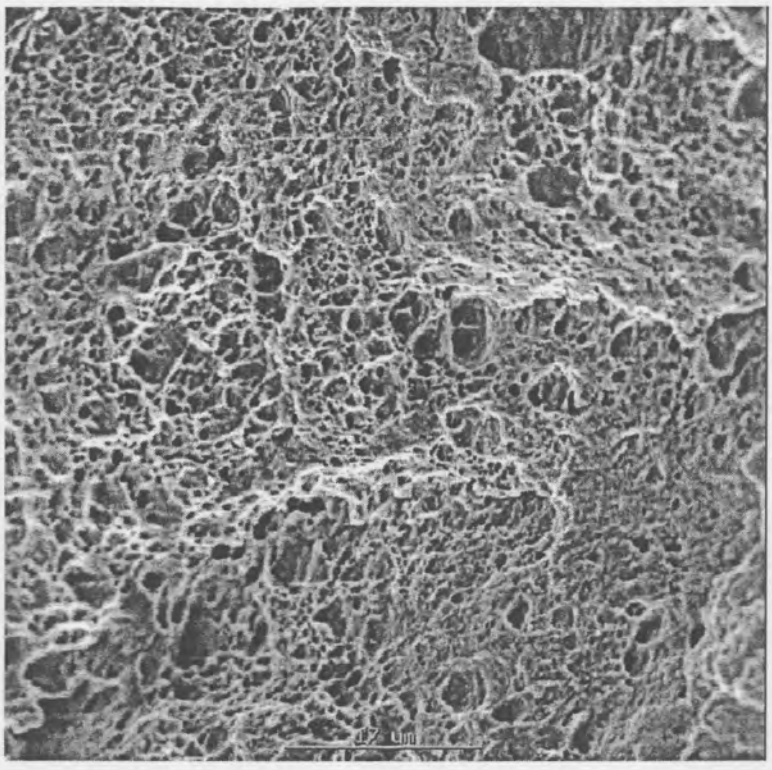

Figure 6.2: High magnification of Figure 6.1 (X20 New). Microvoid coalescence (MVC)

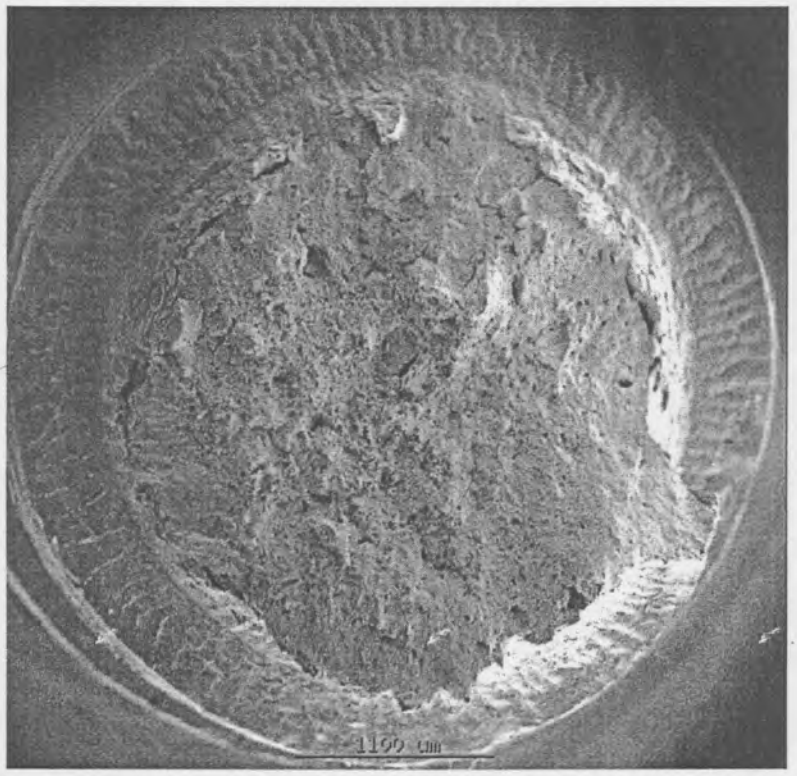

Figure 6.3: X20 Service exposed Material – Ductile fracture surface, 254 MPa

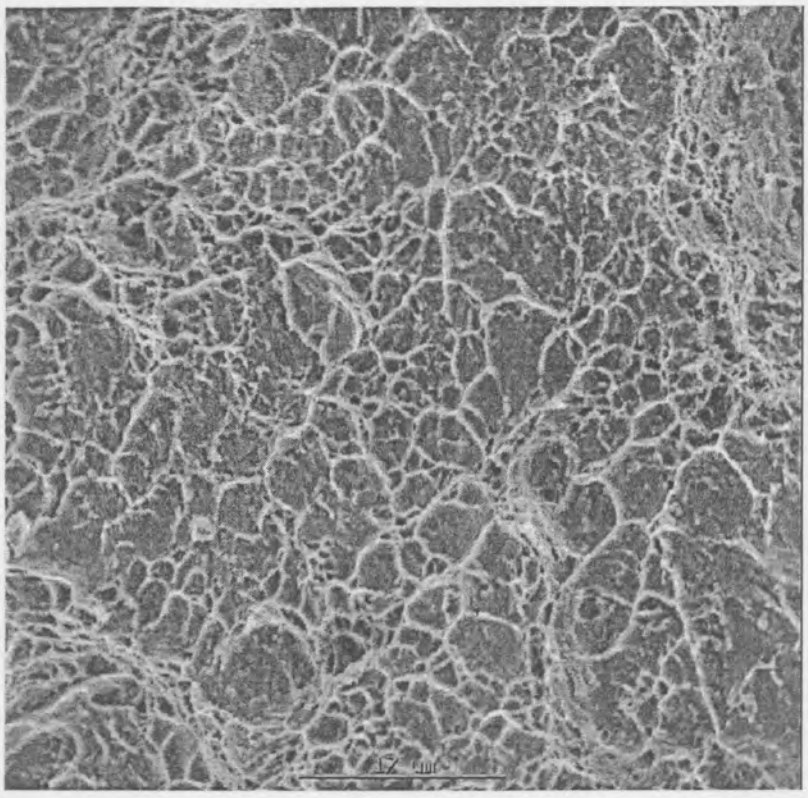

Figure 6.4: High magnification of Figure 6.3 – Microvoid coalescence (MVC)

6.5 METALLOGRAPHY

Metallographic samples were prepared from new and service exposed material after the CGHAZ thermal simulation. The samples tested at 254 MPa (new and service exposed) were also taken and metallographic samples were prepared. The resulting microstructures are shown in Figures 6.5 to 6.10. Descriptions of the structures are given in Table 6.3.

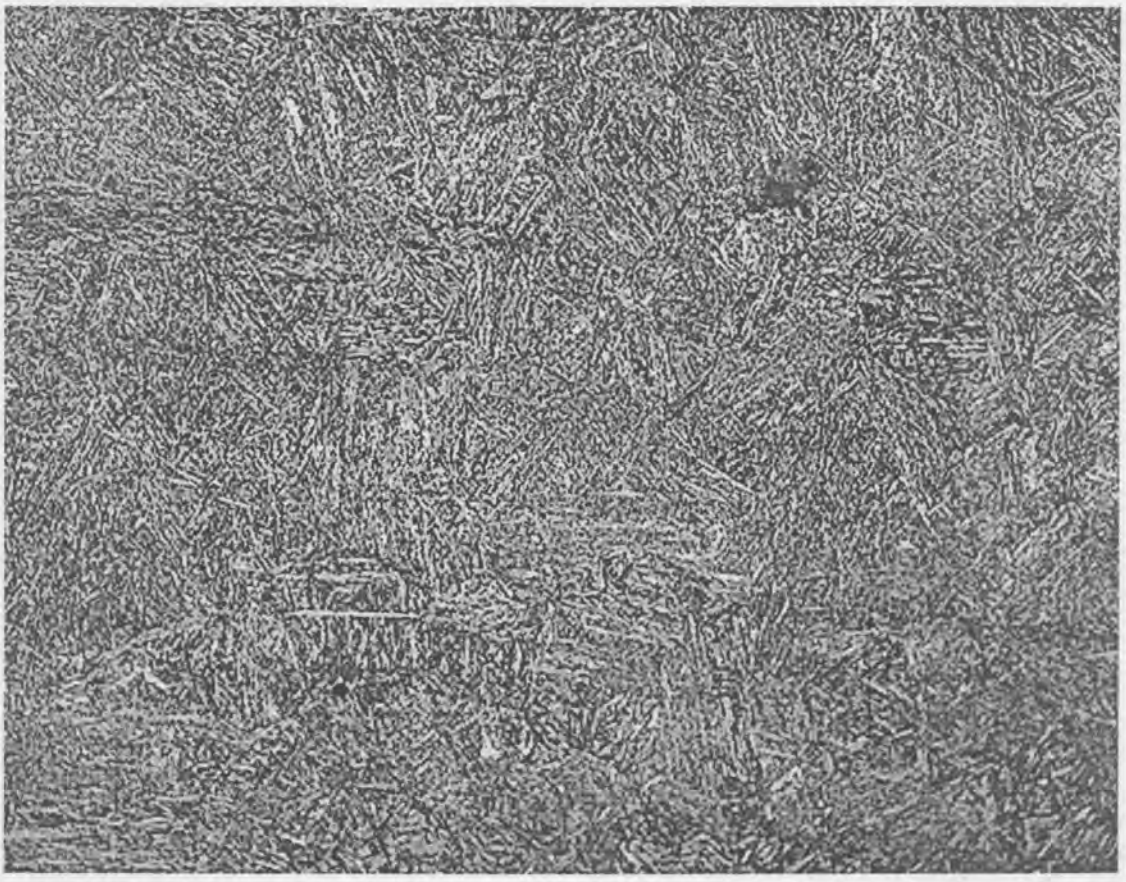

Figure 6.5: Base metal of new material – 200x (After thermal simulation)

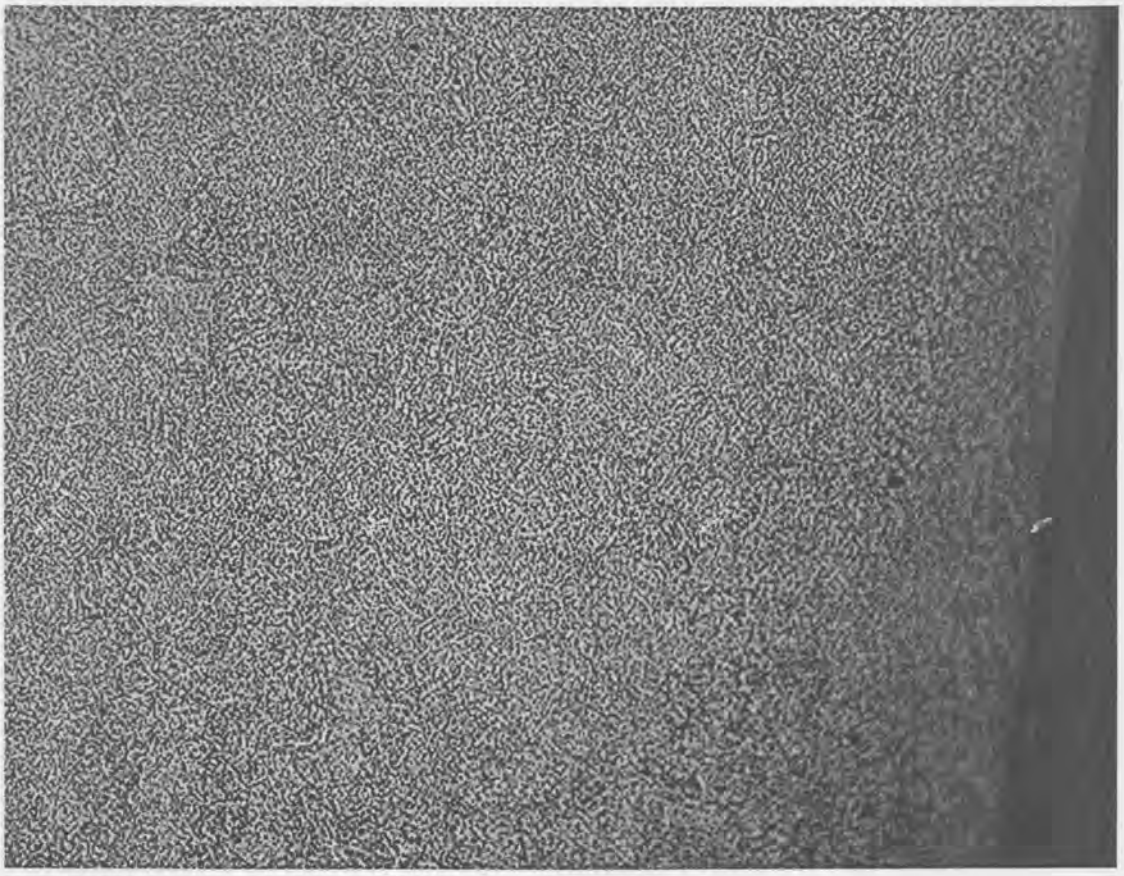

Figure 6.6: CGHAZ of new material – 200x (After thermal simulation)

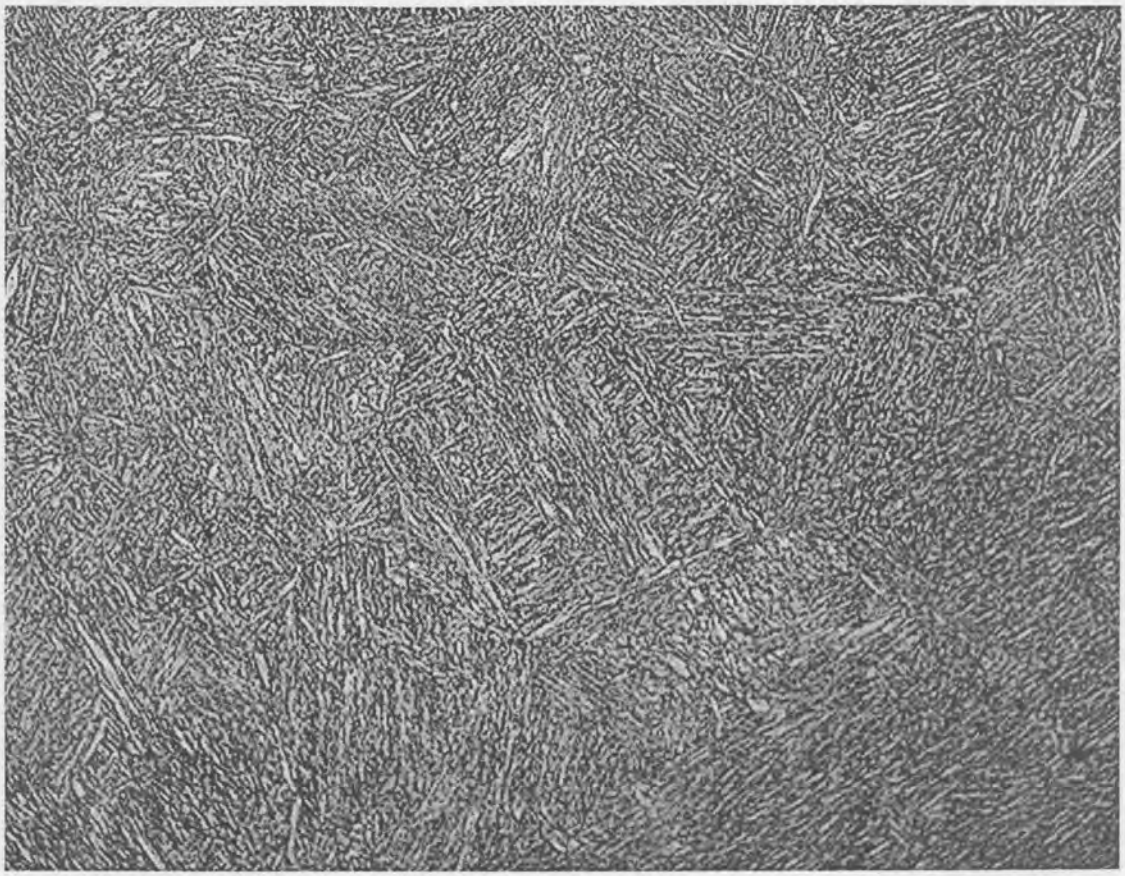

Figure 6.7: Base metal of service exposed material – 200x (After thermal simulation)

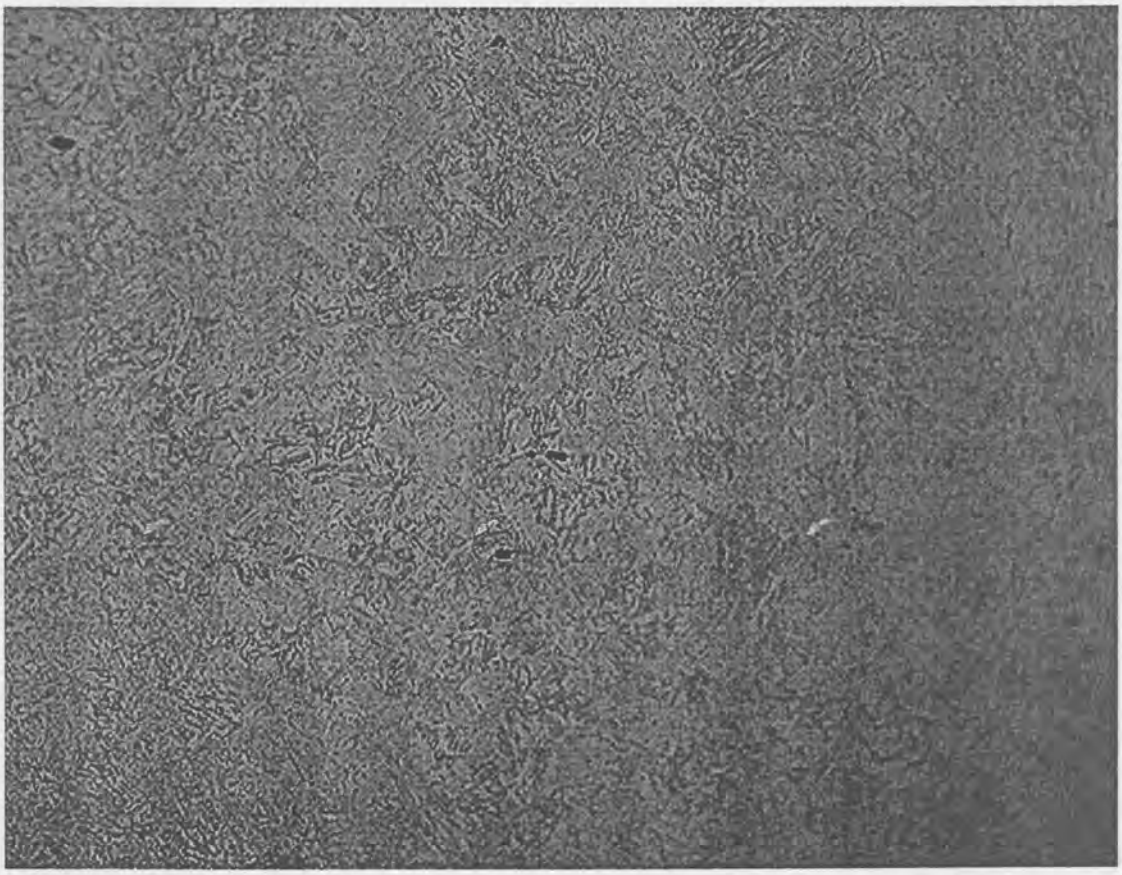

Figure 6.8: CGHAZ of service exposed material – 200x (After thermal simulation)

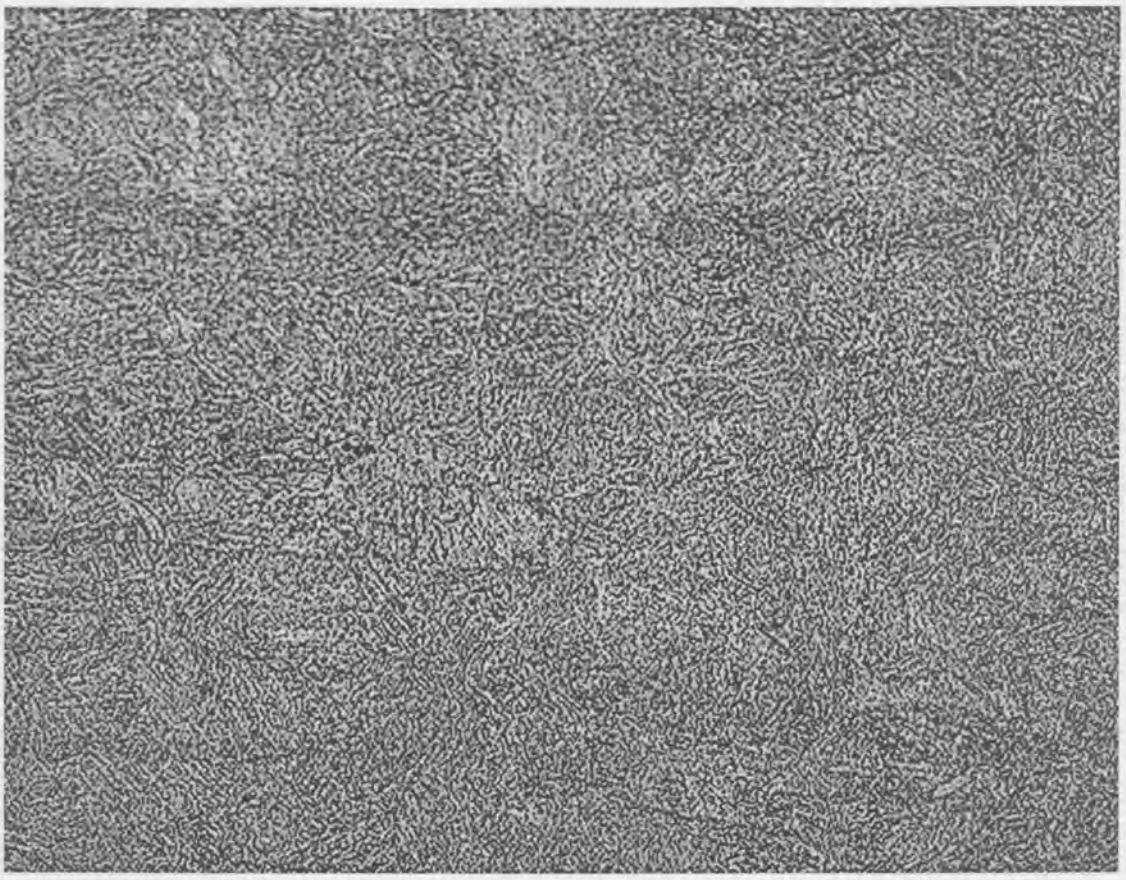

Figure 6.9: Base metal of new material – 200x (After PWHT)

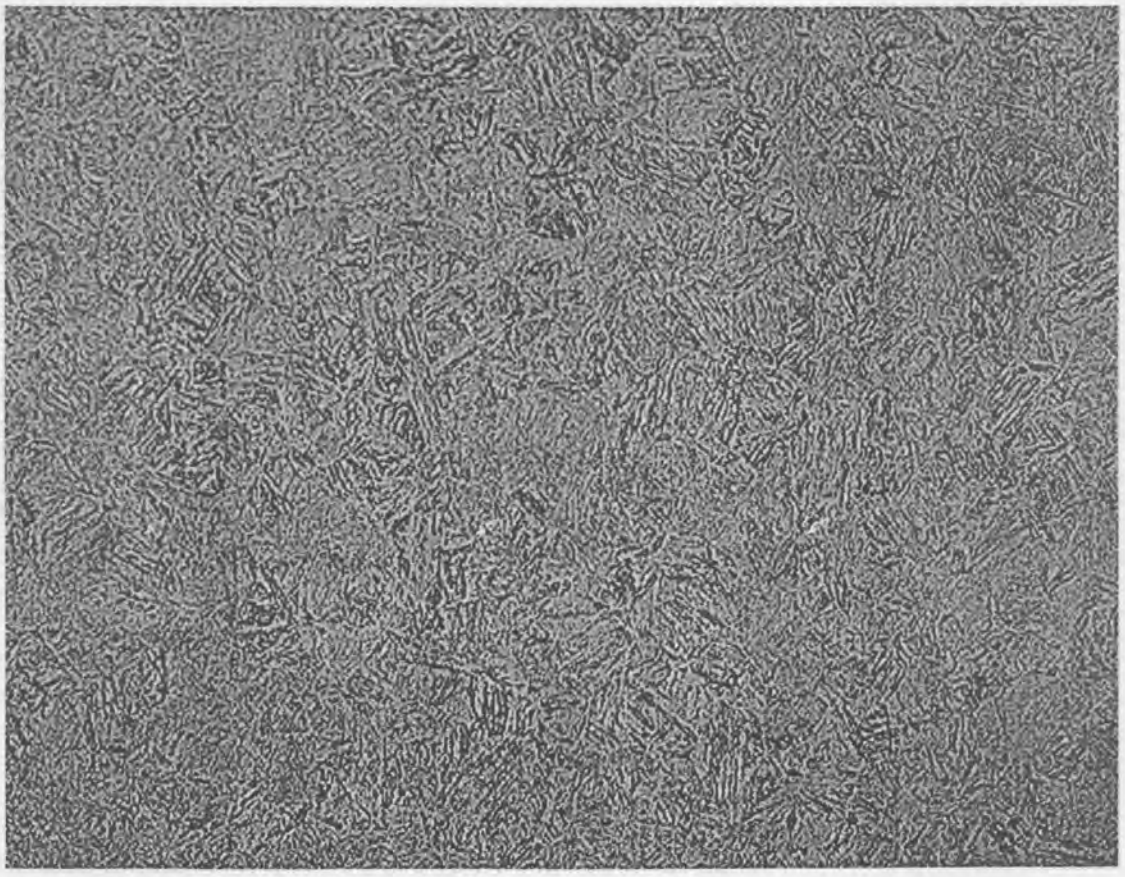

Figure 6.10: CGHAZ of new material – 200x (After PWHT).

Table 6.3: Description of metallographic sample microstructures

Condition	State	Figure No.	Description
As-simulated	New	6.5	Base Metal: Tempered martensite (quenched and tempered condition), with a dispersion of fine carbides on the prior austenite grain boundaries, visible as strings.
		6.6	CGHAZ: Partly tempered martensite. Fine carbides are visible in some of the scattered tempered colonies.
	Service exposed	6.7	Base Metal: Tempered martensite (quenched and tempered condition), with a dispersion of fine carbides on the prior austenite grain boundaries, visible as strings. Some δ-ferrite also present. Some grains also show the ferrite with carbides (these areas are normally softer).
		6.8	CGHAZ: Fine carbides dispersed throughout the structure. Structure looks tempered – probably due to auto tempering during the CGHAZ simulation.
PWHT	New	6.9	Base Metal: Tempered martensite (quenched and tempered condition), with a dispersion of fine carbides on the prior austenite grain boundaries, visible as strings. Overall the structure is more tempered than the structure in the as-simulated condition.
		6.10	CGHAZ: Partly tempered martensite. Some martensite still appears fresh while other martensite areas are more tempered with fine carbides.

6.6 HARDNESS SURVEY

Hardness profiles were determined from the same samples used in the metallography. A Vickers microhardness-testing machine with a load of 300g was used. The profiles start at the centre of the HAZ and extend through to the base metal. The profiles are shown in Graph 6.3.

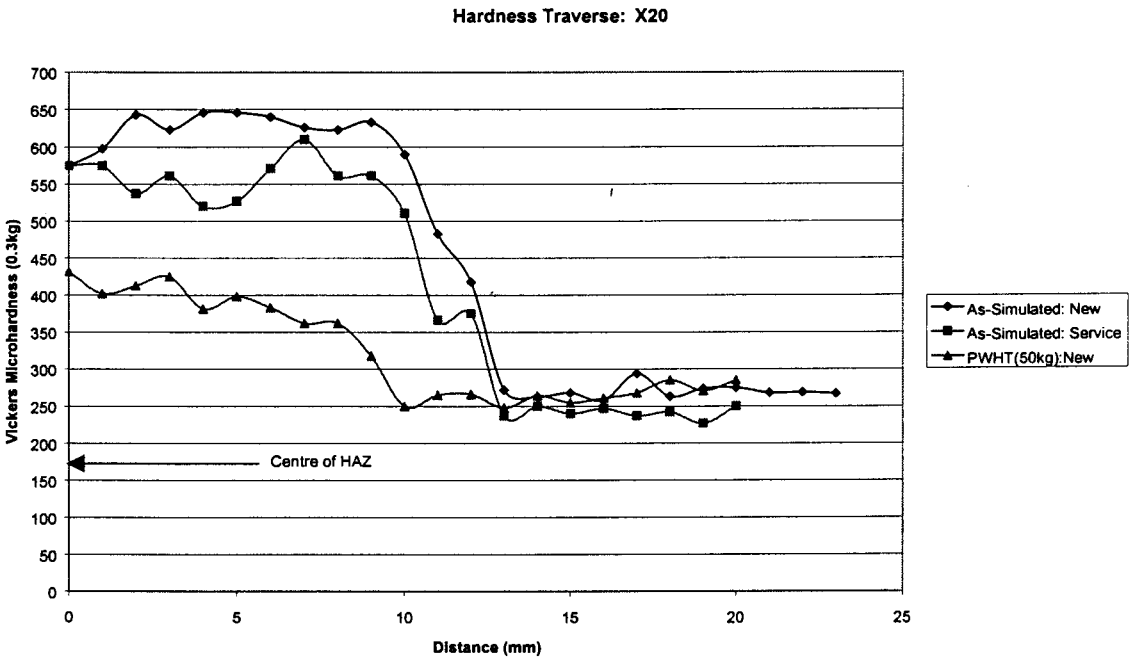

Graph 6.3: Hardness profile of X20 material – New and Service exposed

6.7 DISCUSSION

The results from the spiral notch test revealed a significant difference between the low alloy ferritic grades (½Cr-½Mo-¼V and 2¼Cr-1Mo) and a higher alloyed grade like X20 (12Cr-1Mo). All the samples tested, both new and service-exposed material failed in the base metal area of the sample at all the different testing loads. The failure temperature of the new material for all the samples tested were higher than the comparative service-exposed material. The amount of elongation per sample was higher for the new material than the service-exposed material. The ductility of X20 at elevated temperature is superior to the low alloy ferritic grades. The strength of the material is due to

the high amount of chromium that is present in the structure as chromium carbides as well as molybdenum carbides.

From the SEM photographs it is evident that both the new and service-exposed material failed due to a ductile fracture mechanism. Due to the notch a stress concentration is present and the yield strength of the base metal is lower than the HAZ during the PWHT. The base metal will be the primary region where creep deformation occurs under the influence of a tensile stress up to the point of failure.

The structure of the base metal in the service-exposed condition is such that it will be softer than the base metal of the new material. This leads to the failure in the base metal areas because the yield strength for the base metal is lower than that of the CGHAZ. CGHAZ simulation resulted in similar structures of partly tempered martensite. This is due to the very high hardenability of X20. A fully martensitic structure can thus be obtained in these materials with slower cooling rates in comparison with that of to the two ferritic grades (½Cr-½Mo-¼V and 2¼Cr-1Mo). During cooling of materials with a high hardenability the martensite that formed first is still at a relatively high temperature and longer periods of time and undergoes auto-tempering as the work piece cools down to room temperature. The structure of the sample that underwent PWHT (spiral notch test) showed a tempered structure due to the thermal cycle as expected.

The hardness profiles showed the service-exposed material base metal had a lower hardness than the new material. The hardness of the HAZ's showed some difference. After PWHT the hardness of the HAZ is significantly reduced as toughness and ductility are restored due to the tempering of the hardened structure. The hardness (yield strength) is still higher than that of the base metal, which points to the fact that the base metal is the area where creep deformation was concentrated during PWHT.

6.8 CONCLUSION

X20 material creep strength is obtained due to the high content of chromium as alloying element with molybdenum in small quantities. The hardenability of the steel is very high. PWHT restores toughness and ductility and does not seem to increase the strength, as is the case with ½Cr-½Mo-¼V. Due to the high hardenability, a X20 component during welding operations is held at a certain temperature before PWHT. This could prevent full transformation of the HAZ to martensite and retained austenite could be present before PWHT. The temperature before PWHT must be such that it prevents cracking due to the high hardenability and also to allow almost full transformation. The yield strength of the base metal for new and service-exposed material will always be lower than the HAZ making it the primary region for creep deformation during PWHT to allow stress relief to occur.

6.9 REFERENCES

1. Stahlschlüssel – Key to Steel, 1998

CHAPTER 7: P91 (X10CrMoVNb9-1)

7.1 INTRODUCTION

Up to the 1950's, the highest ferritic alloy used in most boilers was the low alloy 2¼Cr-1Mo. By the end of the 1950's through the 60's 70's and 80's alloy development continued. The end result was P91. A 9%Cr steel with 1% Molybdenum and various alloying elements. The steel is normally used in the quenched and tempered condition and the starting microstructure is tempered martensite.

7.1.1 General Chemical Composition[1]

ELEMENT	min %	max %
C	0.08	0.12
Si	0.20	0.50
Mn	0.30	0.60
P	0	0.020
S	0	0.010
Cr	8.00	9.50
Mo	0.85	1.05
Ni	0	0.40
V	0.18	0.25
Nb	0.06	0.10
Al	0	0.040
N	0.030	0.070

7.1.2 Mechanical Properties[2]

PROPERTY	VALUE
Yield stress	>= 415 MPa
Tensile Strength	585 – 770 MPa
Elongation	>= 20 %
Impact value (DVM)	>= 80 J
Hardness Brinell	218 – 250 HB_{30}

7.2 CHEMICAL ANALYSIS

Eskom accredited methods No 106 (Alloying elements) and 119 (Carbon) were used on the new and service-exposed material. The results are shown in Table 7.1. The original result sheets are attached in Appendix 1.

Element	New Material
Carbon	0.22
Chromium	9.19
Nickel	0.19
Manganese	0.48
Molybdenum	0.86
Vanadium	0.24
Sulphur	0.001
Phosphorus	0.013
Silicon	0.27
Titanium	0.01
Copper	0.05
Cobalt	0.005
Niobium	0.07
Tin	0.01
Tungsten	0.005

Table 7.1: Chemical analysis for new and artificially aged P91 material

The chemical composition of the test material was within specified range for P91 material. Only new material was available for testing.

7.3 SPIRAL NOTCH TEST RESULTS (Constant load, PWHT Thermal Cycle)

Due to fact that no service-exposed material was available, a batch of the new material was artificially aged to represent service-exposed material (described in Chapter 3). The results from the spiral notch tests on the new and artificially aged P91 are shown in Table 7.2 and Graphs 7.1 and 7.2.

Table 7.2: Position of final fracture for P91 steel samples

Nominal Stress (MPa)	P91 New Material	P91 Artificially aged Material
407	Base Metal	Base Metal
356	Base Metal	Base Metal
305	Base Metal	Base Metal
254	Base Metal	Base Metal

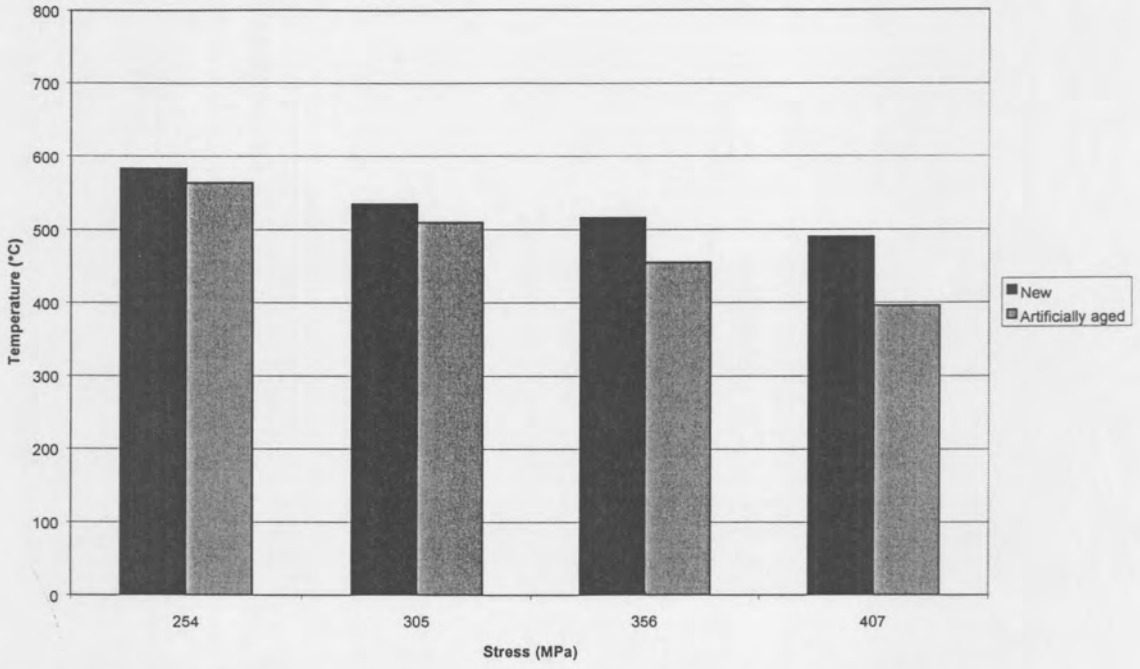

Graph 7.1: Temperature of final fracture for P91 steel samples

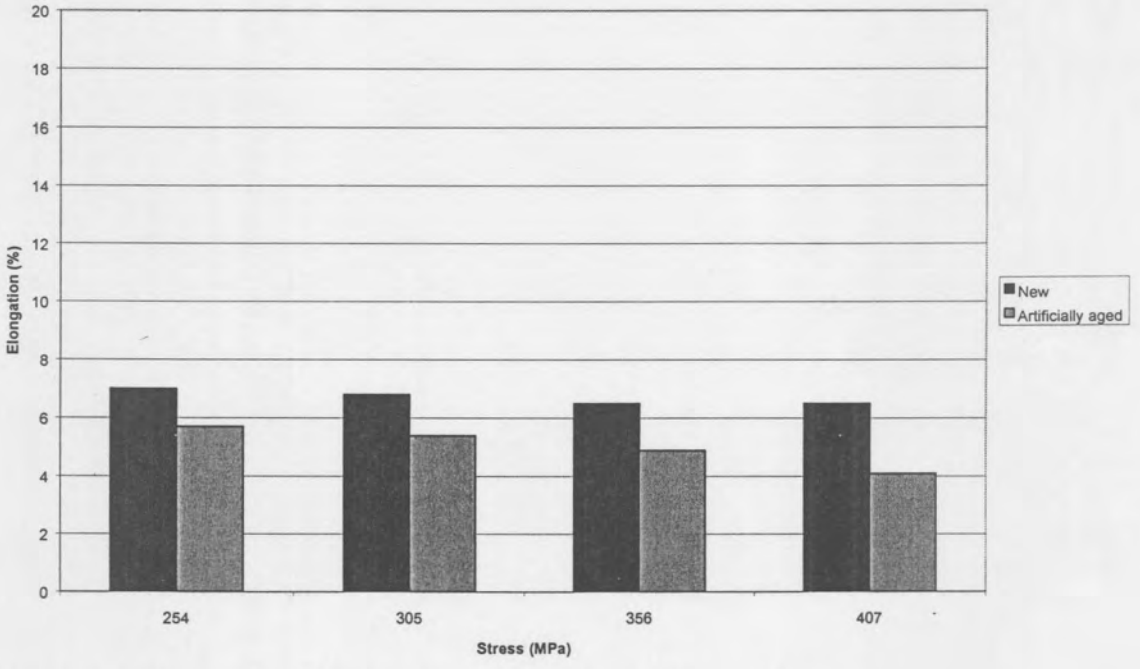

Graph 7.2: Amount of elongation for P91 steel samples

The experimental graphs compiled during these tests are attached in Appendix 2.

7.4 SEM FRACTOGRAPHY

The fracture surfaces of the samples tested at 254 MPa for both new and service exposed material was studied by SEM to confirm the mechanism of fracture. The fracture surfaces are shown in Figures 7.1 to 7.4.

Figure 7.1: P91 New Material – Ductile fracture surface, 254 MPa

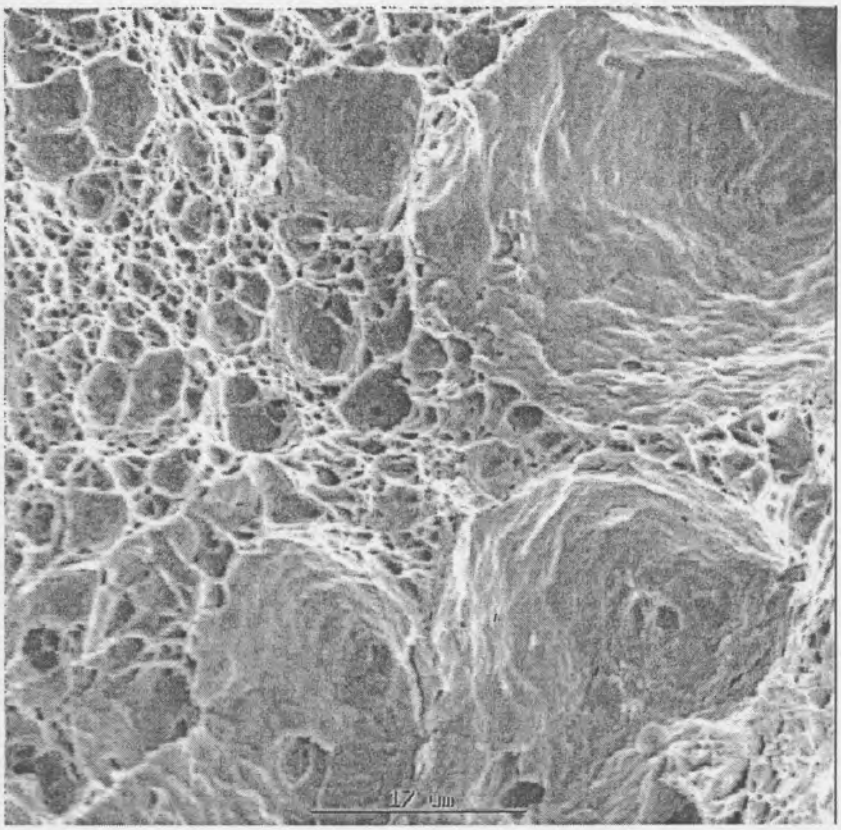

Figure 7.2: High magnification of Figure 7.1 (P91 New). Microvoid coalescence (MVC)

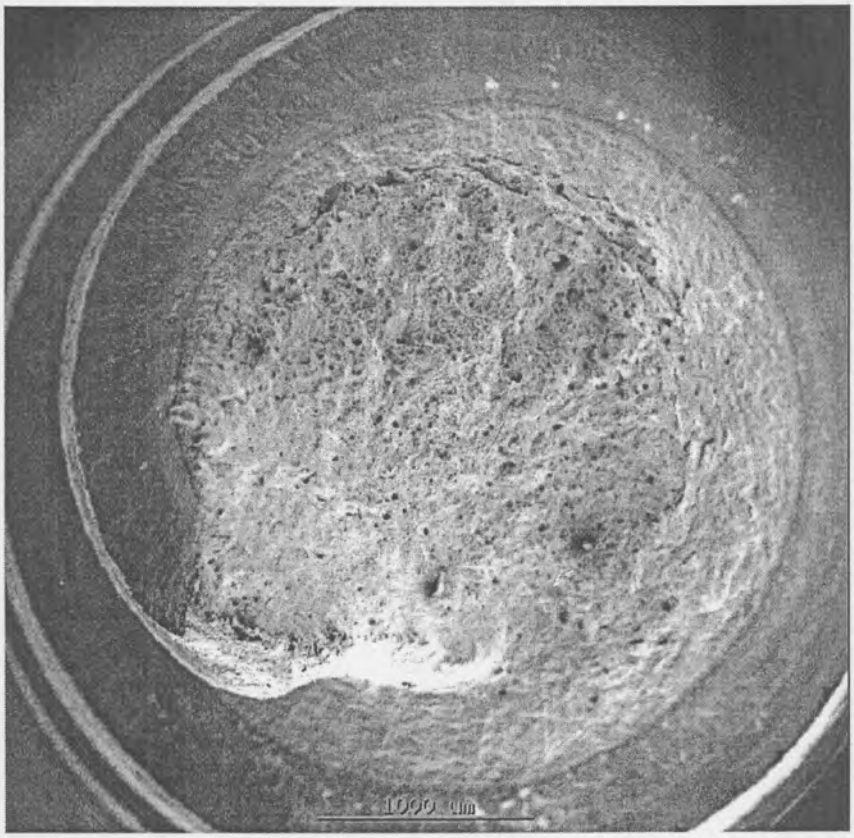

Figure 7.3: P91 Service exposed Material – Ductile fracture surface, 254 MPa

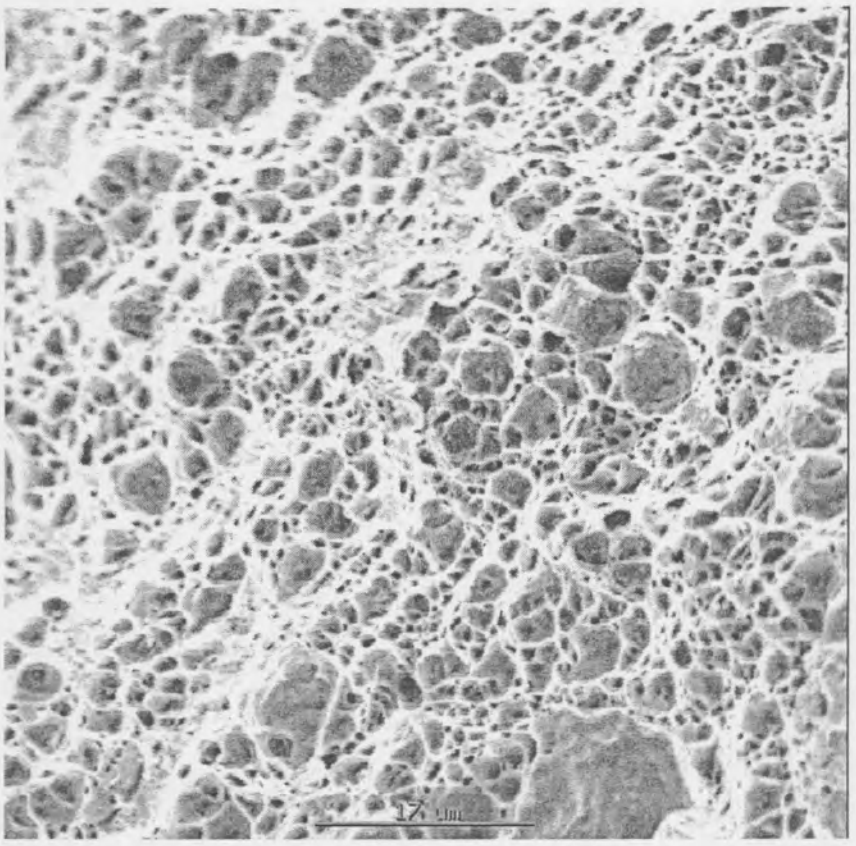

Figure 7.4: High magnification of Figure 7.3 – Microvoid coalescence (MVC)

7.5 METALLOGRAPHY

Metallographic samples were prepared from new and service exposed material after the CGHAZ simulation. The samples tested at 254 MPa (new and artificially aged) were also taken and metallographic samples were prepared. The resulting microstructures are shown in Figures 7.5 to 7.12. Descriptions of the structures are given in Table 7.3.

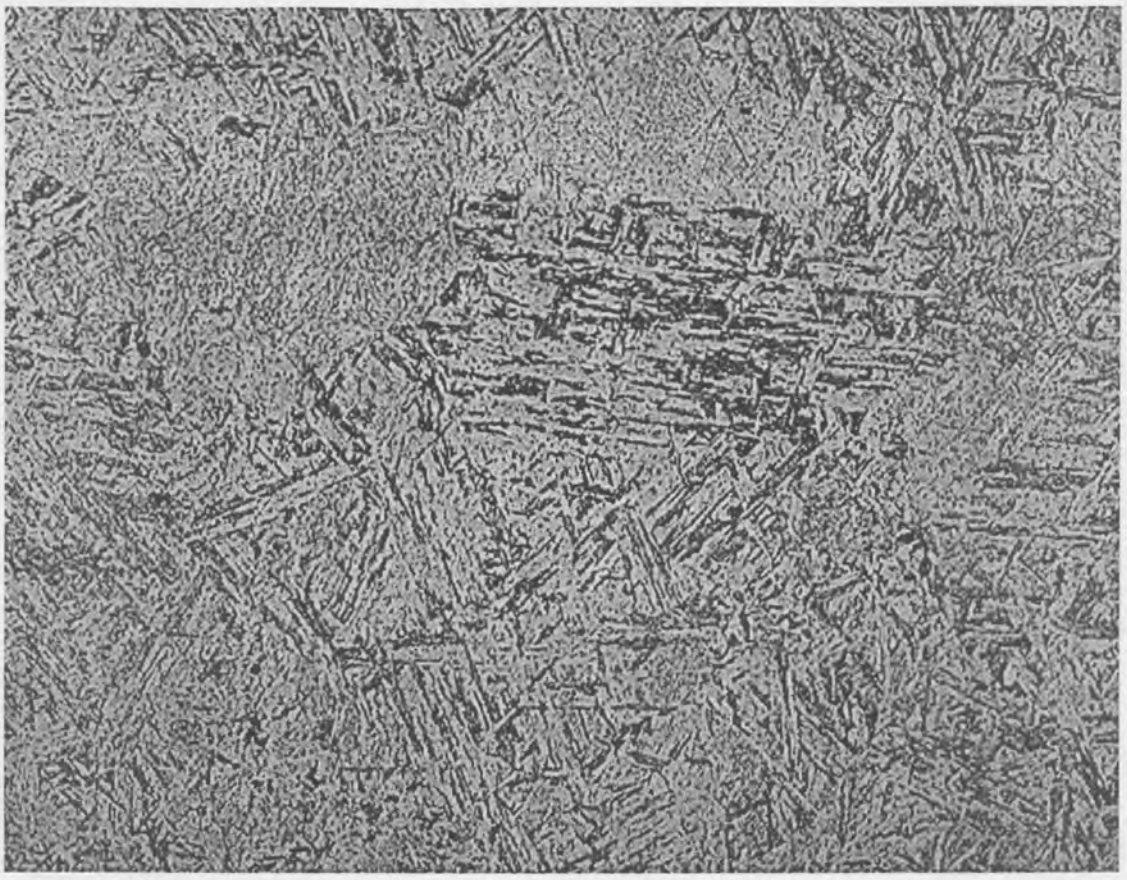

Figure 7.5: Base metal of new material – 200x (After thermal simulation)

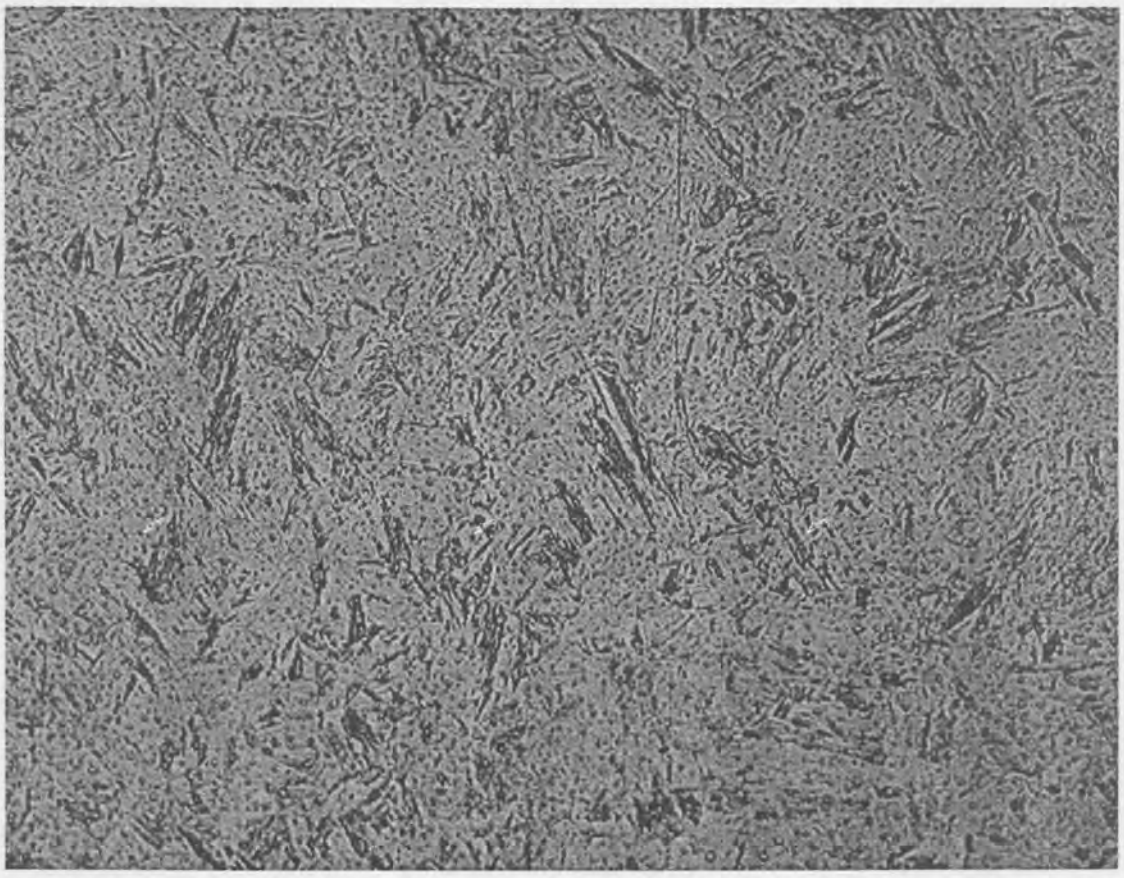

Figure 7.6: CGHAZ of new material – 500x (After thermal simulation)

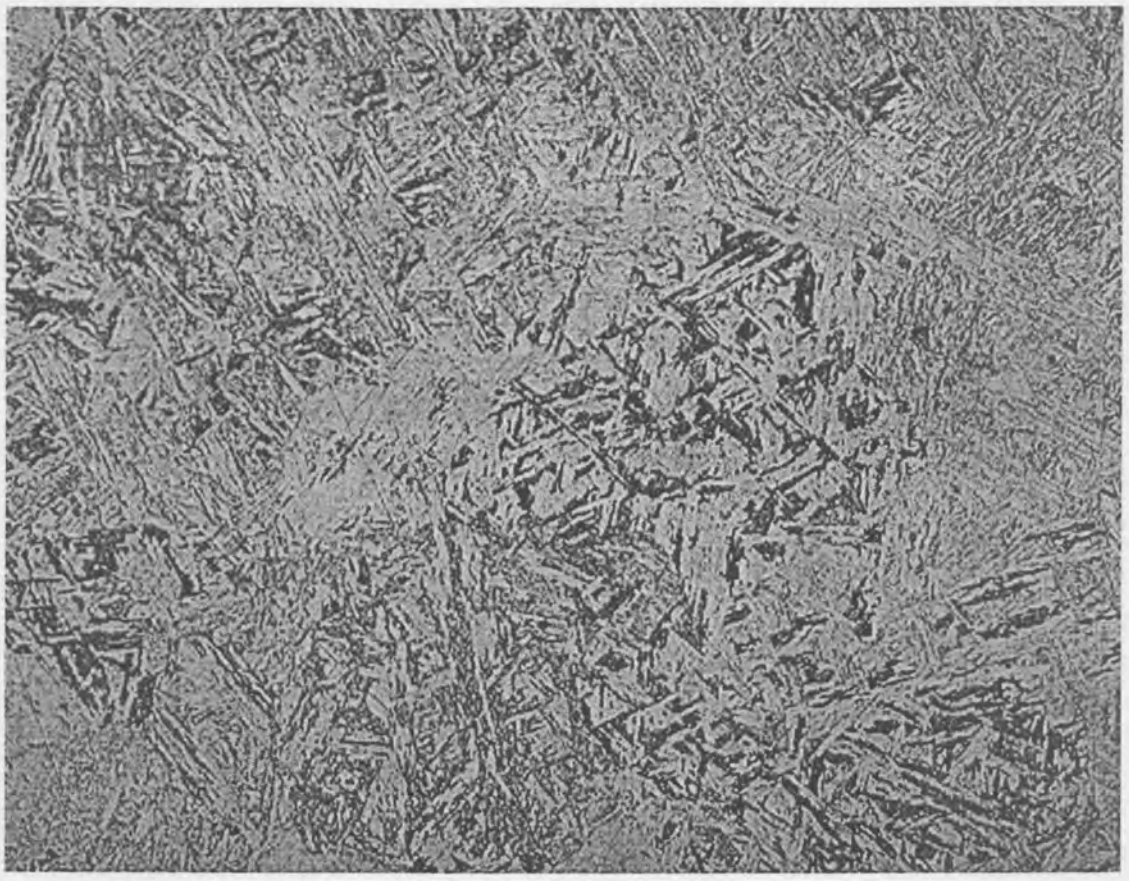

Figure 7.7: Base metal of aged material – 200x (After thermal simulation)

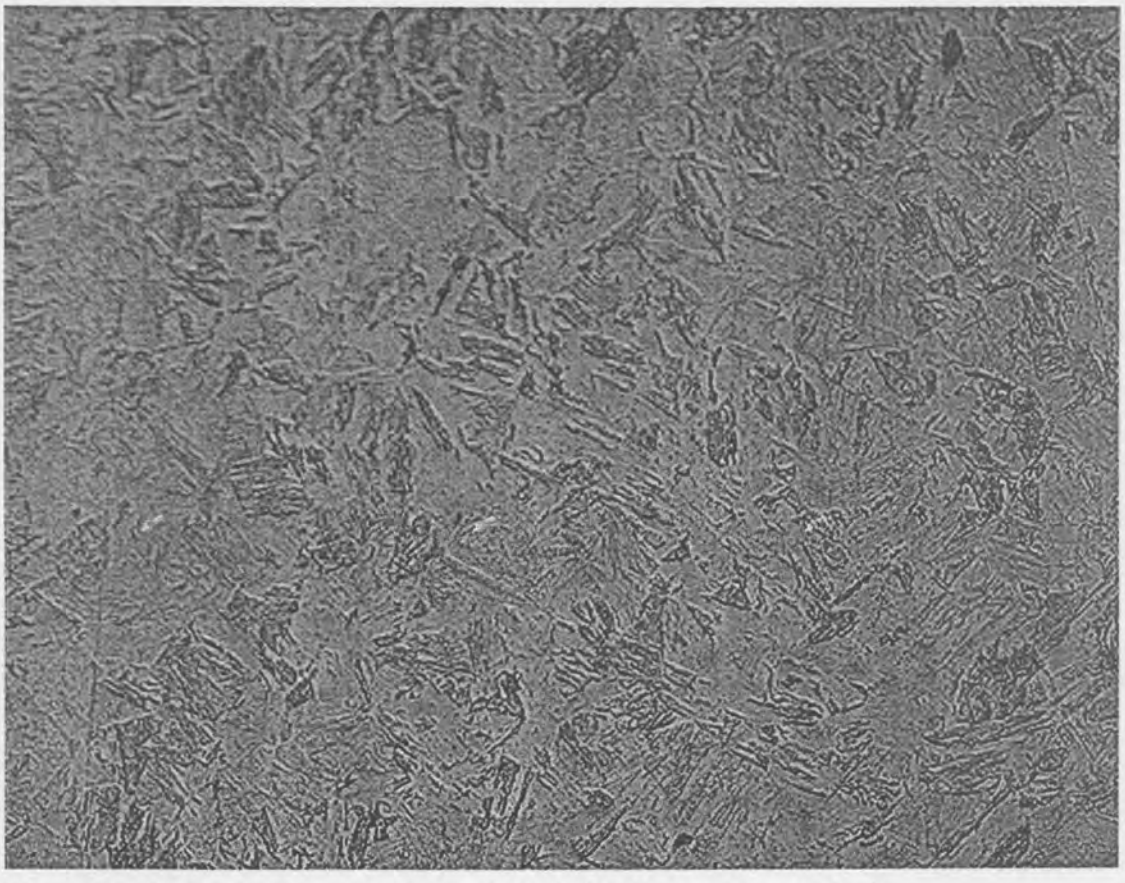

Figure 7.8: CGHAZ of aged material – 500x (After thermal simulation)

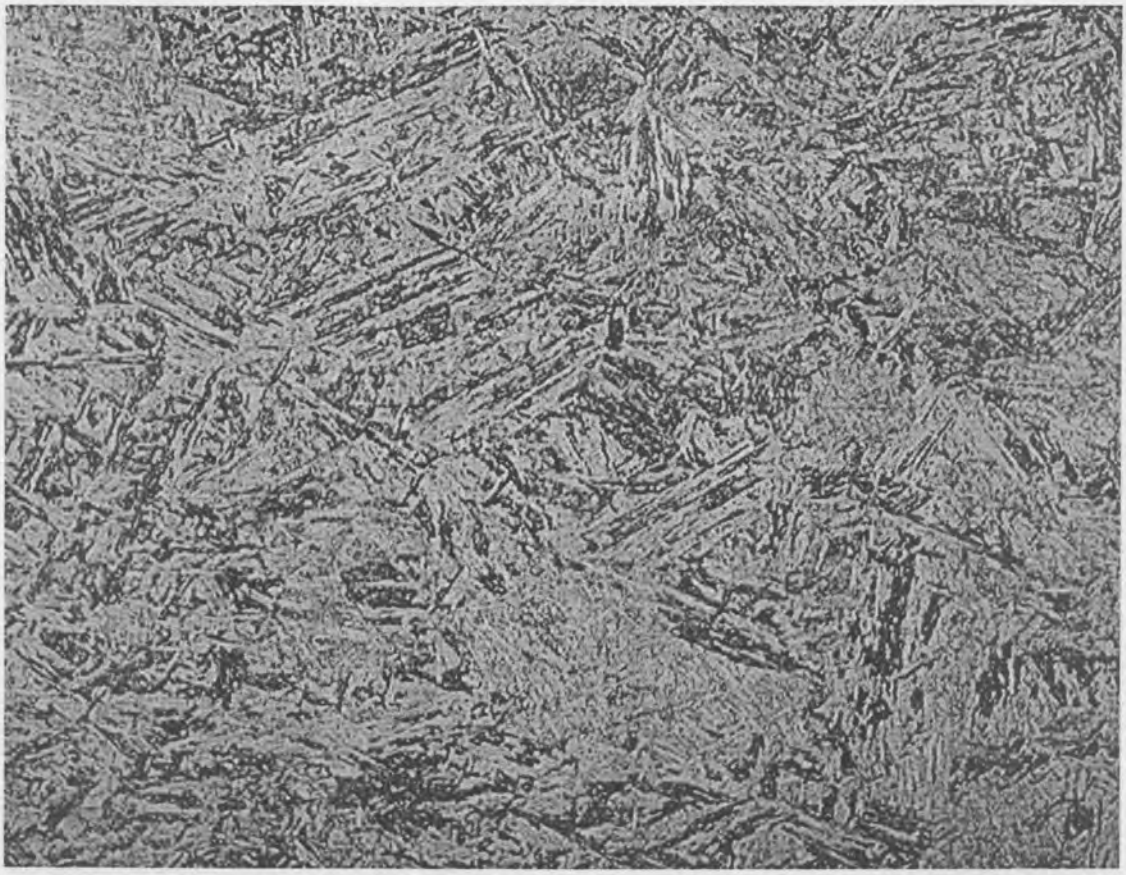

Figure 7.9: Base metal of new material – 200x (After PWHT)

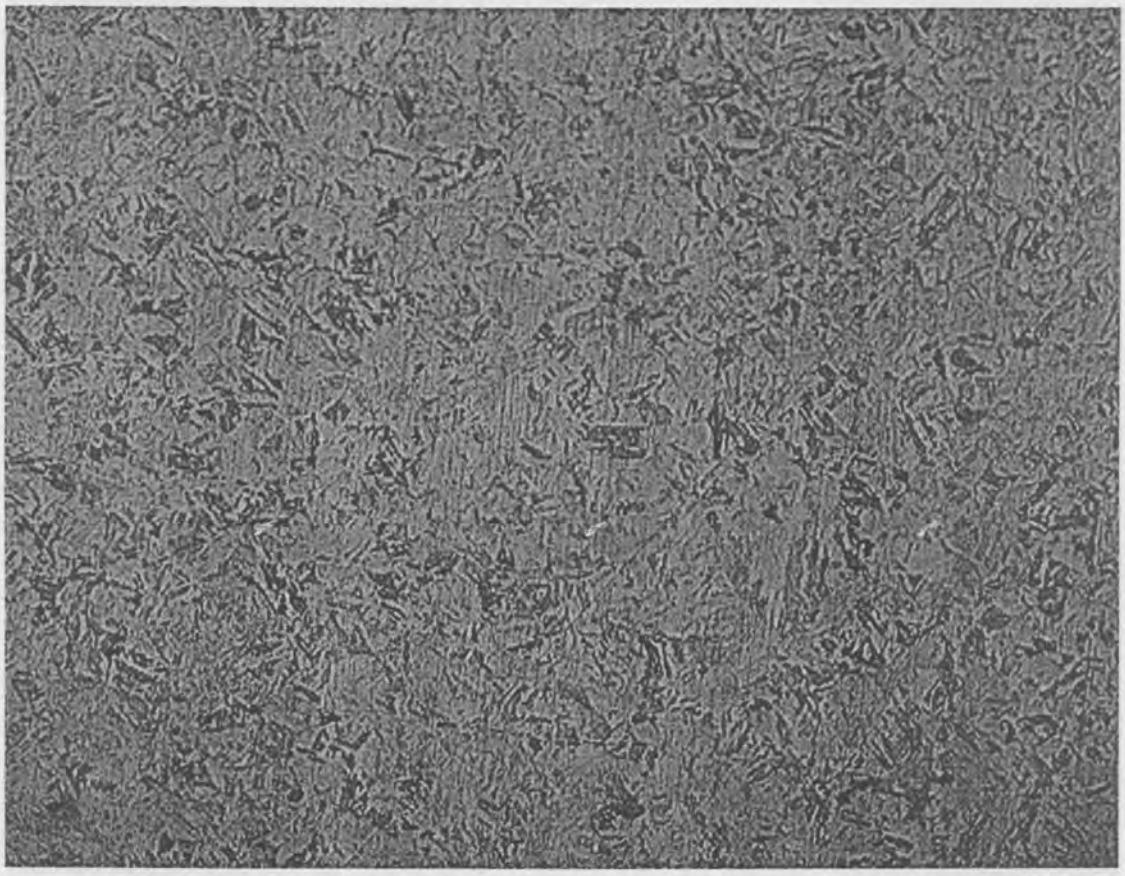

Figure 7.10: CGHAZ of new material – 200x (After PWHT)

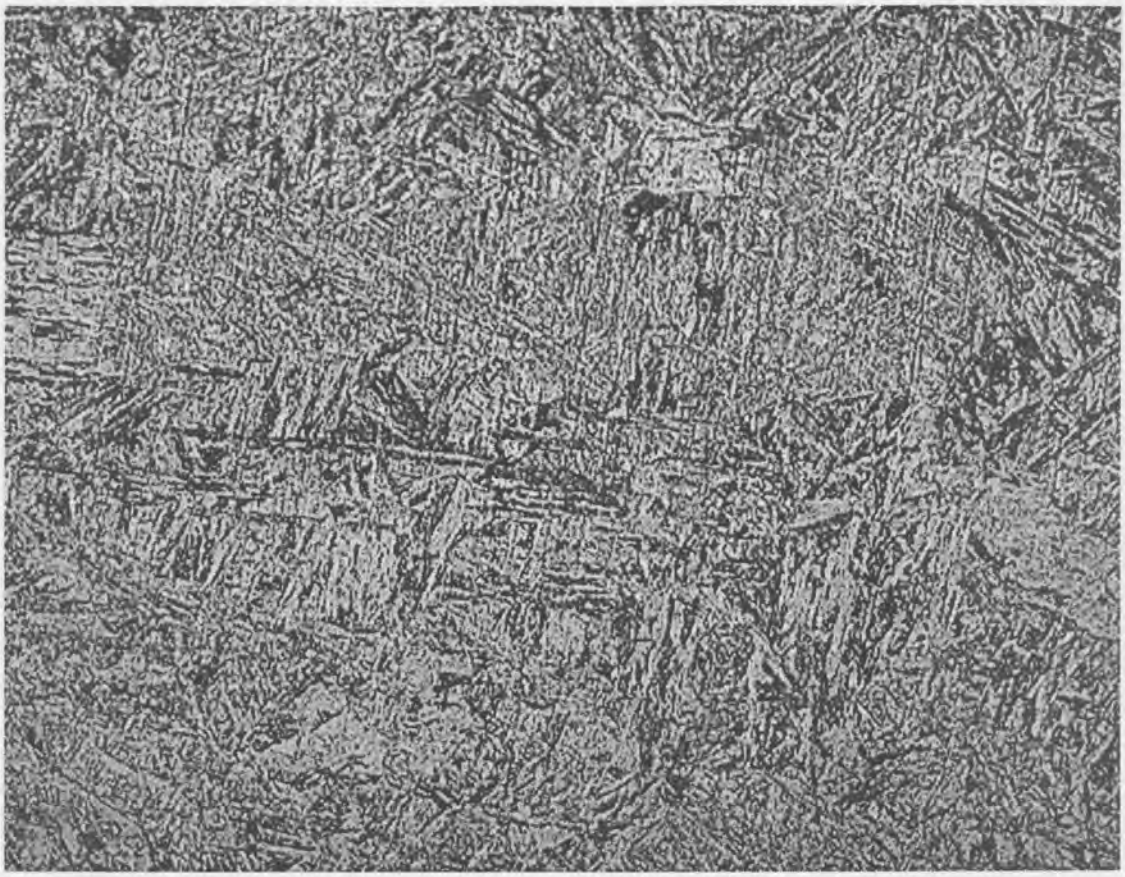

Figure 7.11: Base metal of aged material – 200x (After PWHT)

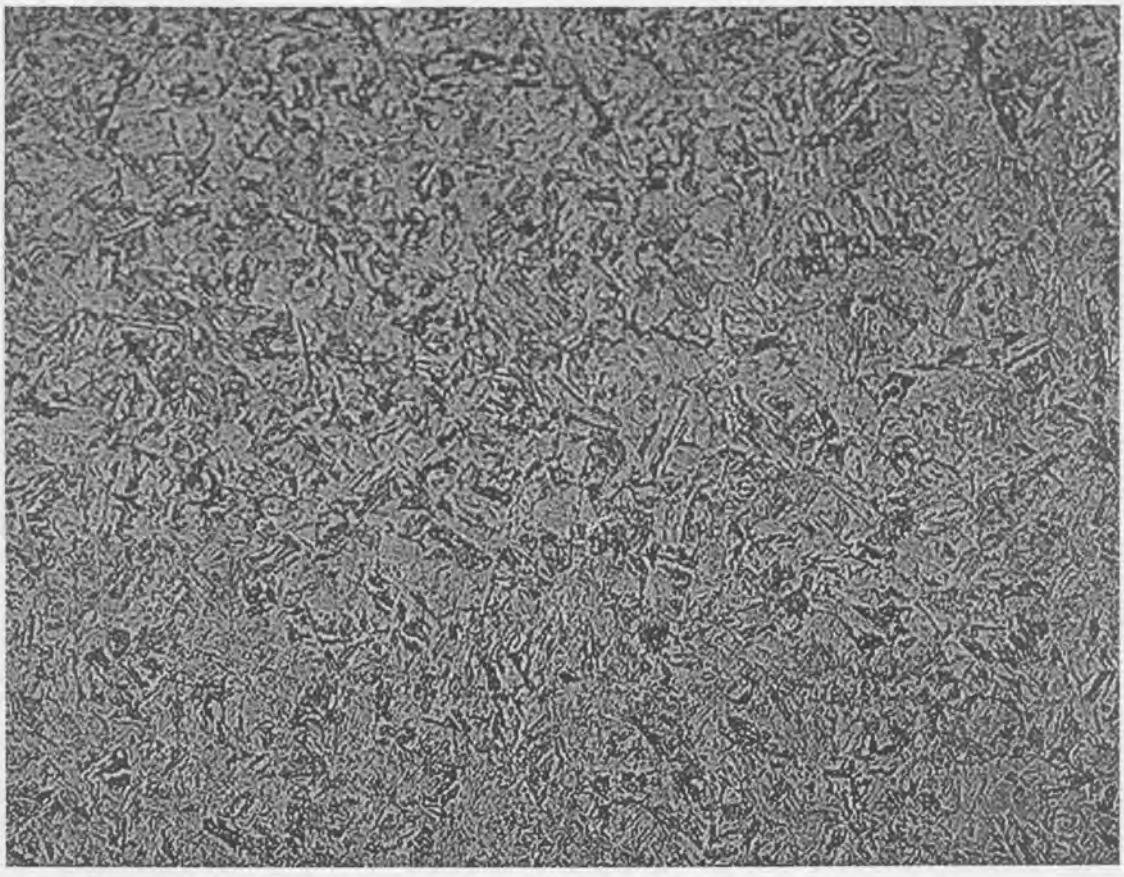

Figure 7.12: CGHAZ of aged material – 200x (After PWHT)

Table 7.3: Description of metallographic sample microstructures

Condition	State	Figure No.	Description
As-simulated	New	7.5	Base Metal: Tempered martensite (quenched and tempered condition), with a dispersion of fine carbides in the martensite laths.
		7.6	CGHAZ: Tempered martensite with areas (colonies) of fresh untempered martensite.
	Artificially Aged	7.7	Base Metal: Tempered martensite (quenched and tempered condition). The grains are more decomposed (tempered) than in the new condition.
		7.8	CGHAZ: Fresh martensite.
PWHT	New	7.9	Base Metal: Tempered martensite.
		7.10	CGHAZ: Tempered martensite with some patches showing fresh martensite.
	Artificially Aged	7.11	Base Metal: Structure shows more tempering. The martensite laths are more broken apart and there are fewer laths visible in the structure.
		7.12	CGHAZ: Partly tempered martensite.

7.6 HARDNESS SURVEY

Hardness profiles were determined from the same samples used in the metallography. A Vickers microhardness-testing machine with a load of 300g was used. The profiles start at the centre of the HAZ and extend through to the base metal. The profiles are shown in Graph 7.3.

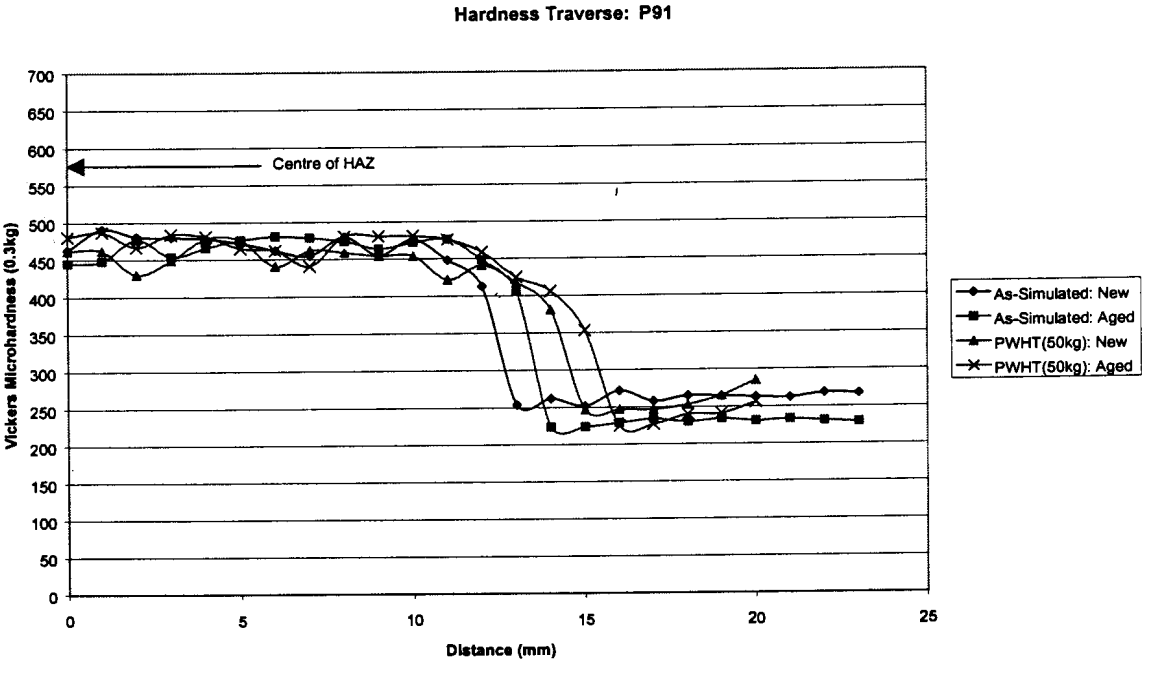

Graph 7.3: Hardness profile of P91 – New and Artificially aged

7.7 DISCUSSION

The results from the spiral notch test were of a similar nature as the results from the tests on X20 material. All the samples tested, both new and artificially aged material failed in the base metal area of the sample at all the different testing loads. The failure temperature of the new material for all the samples tested, was higher than the comparative service-exposed material. The amount of elongation per sample was higher for the new material than the artificially aged material. The ductility of P91 at elevated temperature compares well with the ductility of X20. The strength of the material is due to

the high amount of chromium that is present in the structure as chromium carbides, molybdenum carbides as well as vanadium carbides.

From the SEM photographs it is evident that both the new and artificially aged material failed due to a ductile fracture mechanism. Due to the notch a stress concentration is present and the yield strength of the base metal is lower than that of the HAZ during the PWHT. The base metal will be the primary region for plastic deformation under the influence of a tensile stress until failure.

The structure of the base metal in the artificially aged condition is such that it will be softer than the base metal of the new material. This leads to failure in the base metal areas because the yield strength is lower for the base metal than the CGHAZ. CGHAZ thermal simulation resulted in similar structures of partly tempered martensite with fine carbides within the martensite laths. This is due to the very high hardenability of P91. A fully martensitic structure can thus be obtained in these materials with slower cooling rates in comparison with that of the two ferritic grades (½Cr-½Mo-¼V and 2¼Cr-1Mo). During cooling of materials with a high hardenability the martensite that formed first is still at a relatively high temperature and longer periods of time and undergoes auto-tempering as the work piece cools down to room temperature. The structure of the sample that underwent PWHT (spiral notch test) showed a more tempered state as expected due to the thermal cycle it was subjected to.

The hardness profiles showed that the material in the new and artificially aged condition had almost the same hardness after CGHAZ thermal simulation throughout the HAZ. This confirms the metallography that shows almost no difference of the CGHAZ for both new and aged material. The artificially aged material base metal showed a lower hardness than the new material as expected due to the ageing process. After PWHT the hardness of the HAZ was not significantly reduced, as was the case with X20. The hardness (yield strength) is still higher than that of the base metal, which points out the fact that the base metal is the area where deformation took place during PWHT.

7.8 CONLUSION

P91 material creep strength is obtained due to the high content of chromium as alloying element with molybdenum and vanadium in small quantities. The hardenability of the steel is very high. PWHT restores toughness and ductility and does not seem to increase the strength, as is the case with ½Cr-½Mo-¼V. The yield strength of the base metal for new and service-exposed material will always be lower than that of the HAZ making it the primary region for creep deformation at elevated temperature to provide stress relieving.

7.9 REFERENCES

1. Stahlschlüssel – Key to Steel, 1998
2. Guntz, G., Julien, M., Kottman, G., Pellicani, F., Pouilly, A. and Vaillant, J.C.,"The T91 Book", Vallourec Industries – France, 1990

Private Bag 40175
2022 Cleveland
Telefax (011) 629-5528
Telephone (011) 629-5111

UNIVERSITEIT VAN PRETORIA
UNIVERSITY OF PRETORIA
YUNIBESITHI YA PRETORIA

SANAS ACCREDITED LABORATORY
ISO Guide 25/SABS 0259 (1990)
and EN45001 (1989)

Technology Services International

Chemical Technologies

CERTIFICATE OF ANALYSIS

To: *R LOOTS*

MATERIALS TECHNOLOGY
SCIENTIFIC SERVICES DEPARTMENT
TSI

Report No.: **100119771**
Logged on:
Reported on:

WELDING AT CRAP
AGED MATERIALS

These results are reported on an air-dried basis.

COMMENTS:

pp *Willie Delport*
SENIOR OFFICER (COAL AND X-RAY)
Phone no: *629-5254*

UNIVERSITEIT VAN PRETORIA
UNIVERSITY OF PRETORIA
YUNIBESITHI YA PRETORIA

Private Bag 40175
2022 Cleveland
Telefax (011) 629-5528
Telephone (011) 629-5111

SANAS ACCREDITED LABORATORY
ISO Guide 25/SABS 0259 (1990)
and EN45001 (1989)

Technology Services International

Report No.: 100119771

Logged on:
Reported on:

Sample ID:		200315390	200315392
Description:		1/2 1/2 1/4 NUUT	1/2 1/2 1/4 OUD
Component:	**Units**	**Value:**	**Value:**
CARBON	%	0.14	0.19
CHROMIUM	%	0.46	0.53
NICKEL	%	0.08	0.16
MANGANESE	%	0.51	0.54
MOLYBDENUM	%	0.51	0.54
VANADIUM	%	0.28	0.31
SULPHUR	%	0.01	0.012
PHOSPHORUS	%	0.008	0.014
SILICON	%	0.12	0.24
TITANIUM	%	0.01	0.01
COPPER	%	0.09	0.15
COBALT	%	0.01	0.02
NIOBIUM	%	0.005	0.005
TIN	%	0.01	0.02
TUNGSTEN	%	0.005	0.005

Private Bag 40175
2022 Cleveland
Telefax (011) 629-5528
Telephone (011) 629-5111

UNIVERSITEIT VAN PRETORIA
UNIVERSITY OF PRETORIA
YUNIBESITHI YA PRETORIA

SANAS ACCREDITED LABORATORY
ISO Guide 25/SABS 0259 (1990)
and EN45001 (1989)

Technology Services International

Report No.: 100119771

Logged on:
Reported on:

Sample ID:		200315393	200315394
Description:		2 1/4 NUUT	2 1/4 OUD
Component:	**Units**	**Value:**	**Value:**
CARBON	%	0.11	0.10
CHROMIUM	%	2.41	2.57
NICKEL	%	0.05	0.17
MANGANESE	%	0.49	0.54
MOLYBDENUM	%	0.87	0.91
VANADIUM	%	0.01	0.02
SULPHUR	%	0.001	0.003
PHOSPHORUS	%	0.018	0.021
SILICON	%	0.11	0.04
TITANIUM	%	0.01	0.01
COPPER	%	0.04	0.12
COBALT	%	0.01	0.03
NIOBIUM	%	0.005	0.005
TIN	%	0.01	0.01
TUNGSTEN	%	0.005	0.02

UNIVERSITEIT VAN PRETORIA
UNIVERSITY OF PRETORIA
YUNIBESITHI YA PRETORIA

Private Bag 40175
2022 Cleveland
Telefax (011) 629-5528
Telephone (011) 629-5111

SANAS ACCREDITED LABORATORY
ISO Guide 25/SABS 0259 (1990)
and EN45001 (1989)

Technology Services International

Report No.: 100119771

Logged on:
Reported on:

Sample ID:		200315395	200315396
Description:		X20 NUUT	X20 OUD
Component:	**Units**	**Value:**	**Value:**
CARBON	%	0.22	0.19
CHROMIUM	%	12.05	12.29
NICKEL	%	0.75	0.48
MANGANESE	%	0.59	0.45
MOLYBDENUM	%	0.82	0.78
VANADIUM	%	0.26	0.30
SULPHUR	%	0.004	0.013
PHOSPHORUS	%	0.016	0.020
SILICON	%	0.07	0.13
TITANIUM	%	0.01	0.01
COPPER	%	0.11	0.09
COBALT	%	0.01	0.01
NIOBIUM	%	0.01	0.005
TIN	%	0.01	0.01
TUNGSTEN	%	0.005	0.005

Private Bag 40175
2022 Cleveland
Telefax (011) 629-5528
Telephone (011) 629-5111

UNIVERSITEIT VAN PRETORIA
UNIVERSITY OF PRETORIA
YUNIBESITHI YA PRETORIA

SANAS ACCREDITED LABORATORY
ISO Guide 25/SABS 0259 (1990)
and EN45001 (1989)

Technology Services International

Report No.: 100119771

Logged on:
Reported on:

Sample ID:		200315397
Description:		P91 NEW
Component:	**Units**	**Value:**
CARBON	%	0.22
CHROMIUM	%	9.19
NICKEL	%	0.19
MANGANESE	%	0.48
MOLYBDENUM	%	0.86
VANADIUM	%	0.24
SULPHUR	%	0.001
PHOSPHORUS	%	0.013
SILICON	%	0.27
TITANIUM	%	0.01
COPPER	%	0.05
COBALT	%	0.005
NIOBIUM	%	0.07
TIN	%	0.01
TUNGSTEN	%	0.005

UNIVERSITEIT VAN PRETORIA
UNIVERSITY OF PRETORIA
YUNIBESITHI YA PRETORIA

Private Bag 40175
2022 Cleveland
Telefax (011) 629-5528
Telephone (011) 629-5111

SANAS ACCREDITED LABORATORY
ISO Guide 25/SABS 0259 (1990)
and EN45001 (1989)

Technology Services International

Report No.: 100119771

Logged on:
Reported on:

ALLOYING ELEMENTS IN STEEL ***ESKOM Method No 106 Rev 2 Accredited***
CARBON ***ESKOM Method No 119 Rev 1 Accredited***

Appendix 2: Results from Spiral Notch Tests
½Cr-½Mo-¼V New: 356 MPa

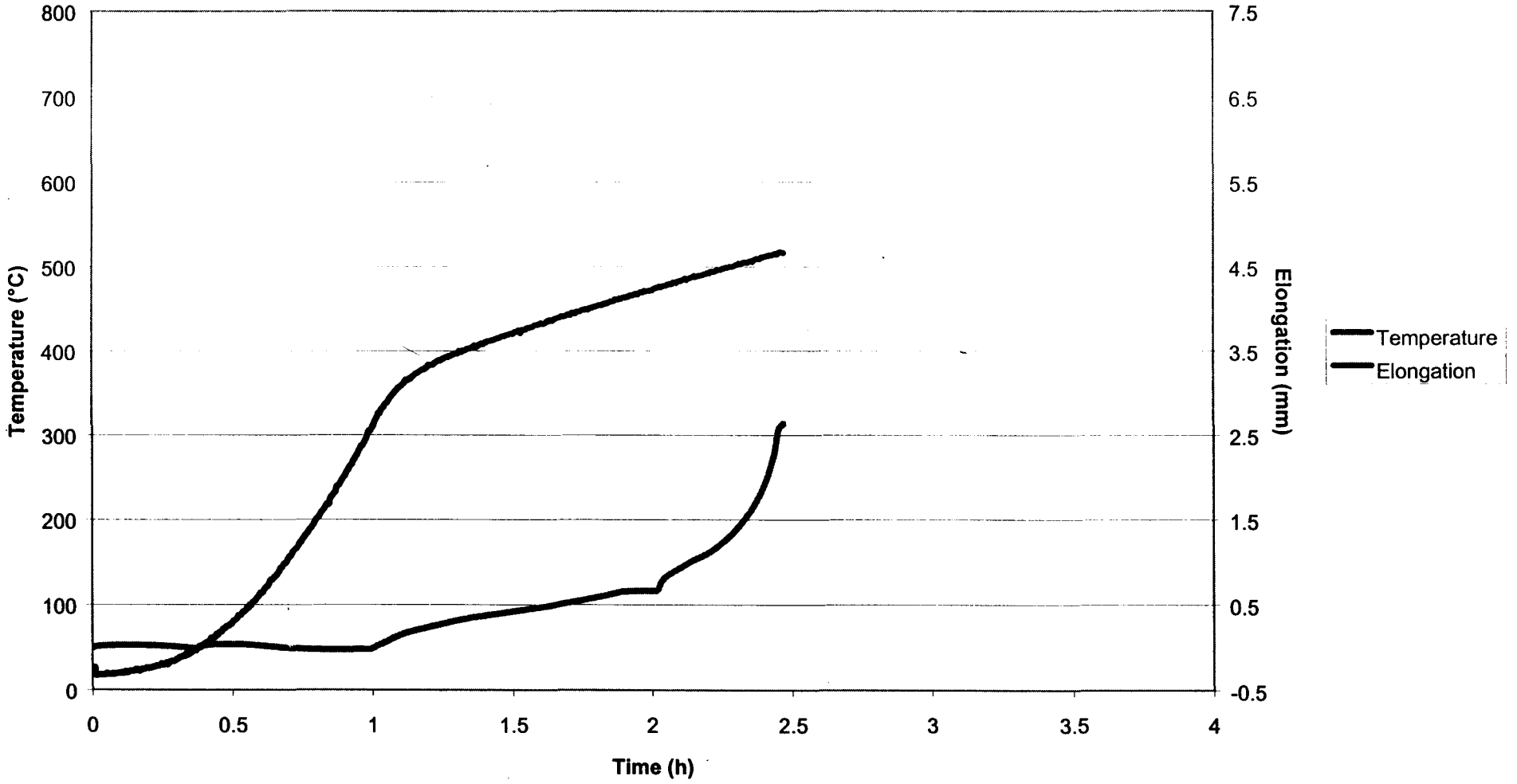

Appendix 2 (Continued)
½Cr-½Mo-¼V New: 305 MPa

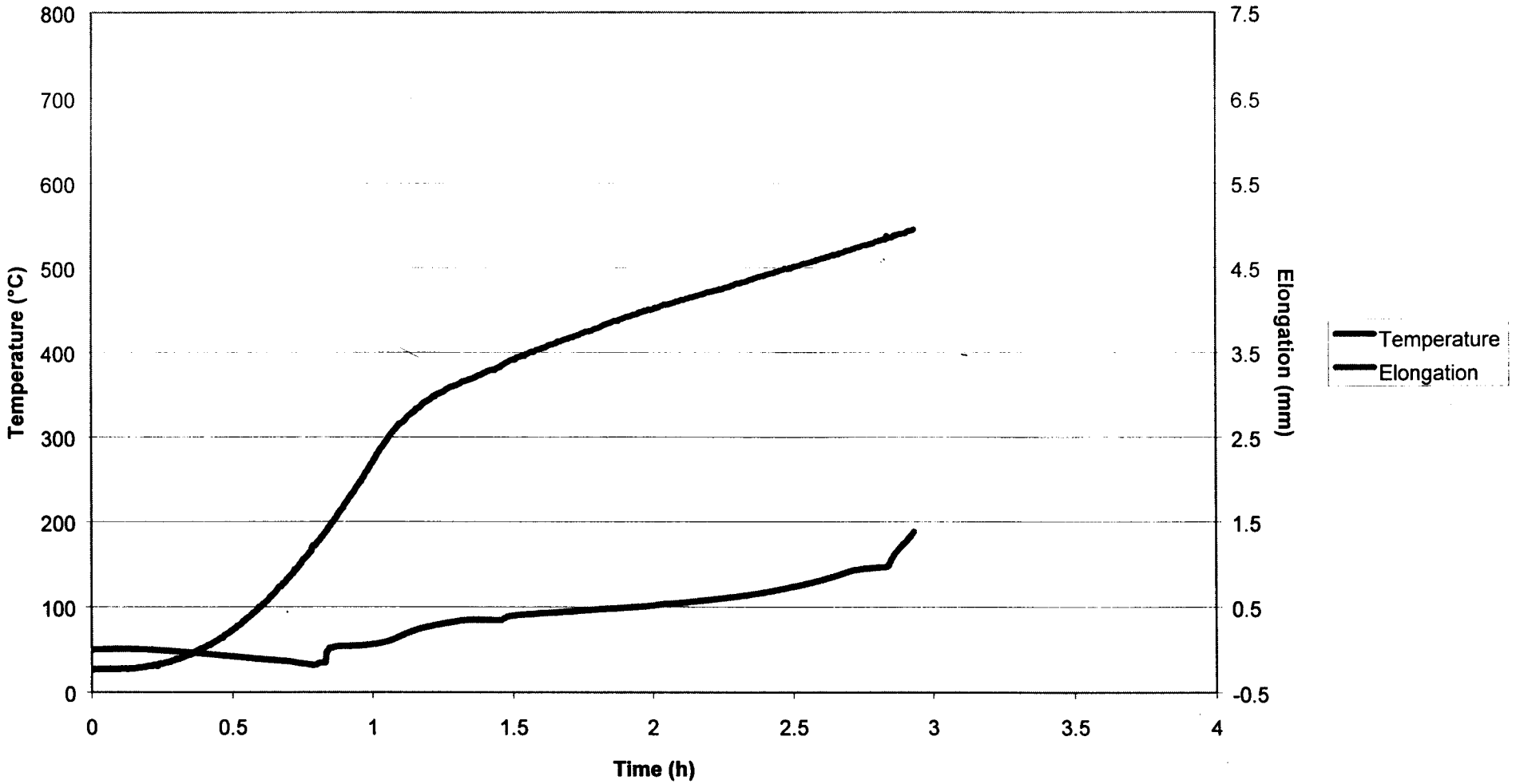

Appendix 2 (Continued)
½Cr-½Mo-¼V New: 204 MPa

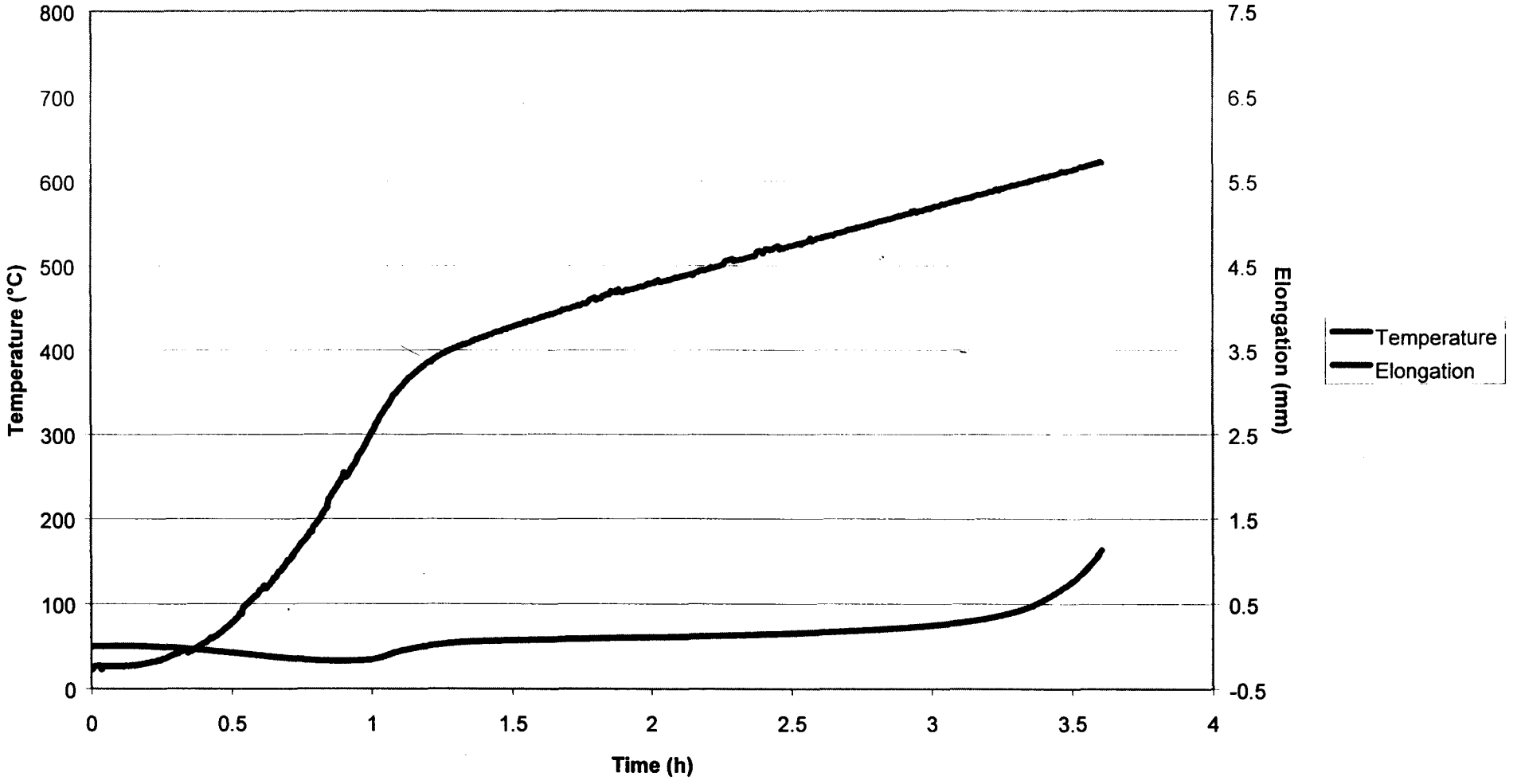

Appendix 2 (Continued)
½Cr-½Mo-¼V Service Exposed: 356 MPa

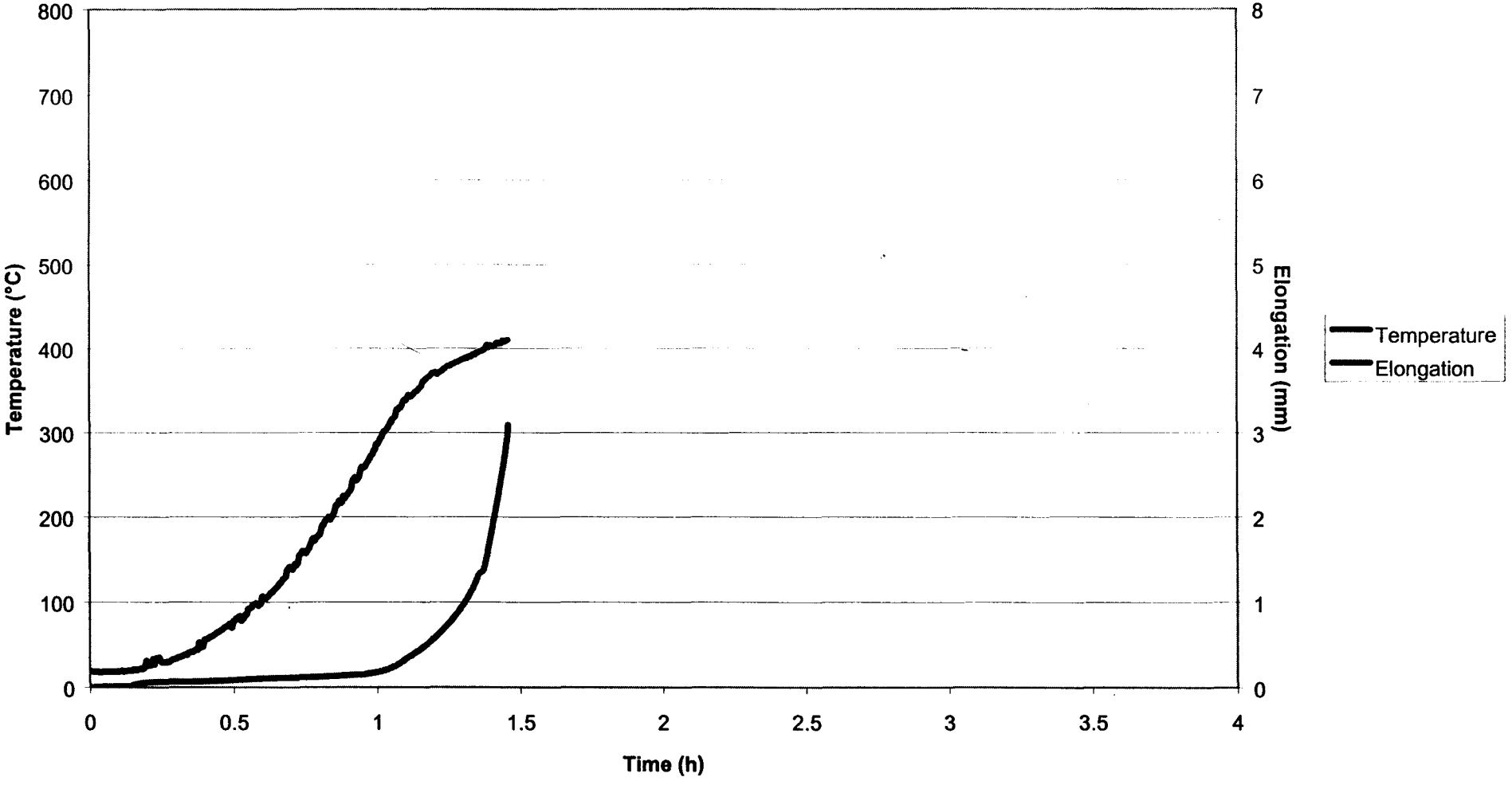

Appendix 2 (Continued)
½Cr-½Mo-¼V Service Exposed: 305 MPa

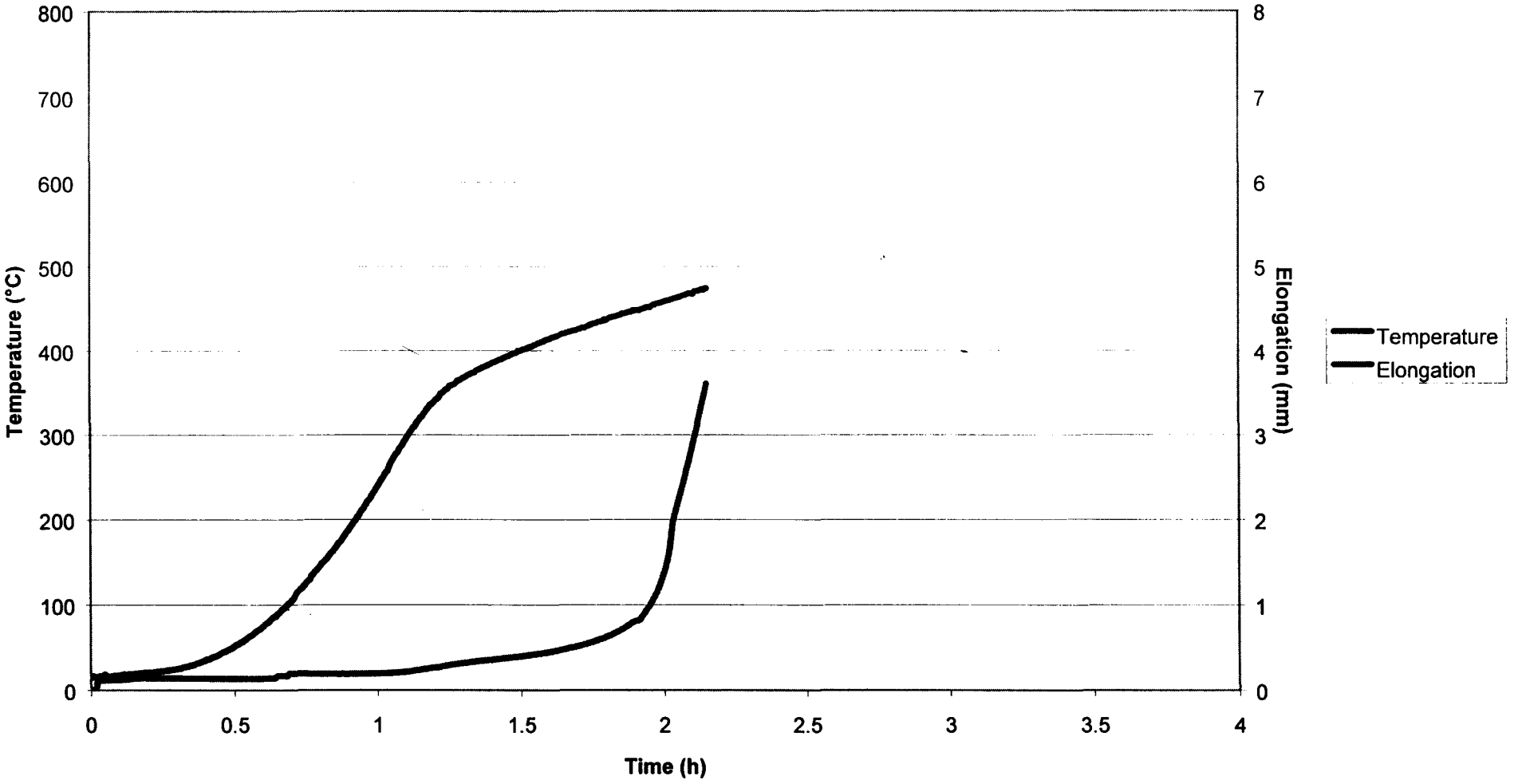

Appendix 2 (Continued)
½Cr-½Mo-¼V Service Exposed: 204 MPa

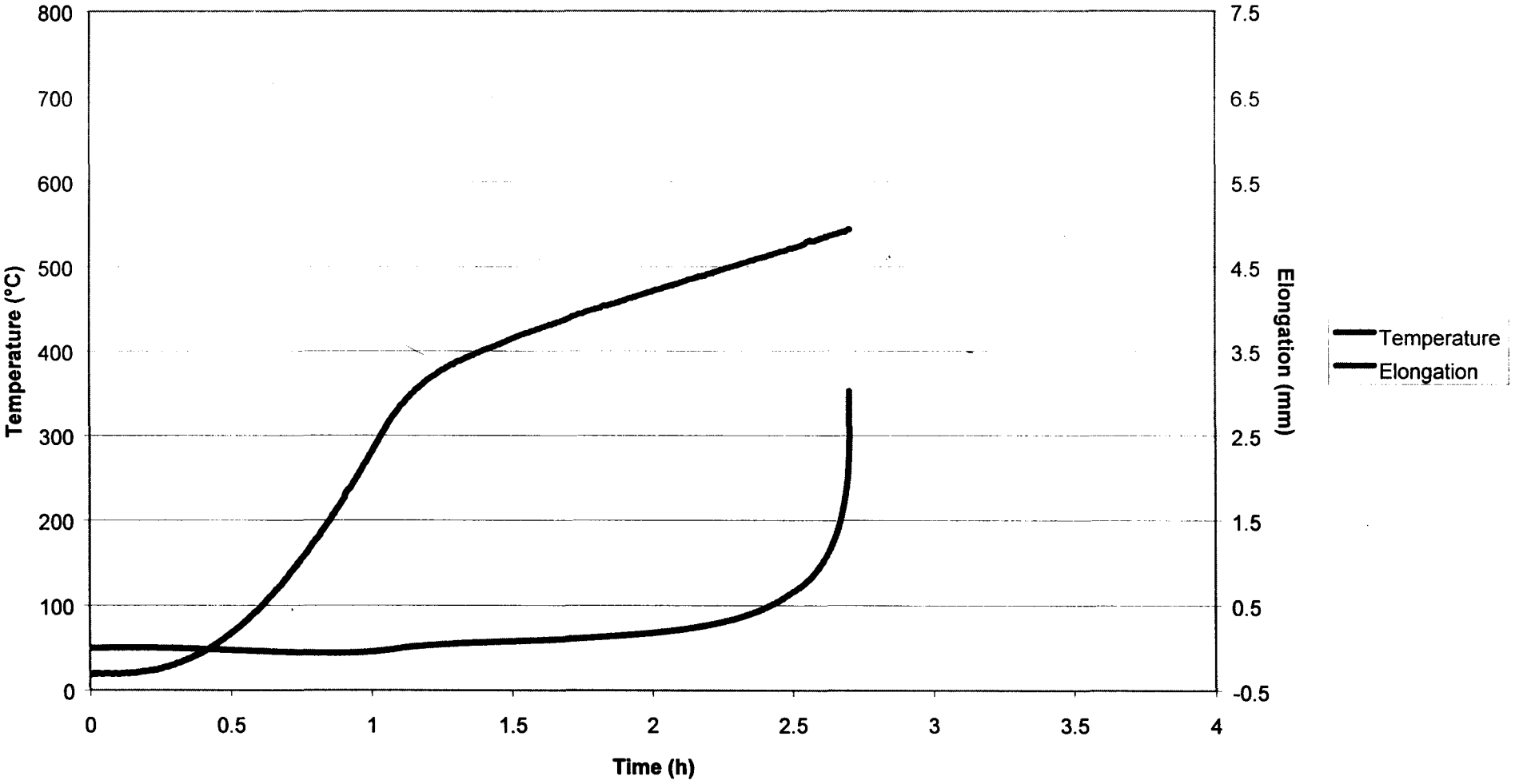

Appendix 2 (Continued)
½Cr-½Mo-¼V Service Exposed: 153 MPa

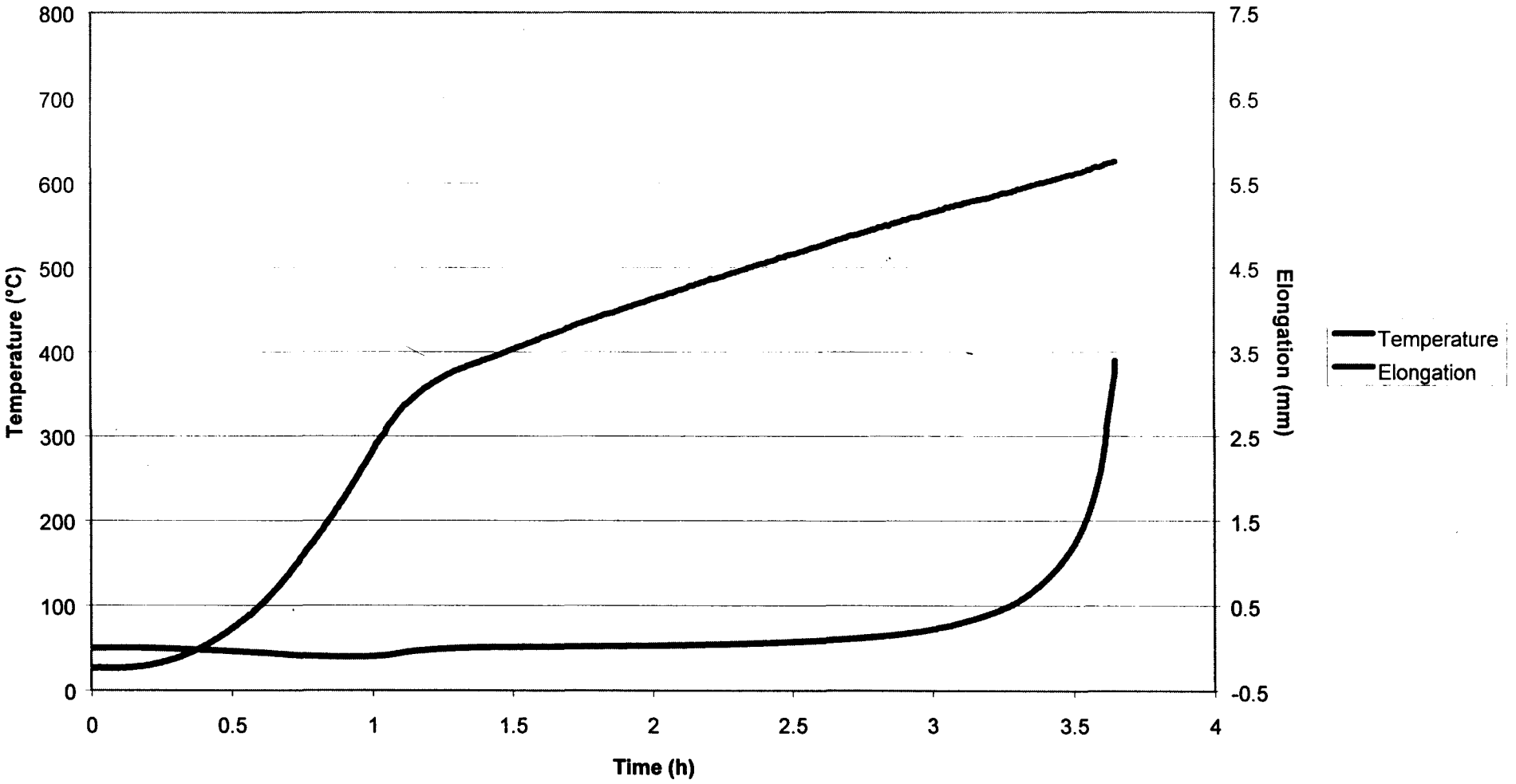

Appendix 2 (Continued)
2¼Cr-1Mo New: 356 MPa

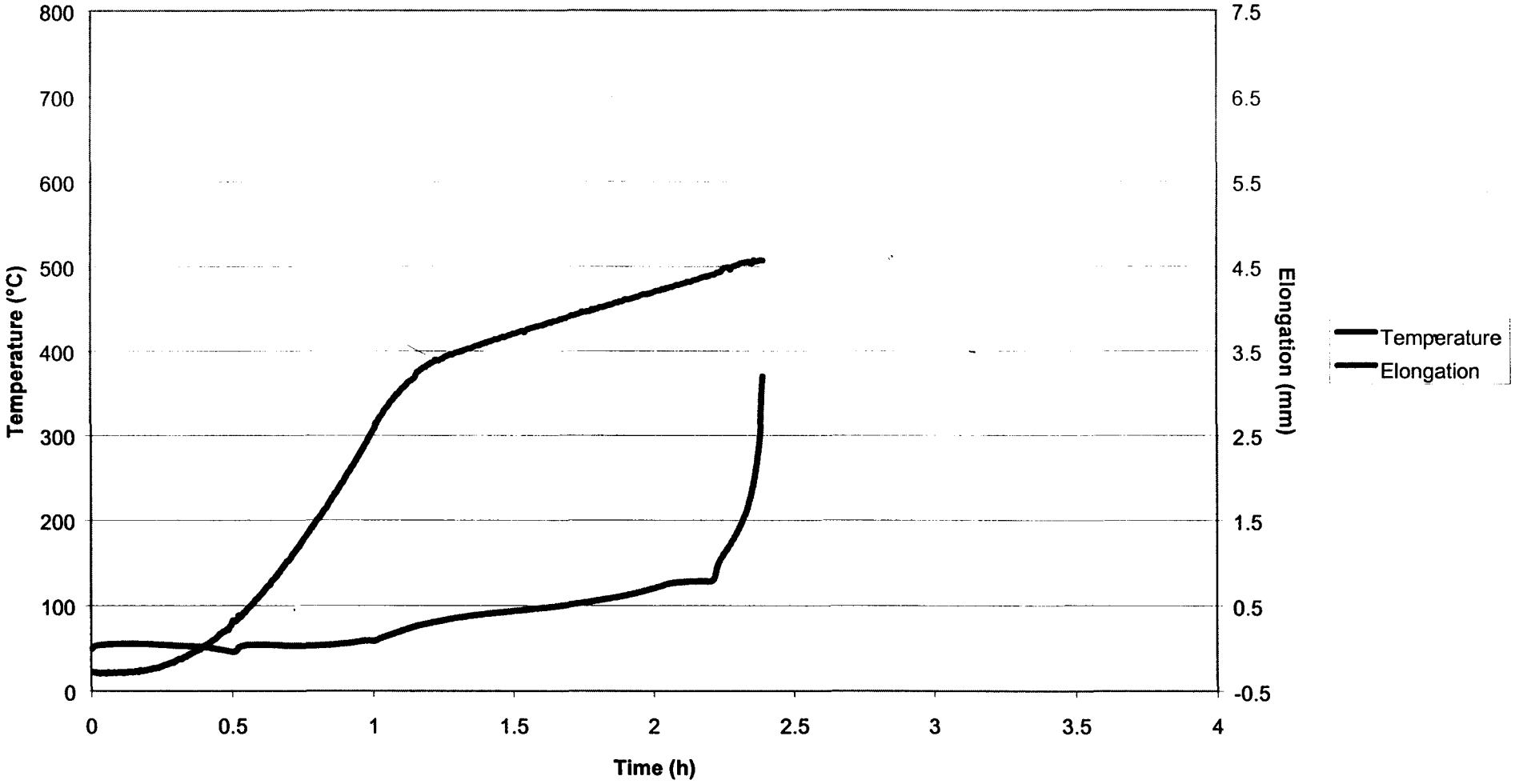

Appendix 2 (Continued)
2¼Cr-1Mo New: 305 MPa

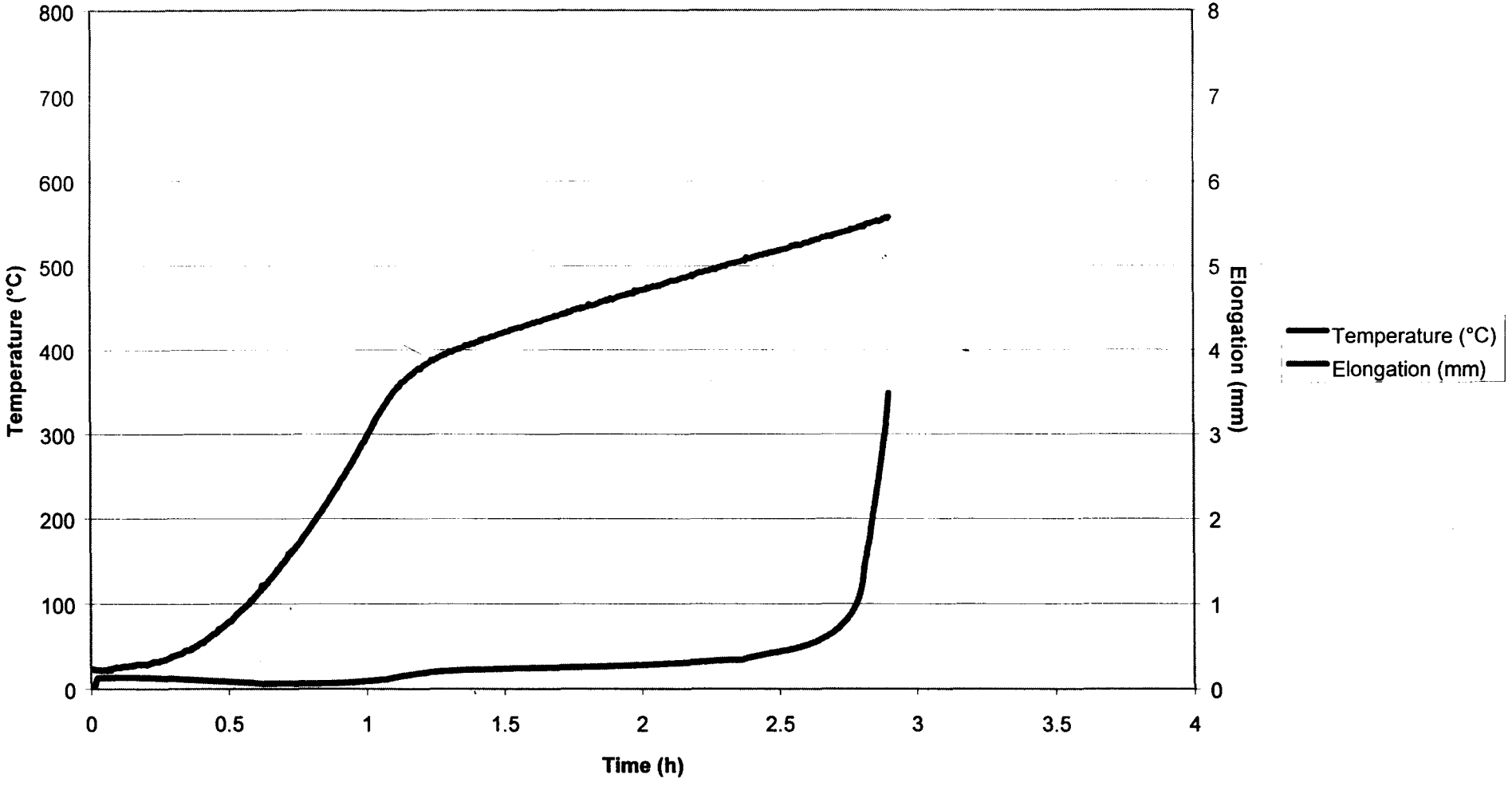

Appendix 2 (Continued)
2¼Cr-1Mo New: 204 MPa

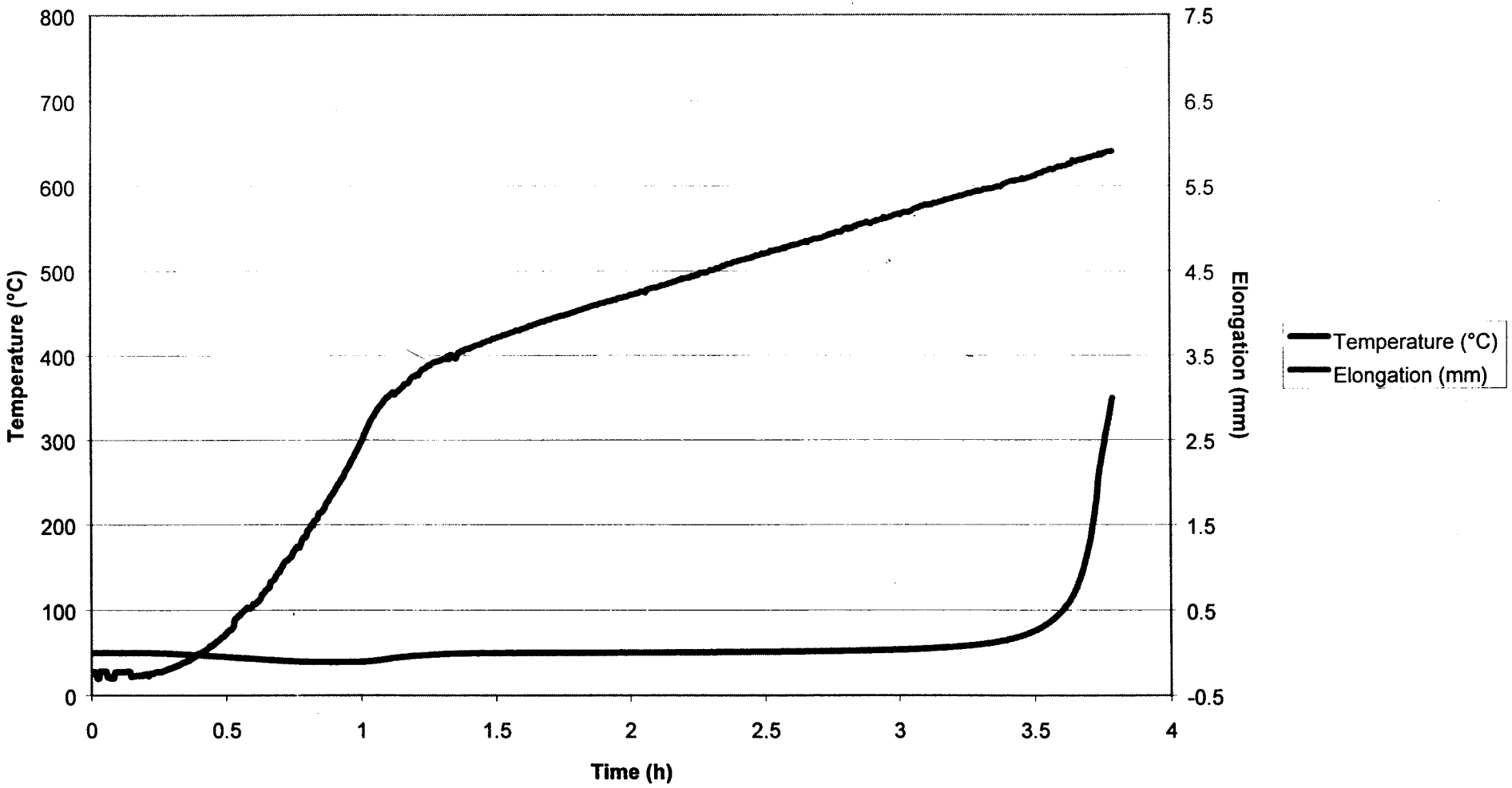

Appendix 2 (Continued)
2¼Cr-1Mo New: 153 MPa

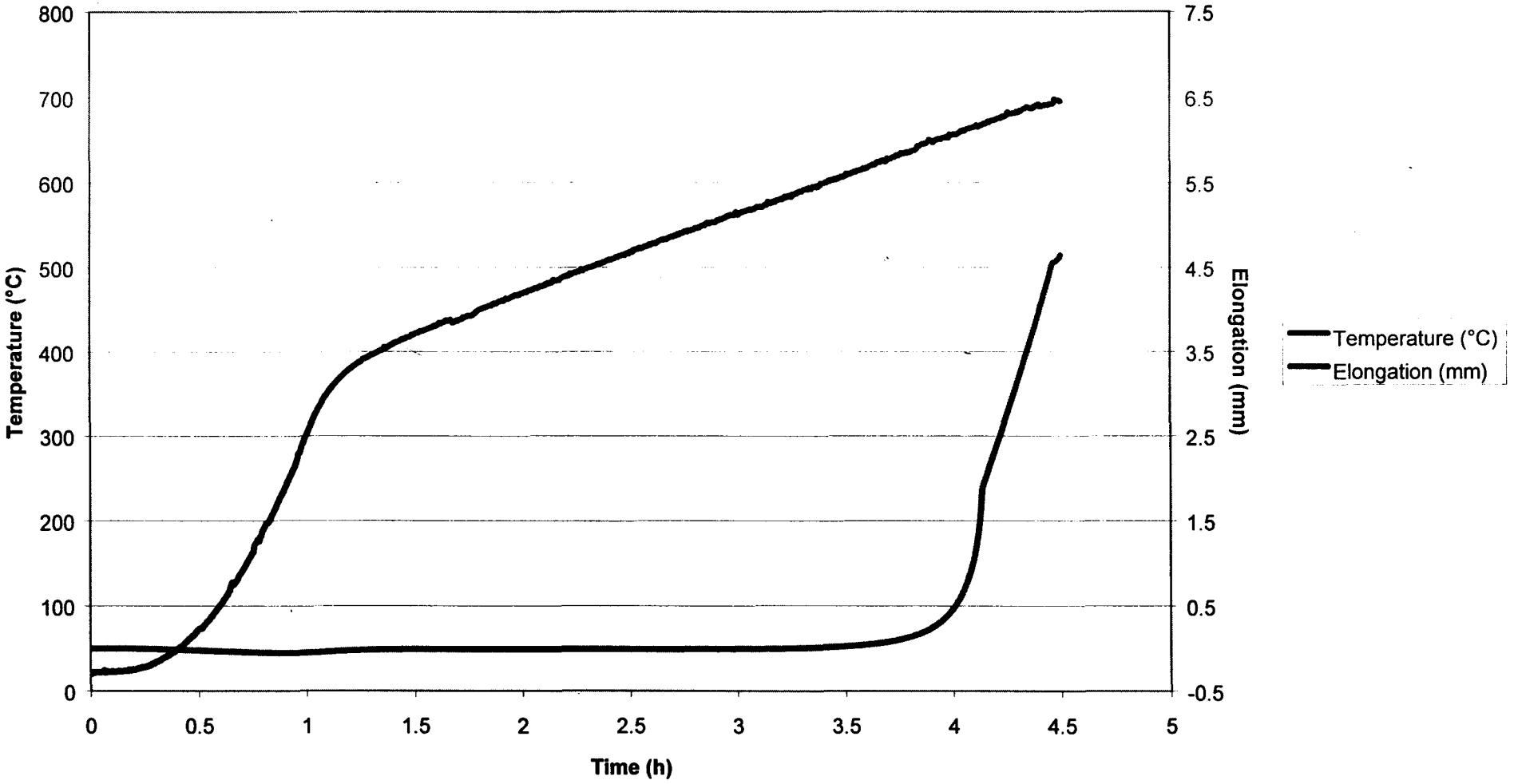

Appendix 2 (Continued)
2¼Cr-1Mo Service Exposed: 356 MPa

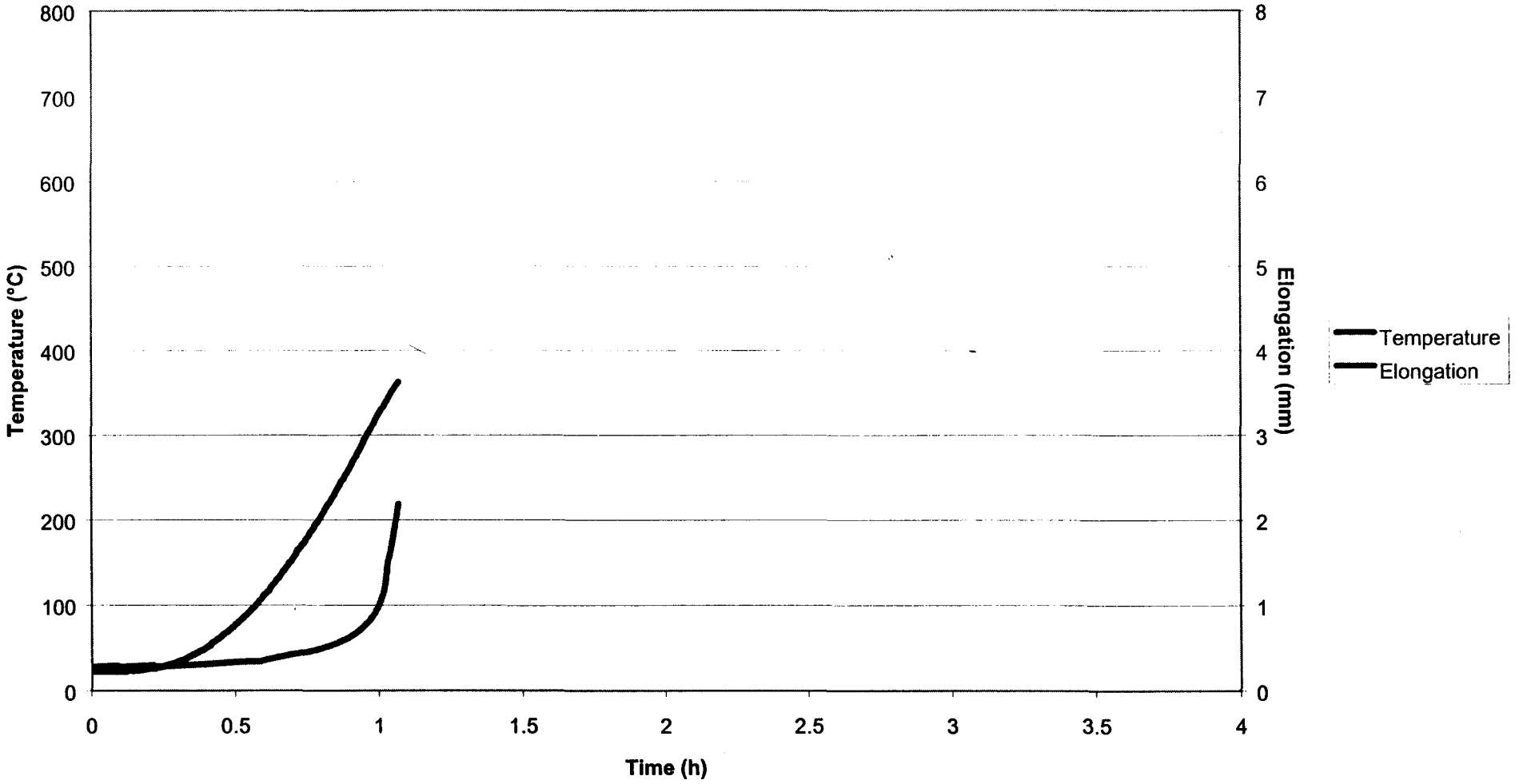

Appendix 2 (Continued)
2¼Cr-1Mo Service Exposed: 305 MPa

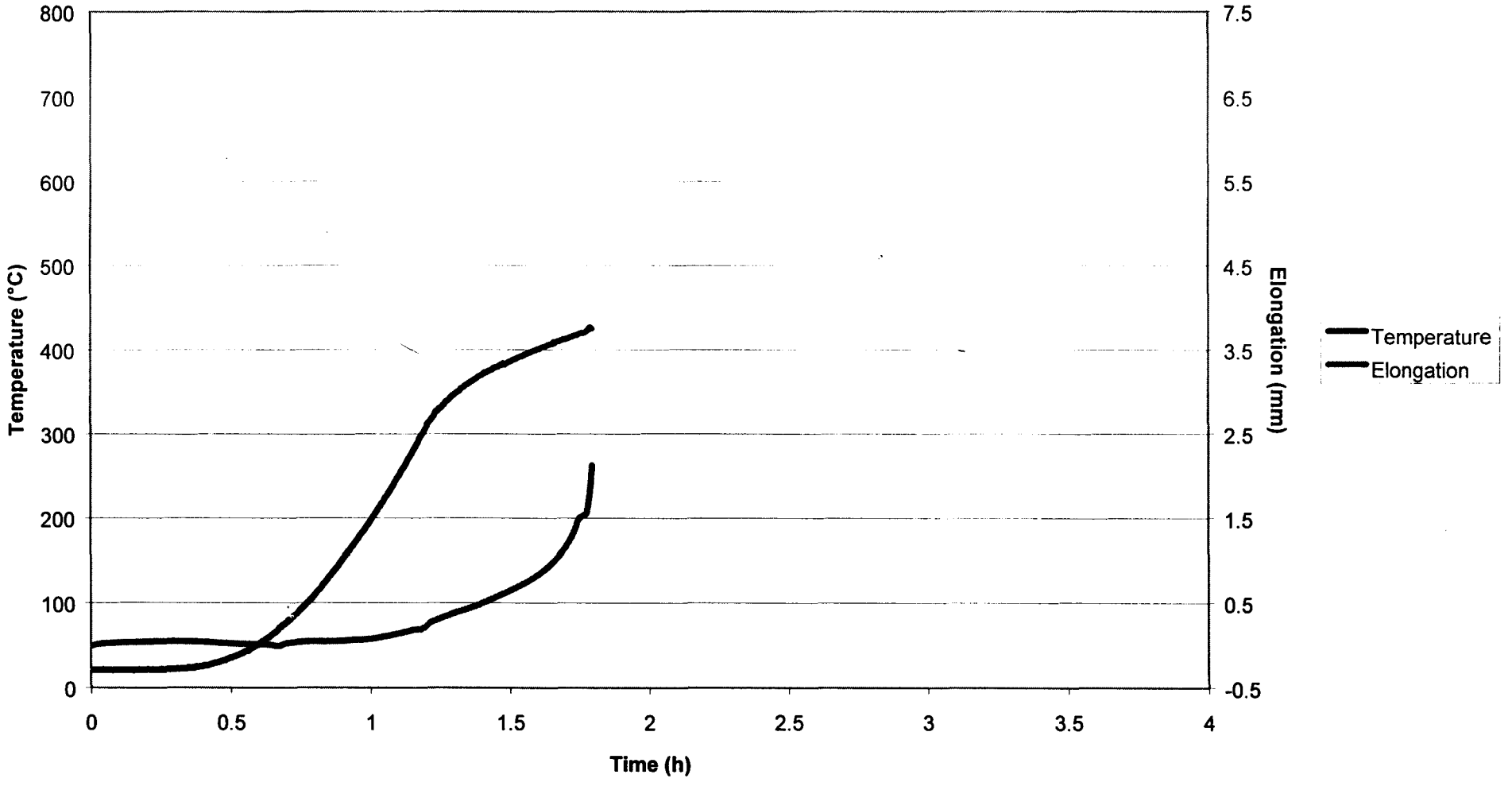

Appendix 2 (Continued)
2¼Cr-1Mo Service Exposed: 204 MPa

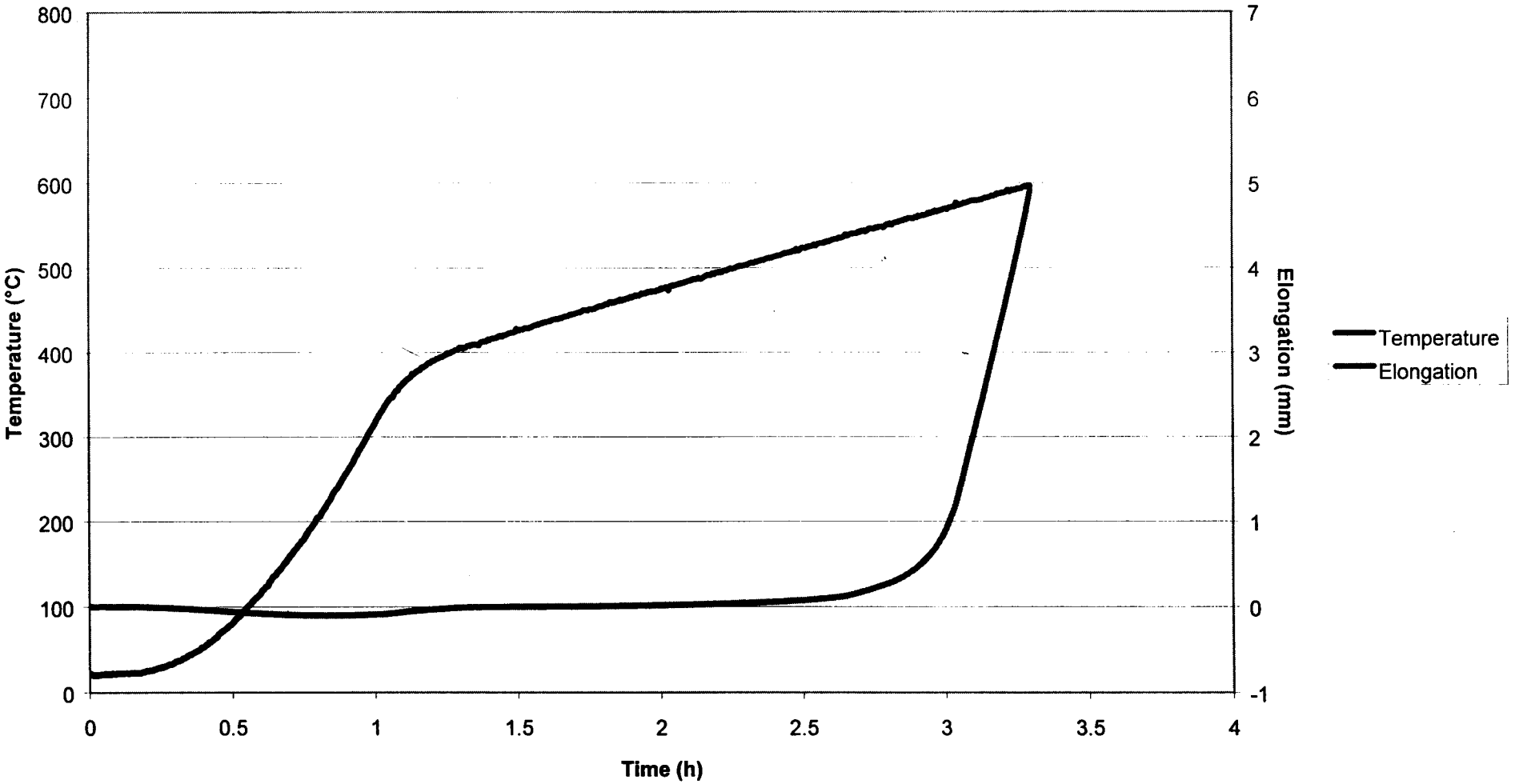

Appendix 2 (Continued)
2¼Cr-1Mo Service Exposed: 153 MPa

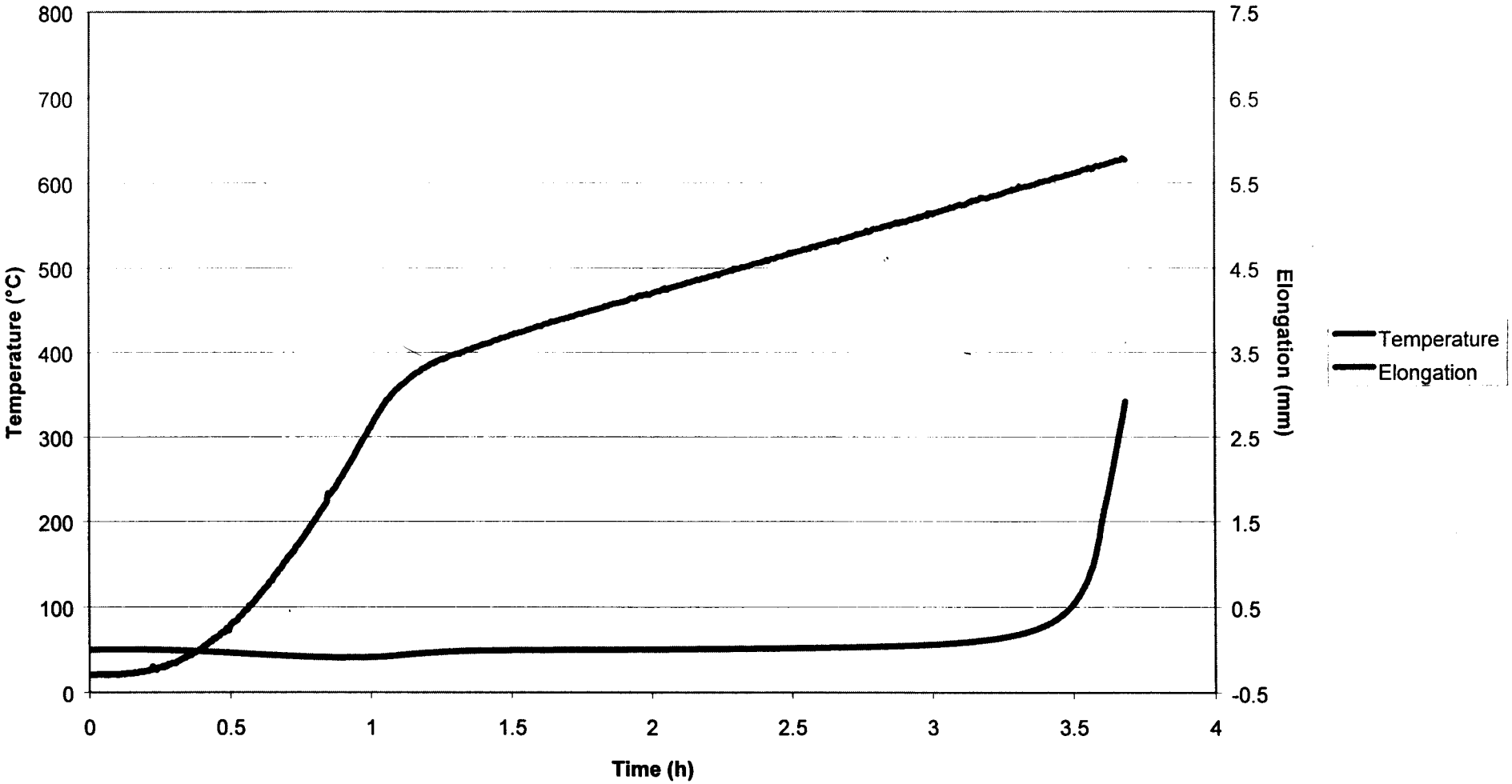

Appendix 2 (Continued)
X20 New: 407 MPa

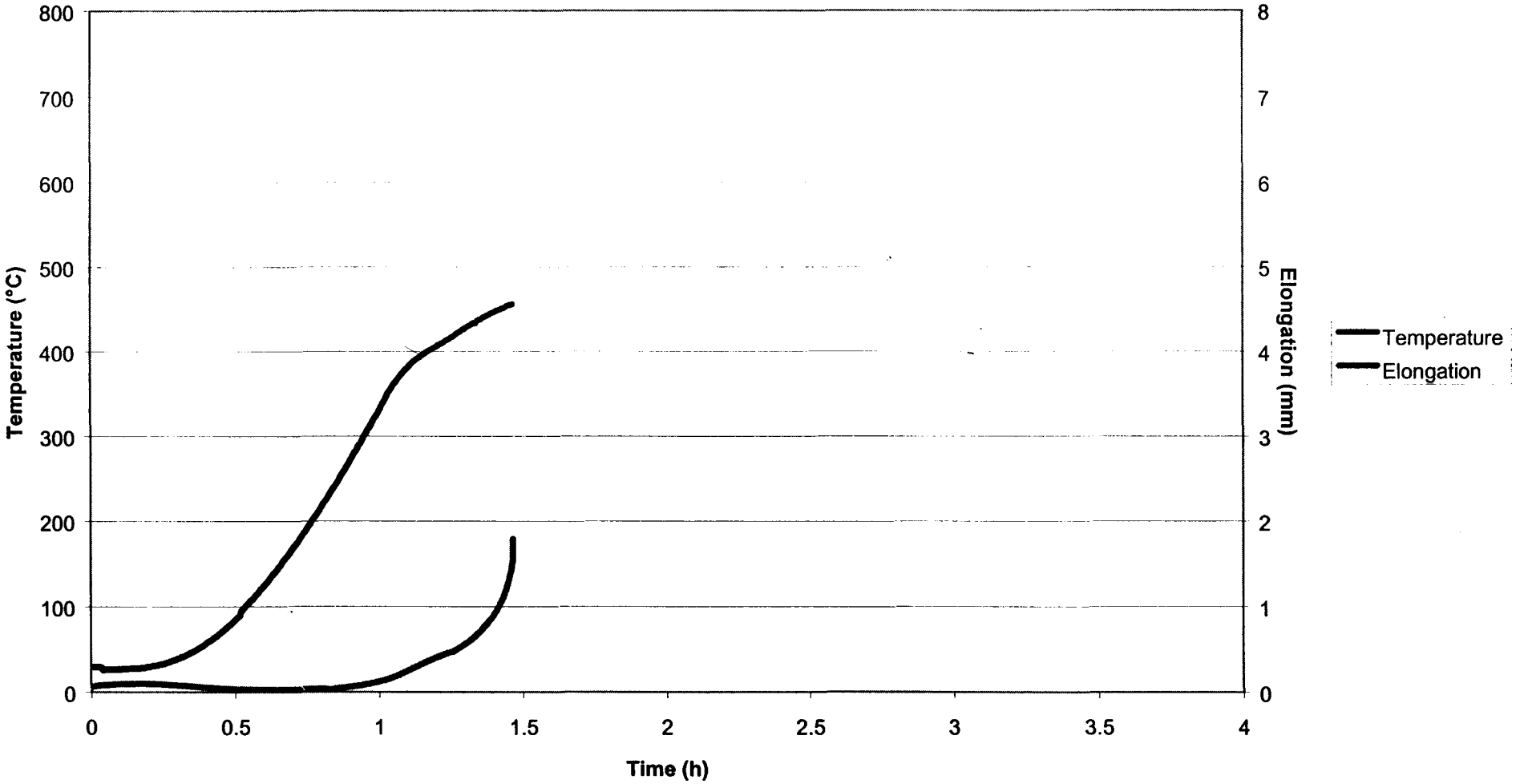

Appendix 2 (Continued)
X20 New: 356 MPa

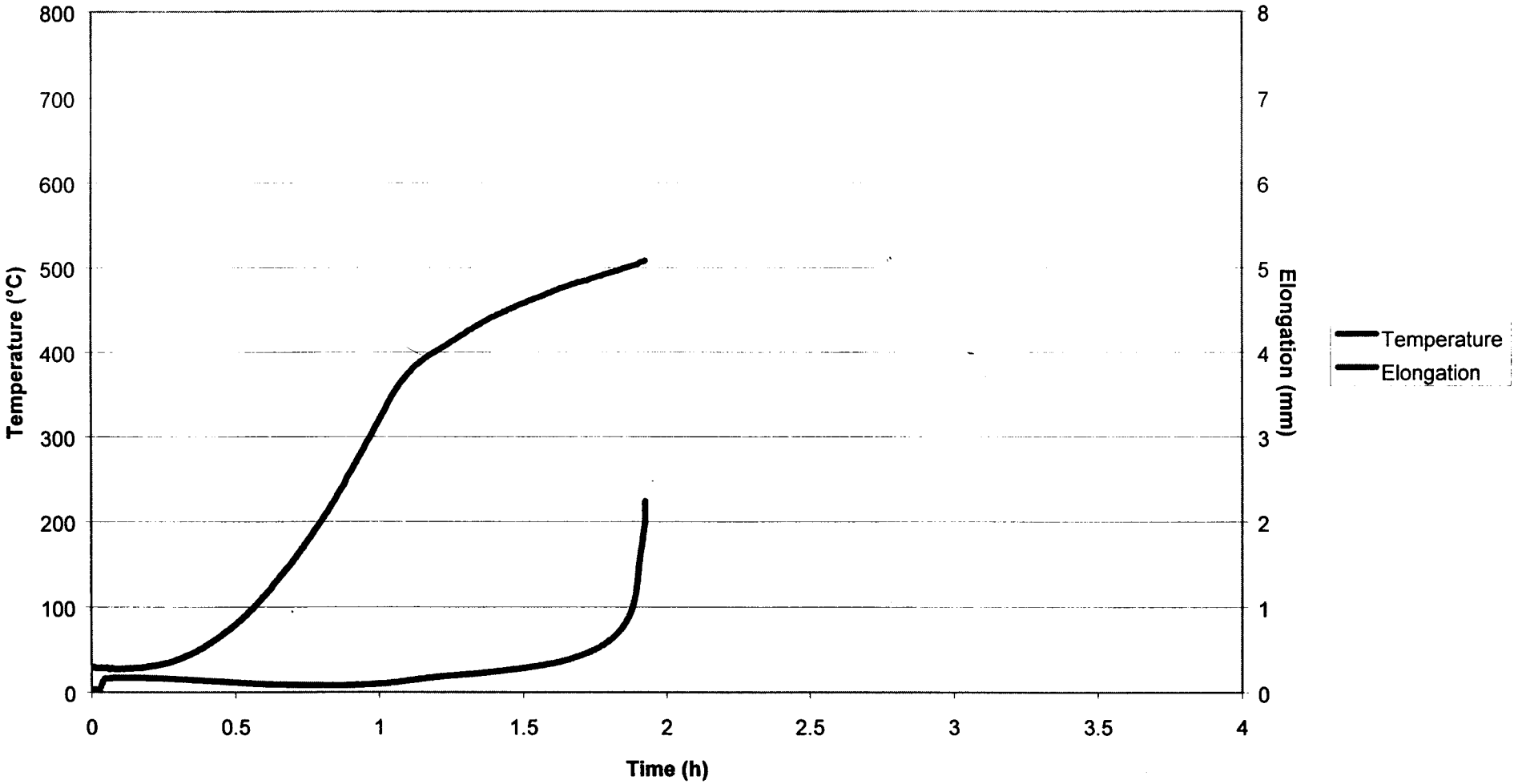

Appendix 2 (Continued)
X20 New: 305 MPa

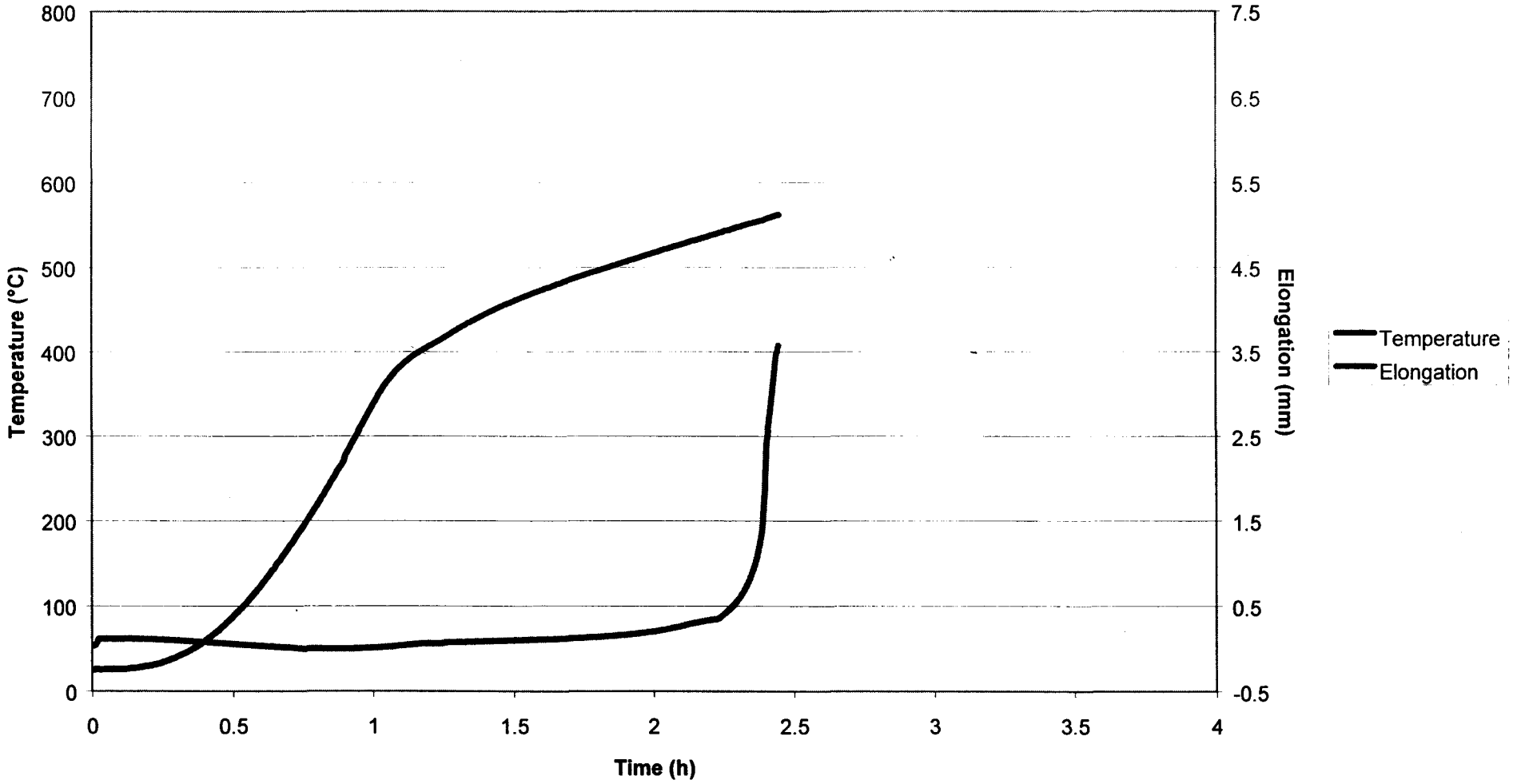

Appendix 2 (Continued)
X20 New: 254 MPa

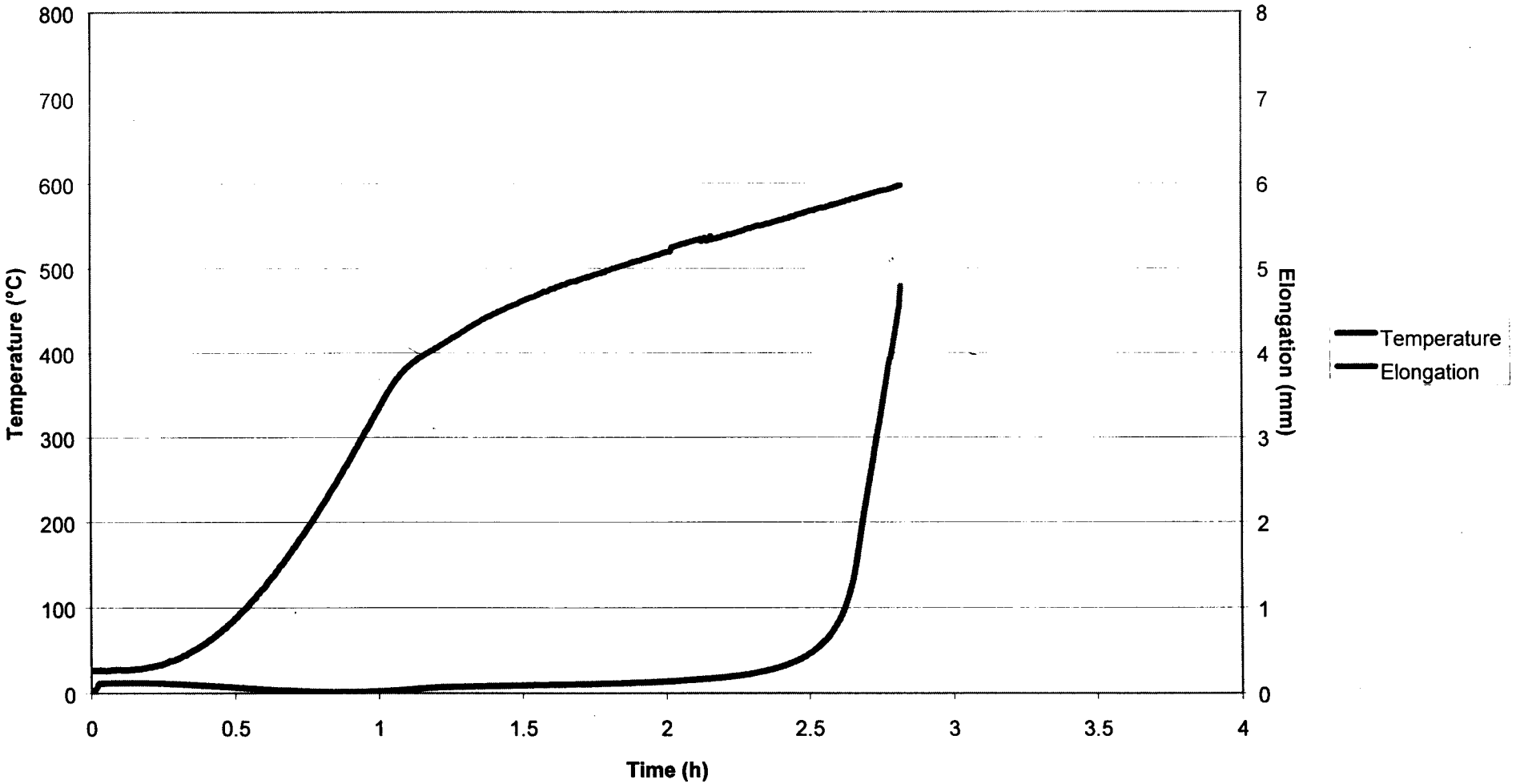

Appendix 2 (Continued)
X20 Service Exposed: 407 MPa

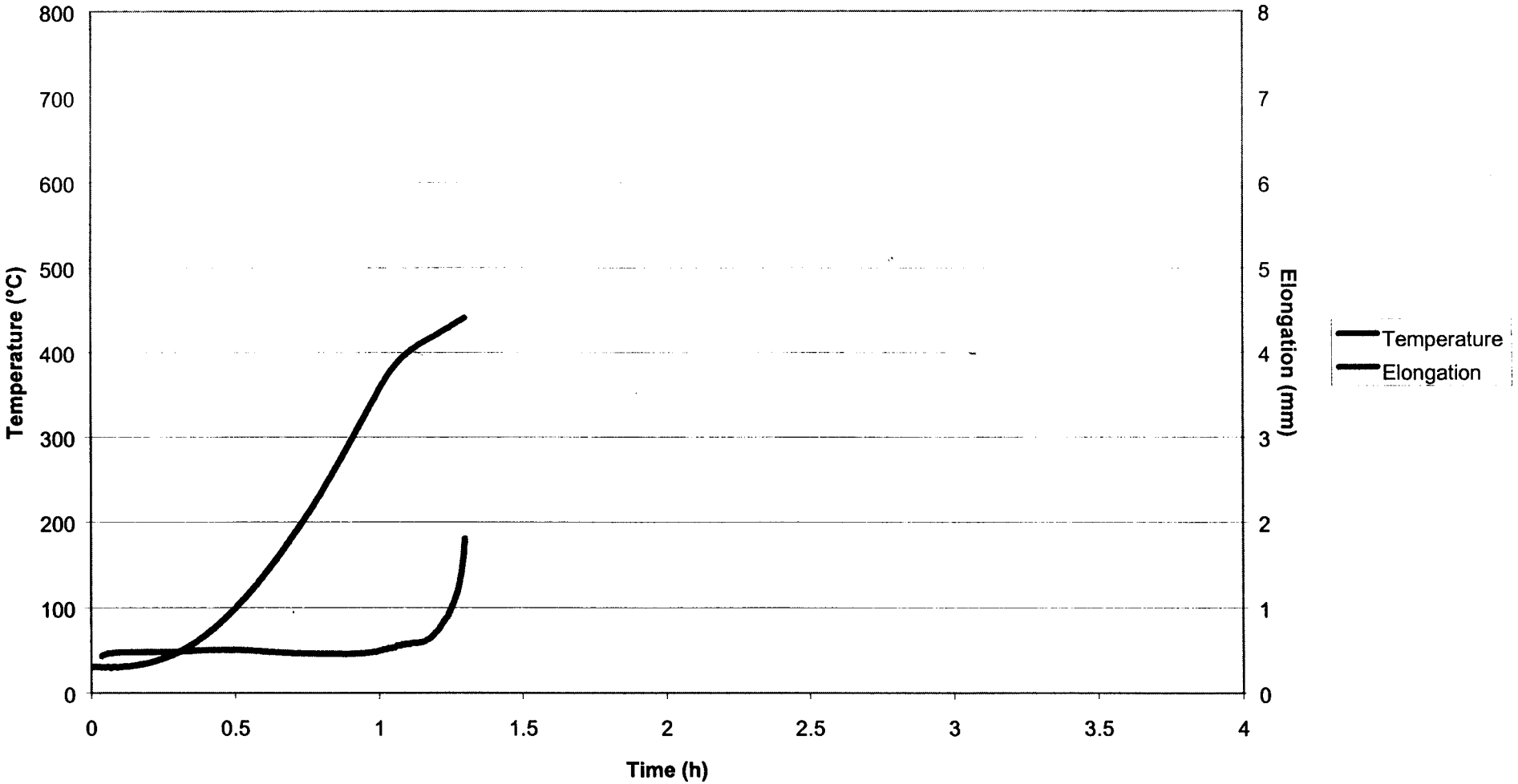

Appendix 2 (Continued)
X20 Service Exposed: 356 MPa

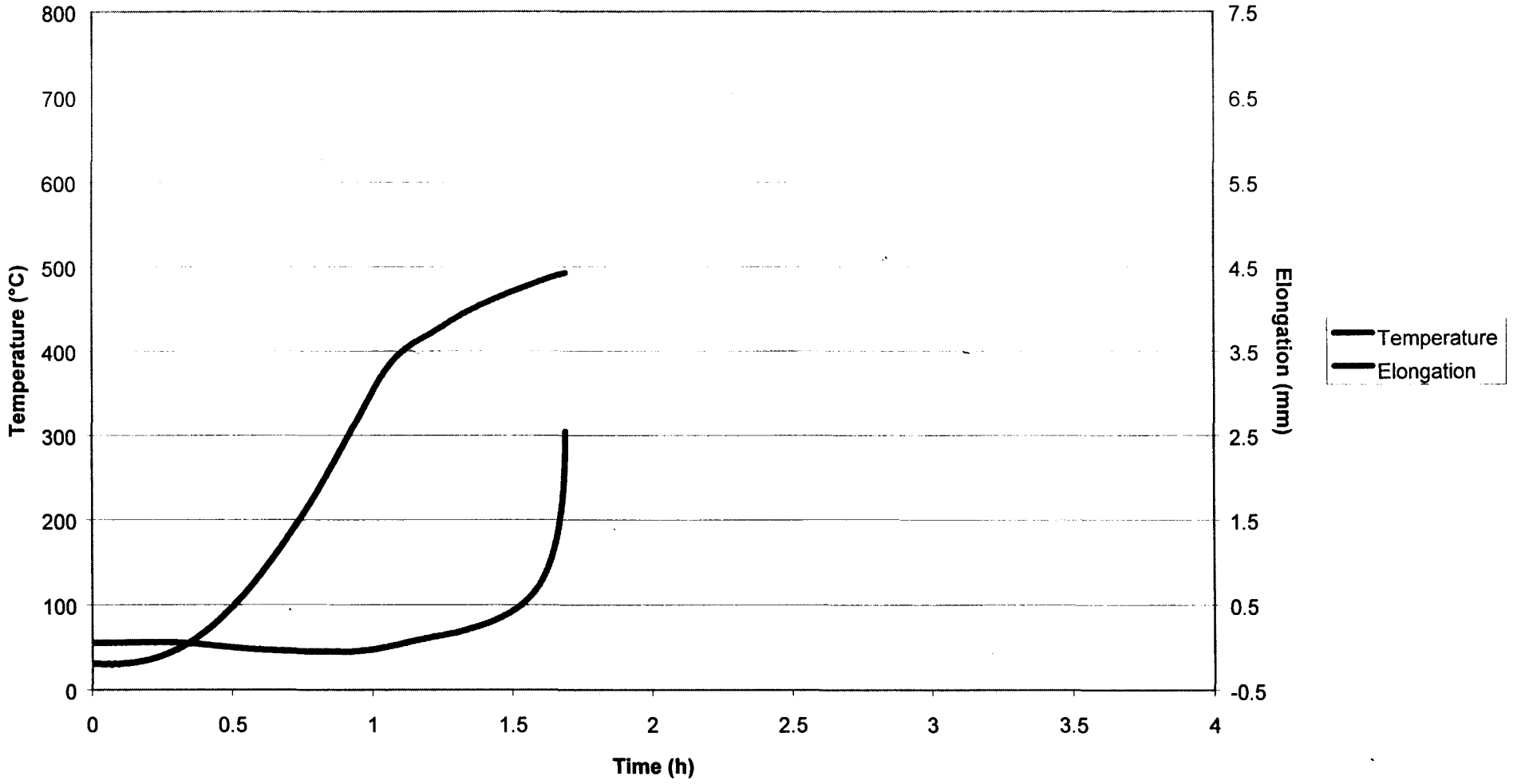

Appendix 2 (Continued)
X20 Service Exposed: 305 MPa

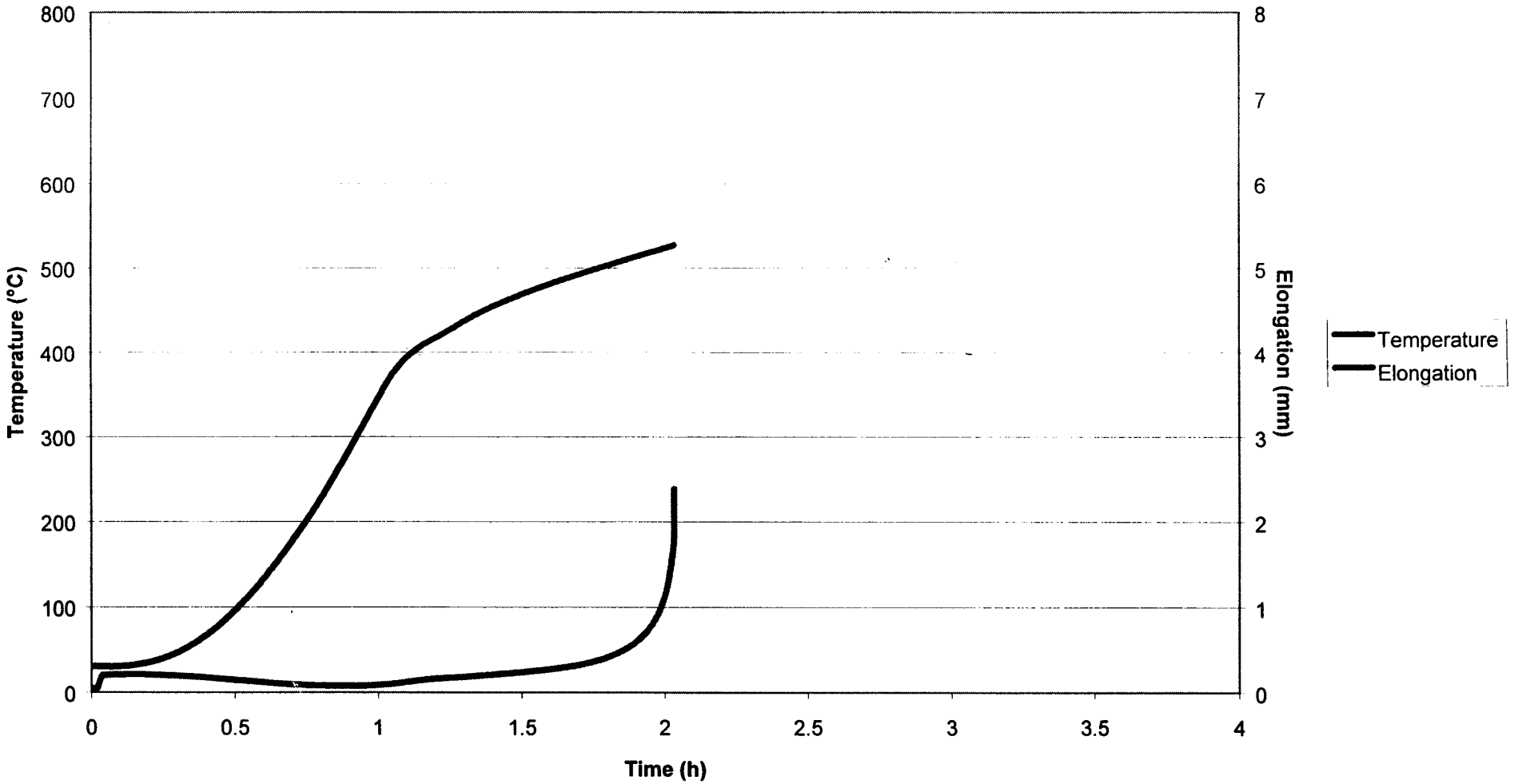

Appendix 2 (Continued)
X20 Service Exposed: 254 MPa

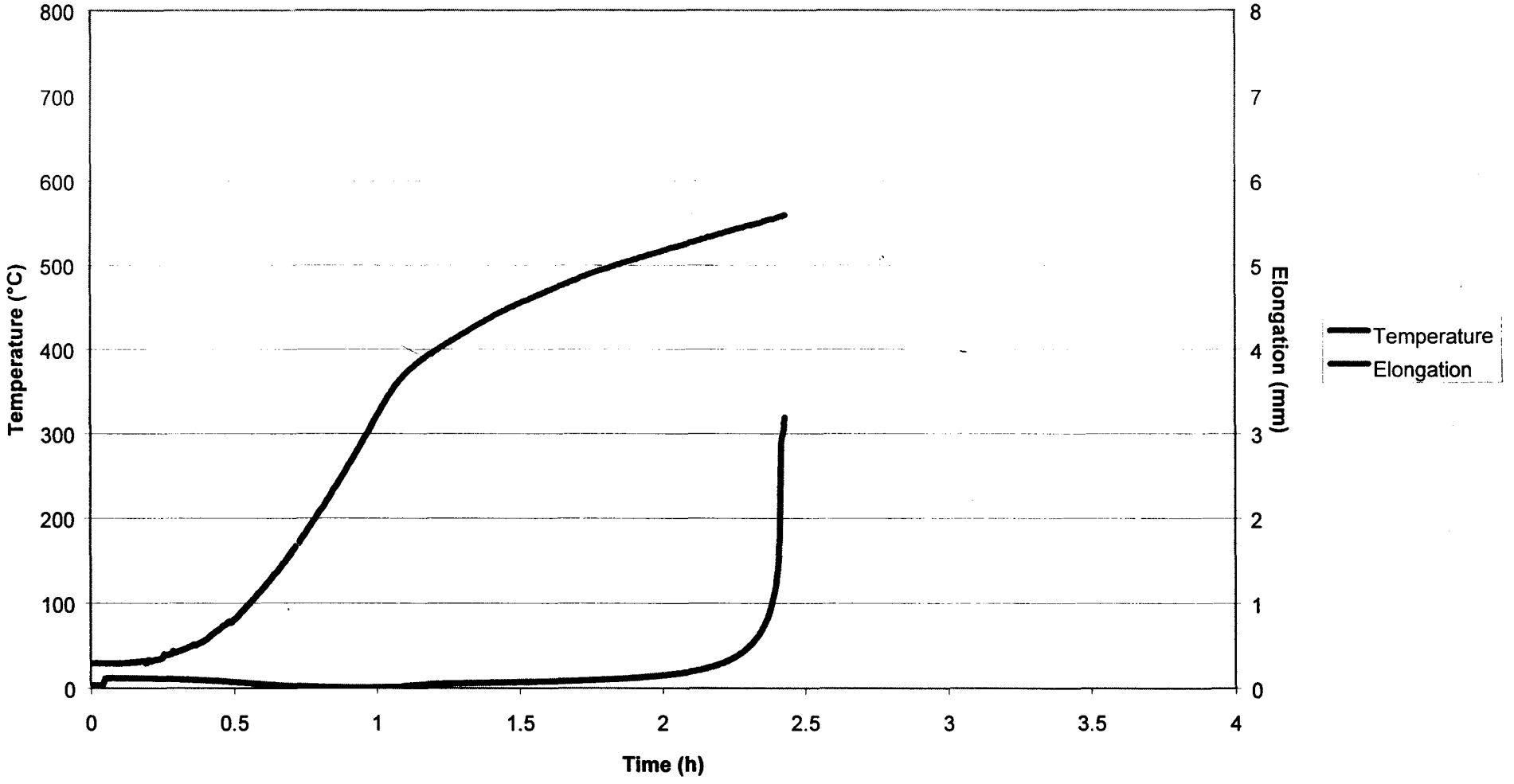

Appendix 2 (Continued)
P91 New: 407 MPa

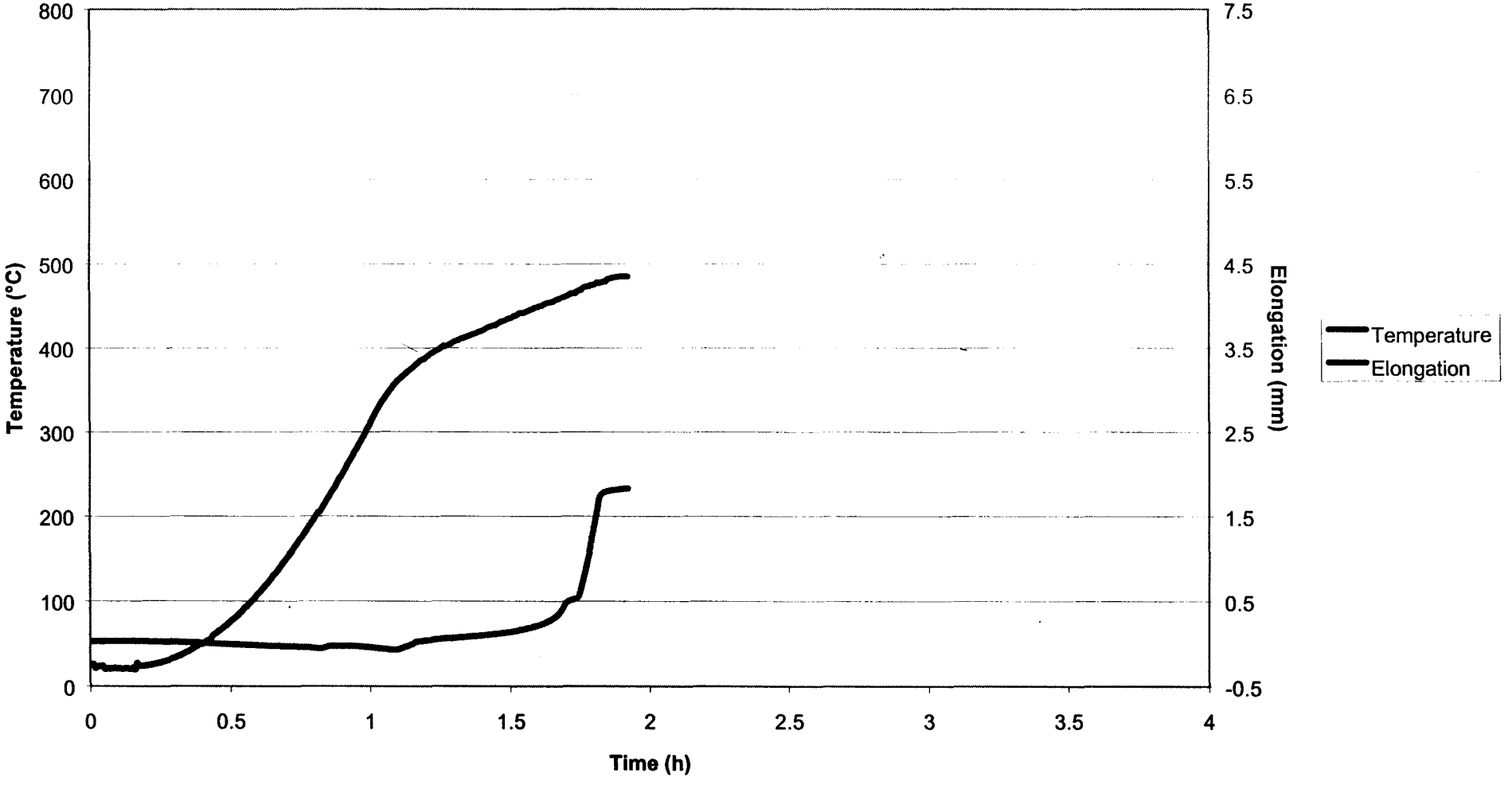

Appendix 2 (Continued)
P91 New: 356 MPa

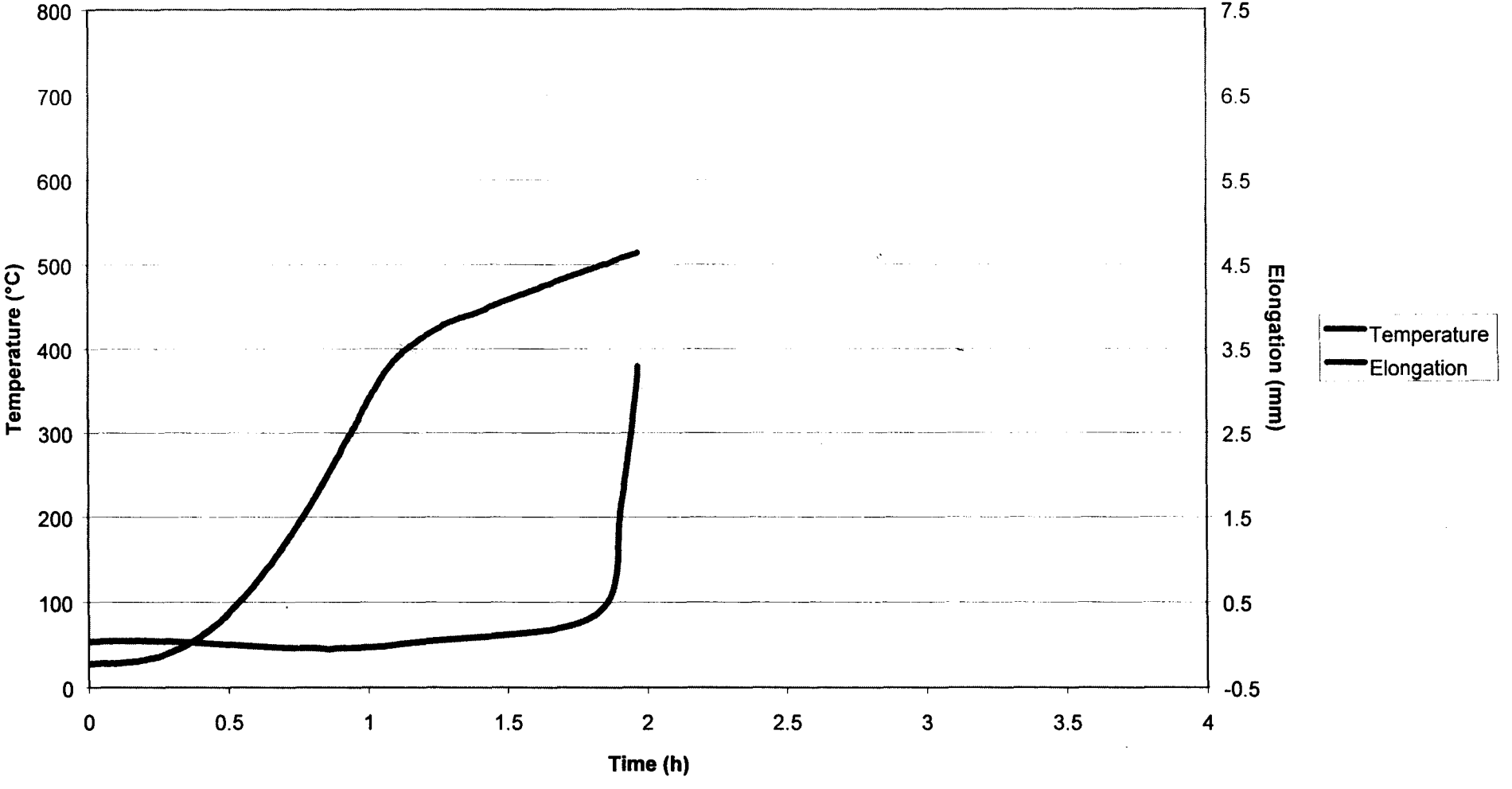

Appendix 2 (Continued)
P91 New: 305 MPa

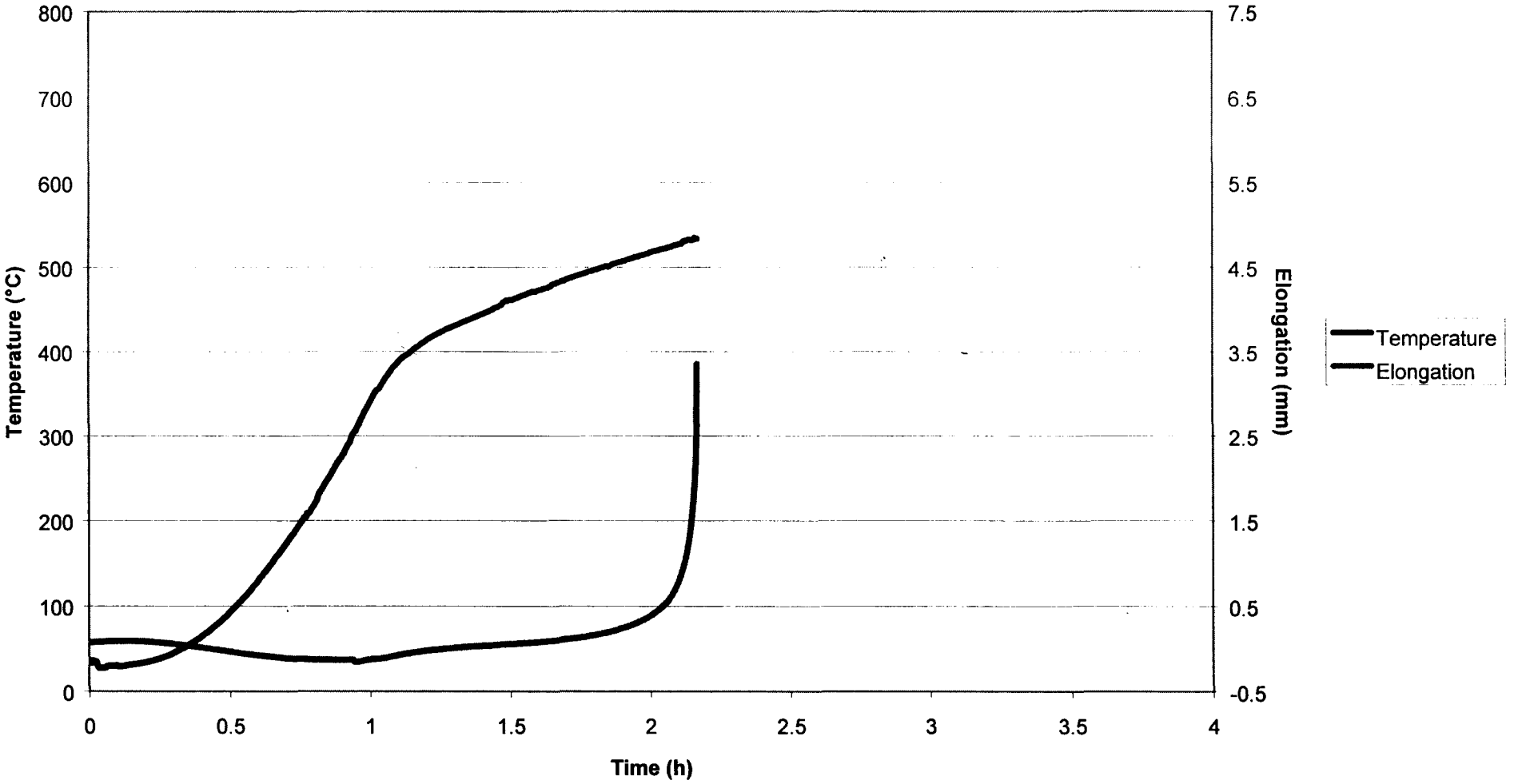

Appendix 2 (Continued)
P91 New: 254 MPa

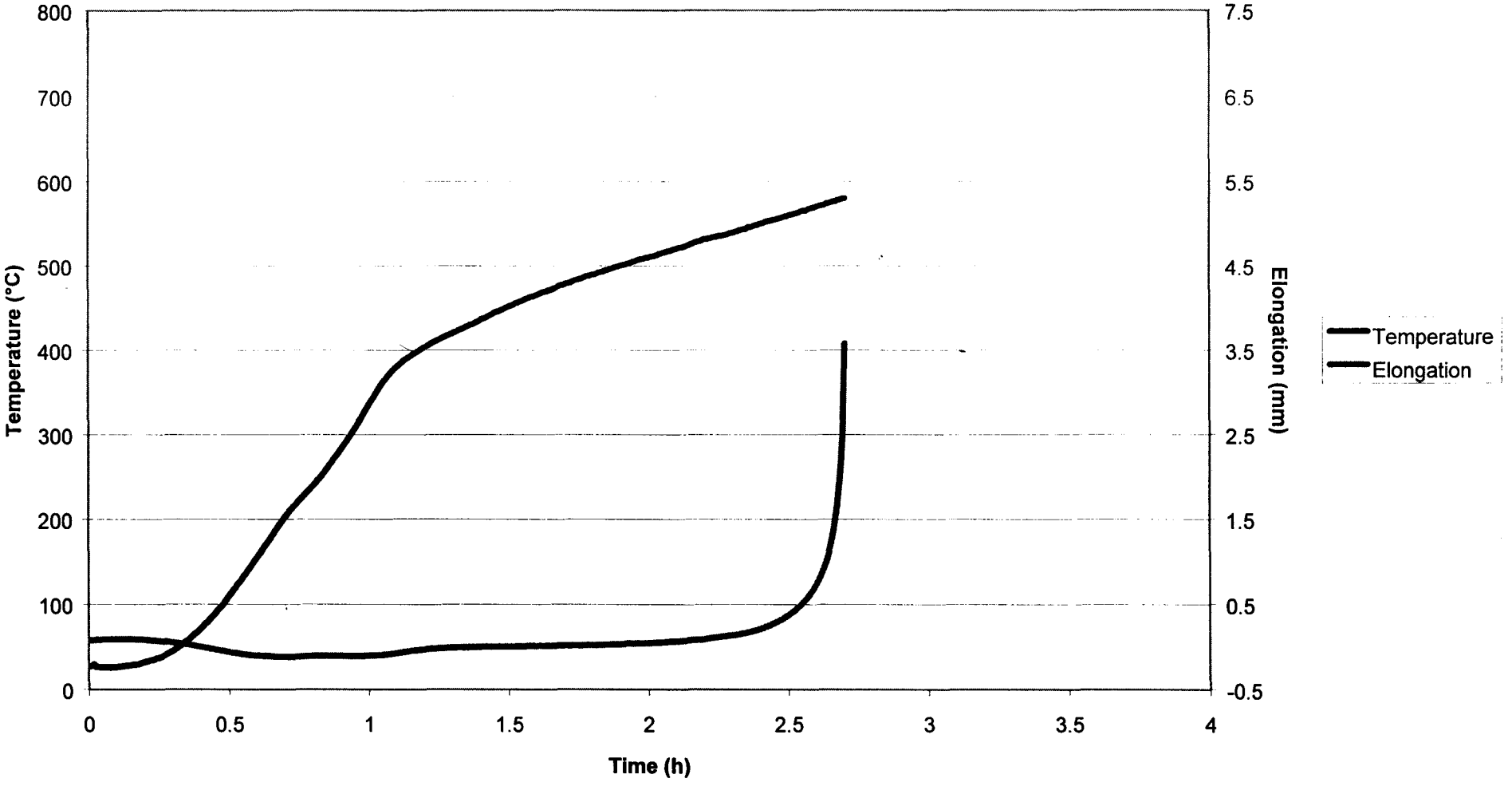

Appendix 2 (Continued)
P91 Artificially Aged: 407 MPa

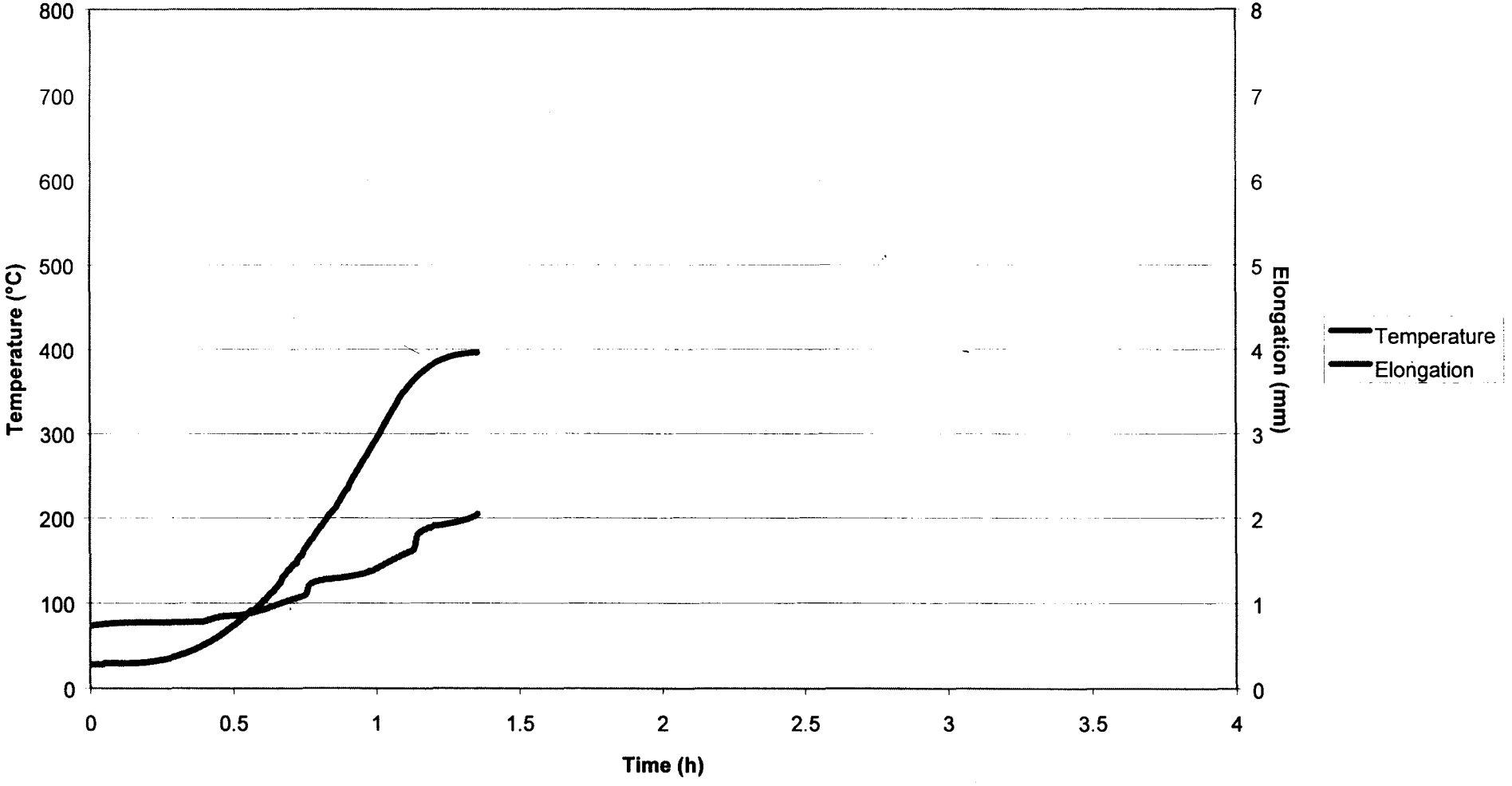

Appendix 2 (Continued)
P91 Artificially Aged: 356 MPa

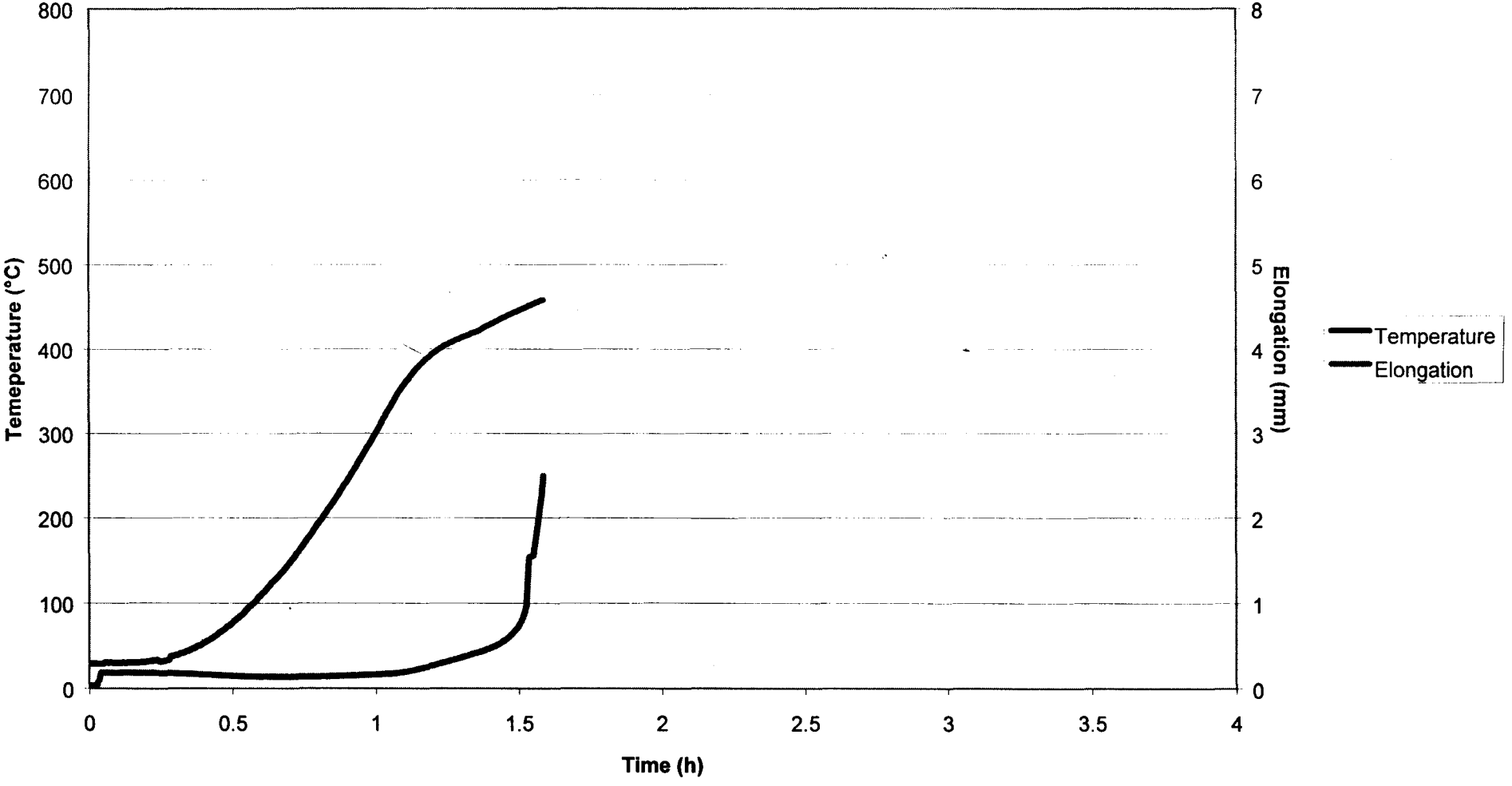

Appendix 2 (Continued)
P91 Artificially Aged: 305 MPa

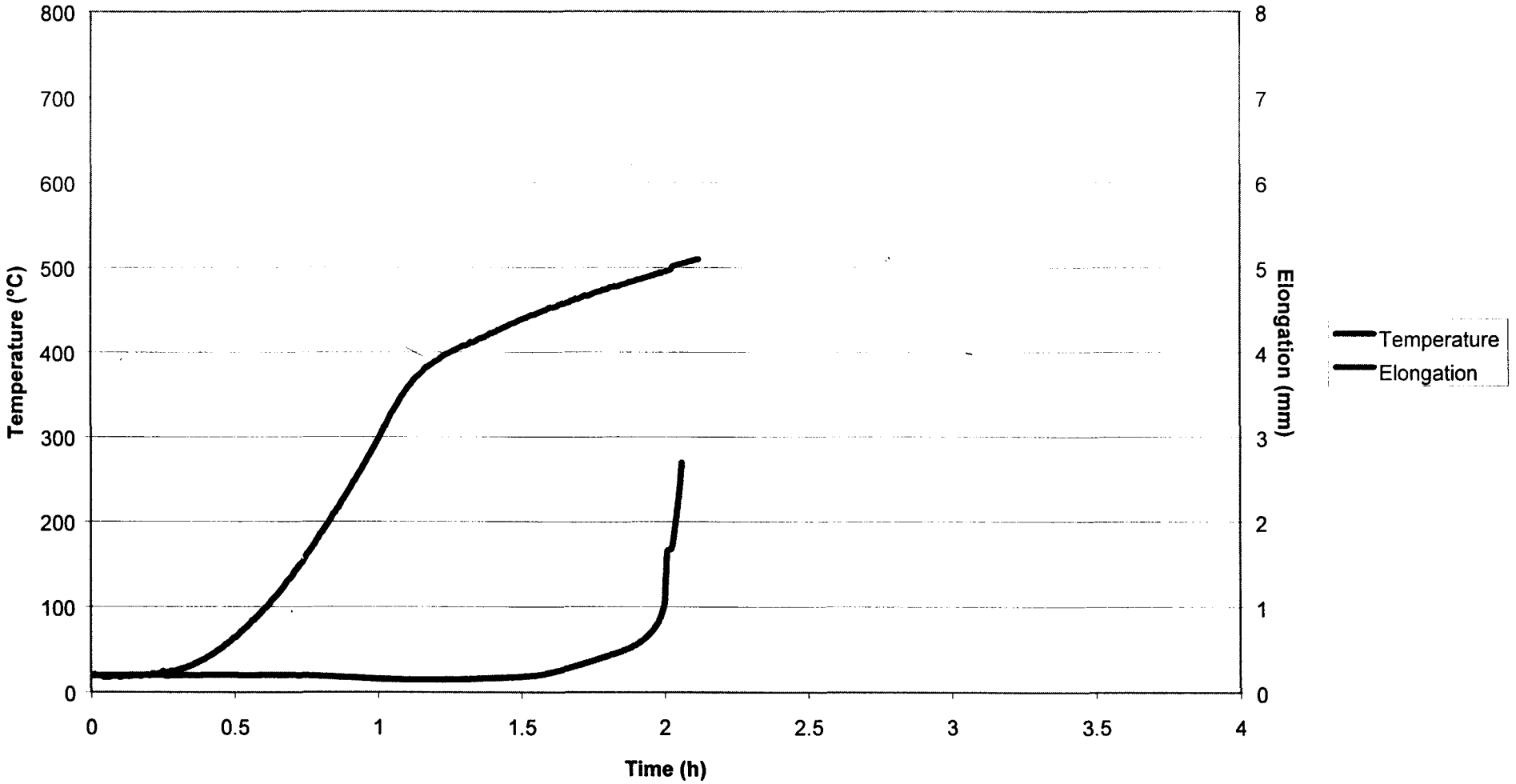

Appendix 2 (Continued)
P91 Artificially Aged: 254 MPa

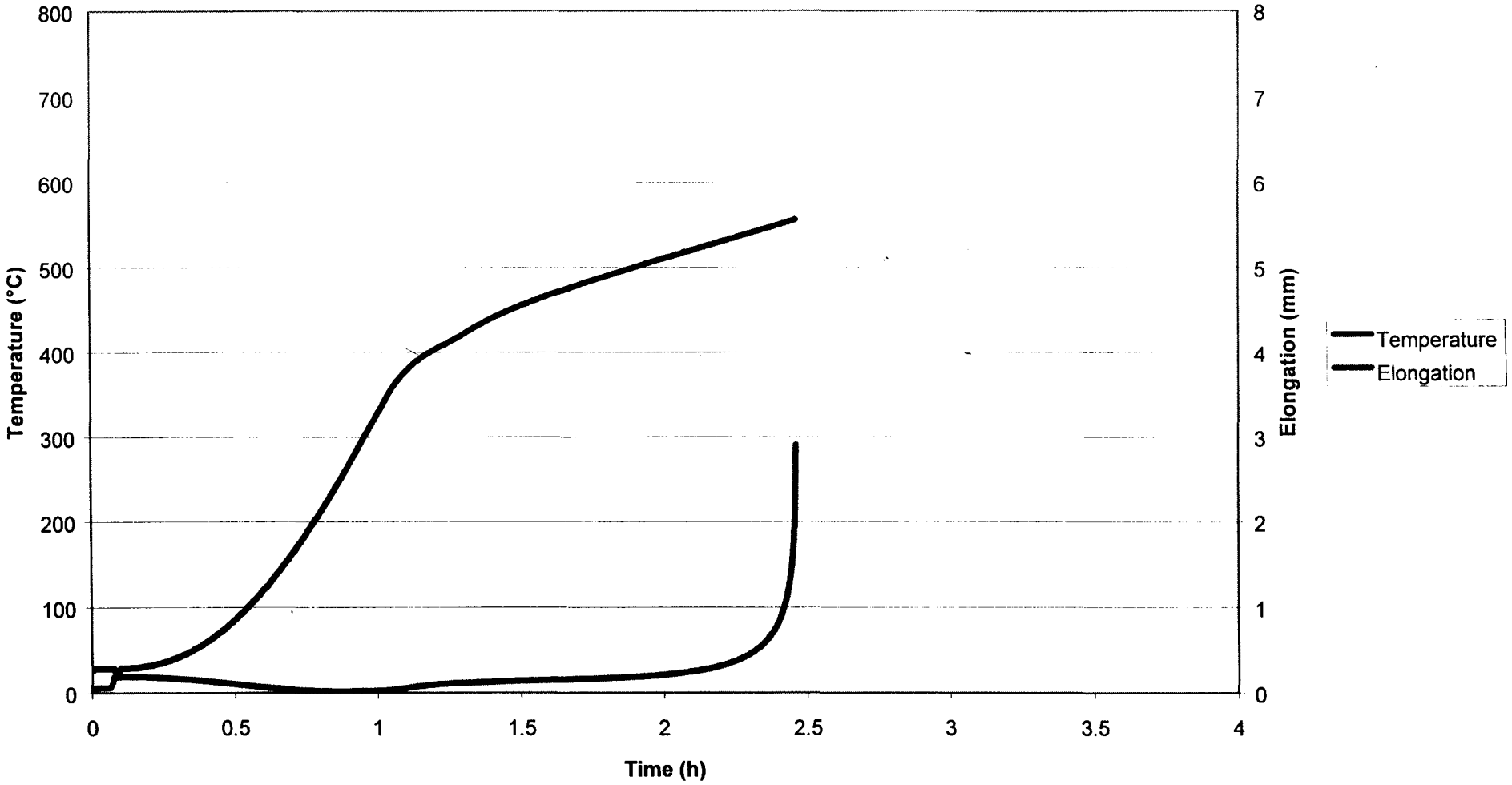

the high amount of chromium that is present in the structure as chromium carbides as well as molybdenum carbides.

From the SEM photographs it is evident that both the new and service-exposed material failed due to a ductile fracture mechanism. Due to the notch a stress concentration is present and the yield strength of the base metal is lower than the HAZ during the PWHT. The base metal will be the primary region where creep deformation occurs under the influence of a tensile stress up to the point of failure.

The structure of the base metal in the service-exposed condition is such that it will be softer than the base metal of the new material. This leads to the failure in the base metal areas because the yield strength for the base metal is lower than that of the CGHAZ. CGHAZ simulation resulted in similar structures of partly tempered martensite. This is due to the very high hardenability of X20. A fully martensitic structure can thus be obtained in these materials with slower cooling rates in comparison with that of to the two ferritic grades (½Cr-½Mo-¼V and 2¼Cr-1Mo). During cooling of materials with a high hardenability the martensite that formed first is still at a relatively high temperature and longer periods of time and undergoes auto-tempering as the work piece cools down to room temperature. The structure of the sample that underwent PWHT (spiral notch test) showed a tempered structure due to the thermal cycle as expected.

The hardness profiles showed the service-exposed material base metal had a lower hardness than the new material. The hardness of the HAZ's showed some difference. After PWHT the hardness of the HAZ is significantly reduced as toughness and ductility are restored due to the tempering of the hardened structure. The hardness (yield strength) is still higher than that of the base metal, which points to the fact that the base metal is the area where creep deformation was concentrated during PWHT.

X20 material creep strength is obtained due to the high content of chromium as alloying element with molybdenum in small quantities. The hardenability of the steel is very high. PWHT restores toughness and ductility and does not seem to increase the strength, as is the case with ½Cr-½Mo-¼V. Due to the high hardenability, a X20 component during welding operations is held at a certain temperature before PWHT. This could prevent full transformation of the HAZ to martensite and retained austenite could be present before PWHT. The temperature before PWHT must be such that it prevents cracking due to the high hardenability and also to allow almost full transformation. The yield strength of the base metal for new and service-exposed material will always be lower than the HAZ making it the primary region for creep deformation during PWHT to allow stress relief to occur.

6.9 REFERENCES

1. Stahlschlüssel – Key to Steel, 1998